Arctic Report Card 2019

Arctic ecosystems and communities are increasingly at risk due to continued warming and declining sea ice

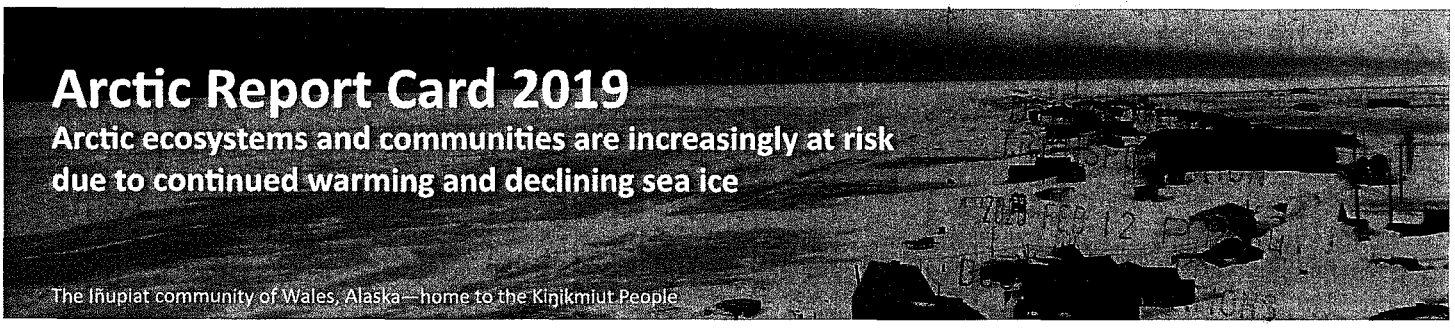

The Iñupiat community of Wales, Alaska—home to the Kiŋikmiut People

2019 Headlines

Arctic ecosystems and communities are increasingly at risk due to continued warming and declining sea ice

The Arctic marine ecosystem and the communities that depend upon it continue to experience unprecedented changes as a result of warming air temperatures, declining sea ice, and warming waters. Arctic Report Card 2019 draws particular attention to the Bering Sea region, where declining winter sea ice exemplifies the potential for sudden and extreme change. Indigenous Elders from the Bering Sea region offer their experiences of living at the forefront of climate change.

Video

Highlights

- The average annual land **surface air temperature** north of 60° N for October 2018-August 2019 was the second warmest since 1900. The warming air temperatures are driving changes in the Arctic environment that affect ecosystems and communities on a regional and global scale.
- The **Greenland Ice Sheet** is losing nearly 267 billion metric tons of ice per year and currently contributing to global average sea-level rise at a rate of about 0.7 mm yr^{-1}.
- **North American Arctic snow cover** in May 2019 was the fifth lowest in 53 years of record. June snow cover was the third lowest.
- **Tundra greening** continues to increase in the Arctic, particularly on the North Slope of Alaska, mainland Canada, and the Russian Far East.
- **Thawing permafrost** throughout the Arctic could be releasing an estimated 300-600 million tons of net carbon per year to the atmosphere.
- Arctic **sea ice extent** at the end of summer 2019 was tied with 2007 and 2016 as the second lowest since satellite observations began in 1979. The **thickness of the sea ice** has also decreased, resulting in an ice cover that is more vulnerable to warming air and ocean temperatures.
- August mean **sea surface temperatures** in 2019 were 1-7°C warmer than the 1982-2010 August mean in the Beaufort and Chukchi Seas, the Laptev Sea, and Baffin Bay.
- Satellite estimates showed **ocean primary productivity** in the Arctic was higher than the long-term average for seven of nine regions, with the Barents Sea and North Atlantic the only regions showing lower than average values.
- Wildlife populations are showing signs of stress. For example, the breeding population of the **ivory gull** in the Canadian Arctic has declined by 70% since the 1980s.
- The **winter sea ice** extent in 2019 narrowly missed surpassing the record low set in 2018, leading to record-breaking warm ocean temperatures in 2019 on the southern shelf. Bottom temperatures on the northern Bering shelf exceeded 4°C for the first time in November 2018.
- **Bering and Barents Seas fisheries** have experienced a northerly shift in the distribution of subarctic and Arctic fish species, linked to the loss of sea ice and changes in bottom water temperature.
- **Indigenous Elders from Bering Sea communities** note that "[i]n a warming Arctic, access to our subsistence foods is shrinking and becoming more hazardous to hunt and fish. At the same time, thawing permafrost and more frequent and higher storm surges increasingly threaten our homes, schools, airports, and utilities."

CAFF Conservation of Arctic Flora and Fauna

AMAP Arctic Monitoring and Assessment Programme

NOAA

December 2019

www.arctic.noaa.gov/Report-Card

Citing the complete report:
Richter-Menge, J., M. L. Druckenmiller, and M. Jeffries, Eds., 2019: Arctic Report Card 2019, https://www.arctic.noaa.gov/Report-Card.

Citing an essay (for example):
Frey, K. E., J. C. Comiso, L. W. Cooper, J. M. Grebmeier, and L. V. Stock, 2019: Arctic Ocean primary productivity: The response of marine algae to climate warming and sea ice decline. *Arctic Report Card 2019*, J. Richter-Menge, M. L. Druckenmiller, and M. Jeffries, Eds., http://www.arctic.noaa.gov/Report-Card.

Table of Contents

Executive Summary

J. Richter-Menge[1], M. L. Druckenmiller[2], and M. Jeffries[3]

[1]University of Alaska Fairbanks, Institute of Northern Engineering, Fairbanks, AK, USA
[2]National Snow and Ice Data Center, Boulder, CO, USA
[3]Cold Regions Research and Engineering Laboratory of the Engineer Research and Development Center, U.S. Army Corps of Engineers, Hanover, NH, USA

The 12 essays featured in Arctic Report Card 2019 provide comprehensive summaries of key land, ice, ocean, and atmosphere observations made throughout the Arctic in the context of historical records. Taken together, the essays also serve to highlight the many strong and complex connections within the Arctic system. It is these connections that magnify the impact of the changing Arctic environment—changes that affect ecosystems and communities on a regional and global scale.

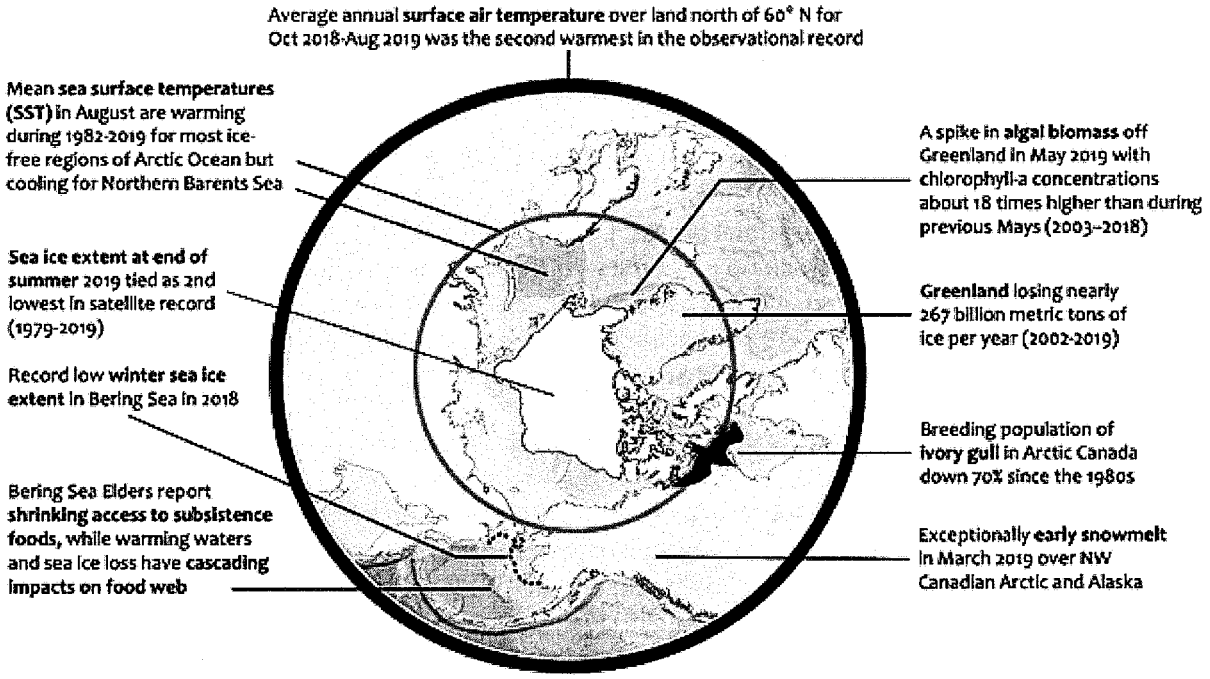

Various essay highlights from across the Arctic.

At the center of the changes observed throughout the Arctic is the persistent warming of the surface air temperature, which began around 1980. At +1.9°C, the annually-averaged land-based surface air temperature anomaly for October 2018-September 2019 is the second highest value (after 2015/16) since 1900. Annually averaged Arctic air temperatures for the past six years (2014-19) all exceed previous records since 1900.

In the marine environment, the decline in the extent and thickness of the Arctic sea ice cover is directly linked to the warming air temperatures. In September 2019, the end-of-summer minimum extent of the sea ice cover was tied for the 2nd lowest (with 2007 and 2016) in the 41-year satellite record. The oldest, thickest ice (>4 years old), which was once widespread within the Arctic Ocean, now makes up just a small fraction of the sea ice cover. In March 1985, at the end-of-winter maximum extent, 33% of

the ice cover within the Arctic Ocean was made up of very old ice, but in March 2019 old ice constituted only 1.2% of the ice cover. First-year ice now dominates the sea ice cover, comprising ~77% of the March 2019 ice cover, compared to about 55% in the 1980s. Overall, the Arctic sea ice cover has transformed from an older, thicker, and stronger ice mass in the 1980s to a younger, thinner, more fragile ice mass in recent years. Because of this transformation, today's sea ice cover is now more vulnerable to melting out in summer, thereby increasing the likelihood of a continuing decrease in minimum ice extent into the future.

The declining trend in the extent of the sea ice cover is also directly linked to observed changes in the sea surface temperatures and ocean primary productivity. Sea surface temperatures in the Arctic Ocean are driven mainly by solar warming. Greater solar warming occurs in ice-free regions of the Arctic Ocean, where the dark ocean surface absorbs solar radiation up to 10 times more readily than the brighter sea ice surface, which largely reflects sunlight. August mean sea surface temperatures show significant warming for 1982-2019 in most regions of the Arctic Ocean that are ice-free in August. For instance, the August mean sea surface temperatures in 2019 were ~1-7°C warmer than the 1982-2010 August mean in the Beaufort and Chukchi Seas, the Laptev Sea, and Baffin Bay.

Primary production in the Arctic Ocean is driven by algae growing in the ice (ice algae) and in the water column (phytoplankton), which provide usable energy to the entire food web through photosynthesis. Recent declines in Arctic sea ice extent have contributed substantially to shifts in patterns of primary production throughout the Arctic Ocean, as related increases in light availability and stratification of the water column stimulate the growth of phytoplankton in the water column. These patterns are often associated with the timing of the seasonal break-up and retreat of the sea ice cover: higher production tends to occur in regions where break-up is relatively early, while lower production tends to occur in regions where break-up is delayed. All regions of the Arctic Ocean have exhibited increasing ocean primary productivity over the 2003-19 period, with the most pronounced increases observed in the Eurasian Arctic, Barents Sea, and Greenland Sea.

Recent conditions in the Bering Sea offer an excellent, albeit disquieting, example of the strong connections within the Arctic marine environment. The Bering Sea forms the transition between the sub-Arctic North Pacific and the Arctic Oceans. The eastern half of the Bering Sea has a broad and shallow shelf that enables an exceptionally productive ecosystem, supporting large numbers of sea birds and marine mammals, the subsistence harvests that numerous Indigenous communities depend on, and more than 40% of the U.S. catch of fish and shellfish (valued at > $1B annually). The summer distribution of fishes and invertebrates living near the seafloor on the Bering Shelf is tied to the extent of the cold bottom water temperatures as determined by the southern extent of sea ice during the preceding winter.

For the past two winters (2018 and 2019) the maximum southern sea ice extent in the Bering Sea was at record low values, at approximately 30% of the long-term mean (1980-2010). The record low sea ice coverage was likely a result of three factors: (1) foremost, abnormally warm, southerly winds during winter limited the maximum sea ice extent by pushing the sea ice northward; (2) the late freeze-up of the southern Chukchi Sea in the preceding falls and delayed ice arrival in the northern Bering Sea; and (3) warm surface ocean temperatures that slowed the advance of ice. The record low sea ice extent and early sea ice retreat disrupted the formation of very cold bottom water temperatures on the Bering Shelf. The warmer bottom water temperatures observed during 2018 created a wide corridor within the shallow continental shelf allowing sub-Arctic fish species to move northward into regions typically occupied by northern shelf and Arctic species. In the Atlantic sector's Barents Sea, there has been a

similar northward shift in fish species associated with warming bottom water temperatures and loss of sea ice. Regional patterns of sea ice loss may also be connected to an observed decline in the breeding population of ivory gulls in the Canadian Arctic.

On land, the warming surface air temperature is causing a decrease in the extent of the Arctic snow cover, an increase in the overall amount of Arctic vegetation, and the thawing of perennially-frozen ground, known as permafrost. These components of the Arctic environment are interconnected and understood to influence wildlife. Thawing permafrost detrimentally affects municipal infrastructure, community shorelines, and Indigenous Peoples' traditional means for storing food in ice cellars. Warming conditions also promote the microbial conversion of carbon that is stored in permafrost into the greenhouse gases carbon dioxide and methane. These gases are released to the atmosphere, further trapping thermal radiation reflected from the Earth's surface in an accelerating feedback loop to global climate warming. The Greenland ice sheet is also melting under the persistent rise of surface air temperatures and, as a result, contributing to global average sea level rise at a current rate of about 0.7 mm yr^{-1}. During the 2019 melt season, the extent and magnitude of ice loss over the Greenland ice sheet rivaled 2012, the previous year of record ice loss.

Coming full circle, the decreasing extent of sea ice and snow cover along with the melting Greenland ice sheet leads to an acceleration in the rate of warming of surface air temperatures in the Arctic. When these bright, white surfaces melt, they expose darker surfaces (e.g., open ocean, rock, or vegetation). The white surfaces of snow and ice reflect sunlight back to space, helping cool the Arctic region. The darker surfaces of land and ocean absorb sunlight, warming the Arctic region. Hence, the increase in the relative amount of open water and snow-free land leads to warming surface air temperatures, which in turn lead to more melting and more warming. This cycle is a critical reason why the Arctic has warmed at more than twice the rate of the global mean since the mid-1990s, a phenomenon known as Arctic amplification of global warming. This warming is transforming Arctic ecosystems and presenting unique challenges for the region's Indigenous peoples who rely on the stability of the environment for cultural and economic well-being, as well as for subsistence foods taken from their local lands and waters. The impacts of a changing Arctic are not confined to those who live there. Through global sea-level rise, the release of permafrost carbon, and its role in regulating global weather patterns, the Arctic is vitally connected to people worldwide.

December 6, 2019

Surface Air Temperature

J. E. Overland[1], E. Hanna[2], I. Hanssen-Bauer[3], S. -J. Kim[4], J. E. Walsh[5], M. Wang[6], U. S. Bhatt[7], R. L. Thoman[8], and T. J. Ballinger[9]

[1]Pacific Marine Environmental Laboratory, NOAA, Seattle, WA, USA
[2]School of Geography and Lincoln Centre for Water and Planetary Health, University of Lincoln, Lincoln, UK
[3]Norwegian Meteorological Institute, Blindern, Oslo, Norway
[4]Korea Polar Research Institute, Incheon, Republic of Korea
[5]International Arctic Research Center, University of Alaska Fairbanks, Fairbanks, AK, USA
[6]Joint Institute for the Study of the Atmosphere and Ocean, University of Washington, Seattle, WA, USA
[7]Geophysical Institute, University of Alaska Fairbanks, Fairbanks, AK, USA
[8]International Arctic Research Center, University of Alaska Fairbanks, Fairbanks, AK, USA
[9]Department of Geography, Texas State University, San Marcos, TX, USA

Highlights

- The average annual surface air temperature over land north of 60° N for October 2018 to September 2019 was the second warmest (after 2015/16) in the observational record beginning in 1900. Arctic temperatures for the past six years (2014-19) have all exceeded previous records.
- Annual Arctic air temperature continues to increase at more than double the magnitude of the global mean air temperature increase.
- Alaska had warmer than normal air temperatures throughout the year, especially in winter, that were associated with unusual southerly winds and a lack of Bering Sea ice, similar to winter 2018.
- Especially warm localized air temperatures during spring and summer over west Greenland supported extensive ice sheet melt events and early regional snow melt.

Introduction

Arctic surface air temperature is an indicator of both regional and global climate change. Although there are year-to-year and regional differences in air temperatures, driven by natural variability, the magnitude, persistence, and Arctic-wide patterns of recent temperature increases are indicators of global climate change from increasing concentrations of atmospheric greenhouse gases (Overland 2009; Notz and Stroeve 2016). Warming atmospheric temperatures also act as a driver of Arctic changes in the ocean and on land. A linear relationship between global temperature change and Arctic sea ice area decline suggests a direct climate forcing (Mahlstein and Knutti 2012). Similarly, tundra greening, especially along coastlines, and glacier mass loss are also the result from air temperature increases. We report on the spatial and temporal variability of Arctic air temperatures during October 2018 through September 2019.

Mean annual land surface air temperature

At +1.9°C, the mean annual surface air temperature (SAT) anomaly for October 2018-September 2019 for land weather stations north of 60° N, relative to the 1981-2010 mean, is the second highest value (after 2015/16) in the observational record starting in 1900 (Fig. 1). Observed annual mean Arctic temperatures over the past six years (2014-19) all exceed previous records. Since the mid-1990s the Arctic has warmed at more than twice the magnitude of global mean temperature increases; a phenomenon known as Arctic amplification (Fig. 1).

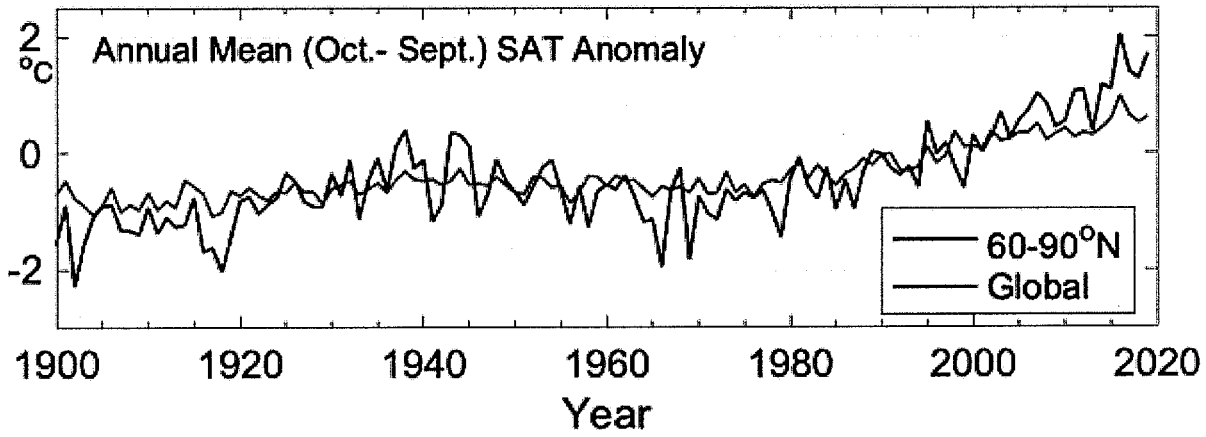

Fig. 1. Arctic (land stations north of 60° N; blue line) and global (red line) mean annual land surface air temperature (SAT) anomalies (in °C) for the period 1900-2019 relative to the 1981-2010 mean value. Note that there were few stations in the Arctic, particularly in northern Canada, before 1940. Source: CRUTEM4 dataset, which is available at www.cru.uea.ac.uk/cru/data/temperature/.

While there is currently no consensus on the reasons for Arctic amplification, proposed mechanisms include: reduced summer albedo due to sea ice and snow cover loss (Pithan and Mauritsen 2014), the increase of water vapor and clouds in the Arctic atmosphere (Dufour et al. 2016; Kim et al. 2017), lapse-rate feedback (decreases in tropospheric temperature with height: Stuecker et al. 2018), and decreased air pollution (Acosta Navarro et al. 2016).

Air temperature variation

Seasonal air temperature variations are divided into autumn 2018 (October, November, December [OND]), and winter (January, February, March [JFM]), spring (April, May, June [AMJ]), and summer (July, August, September [JAS]) of 2019 (Fig. 2). These SAT divisions are chosen to coincide with the seasonal cycles of key Arctic variables. For instance, the summer sea ice minimum occurs in September and autumn cooling continues through December.

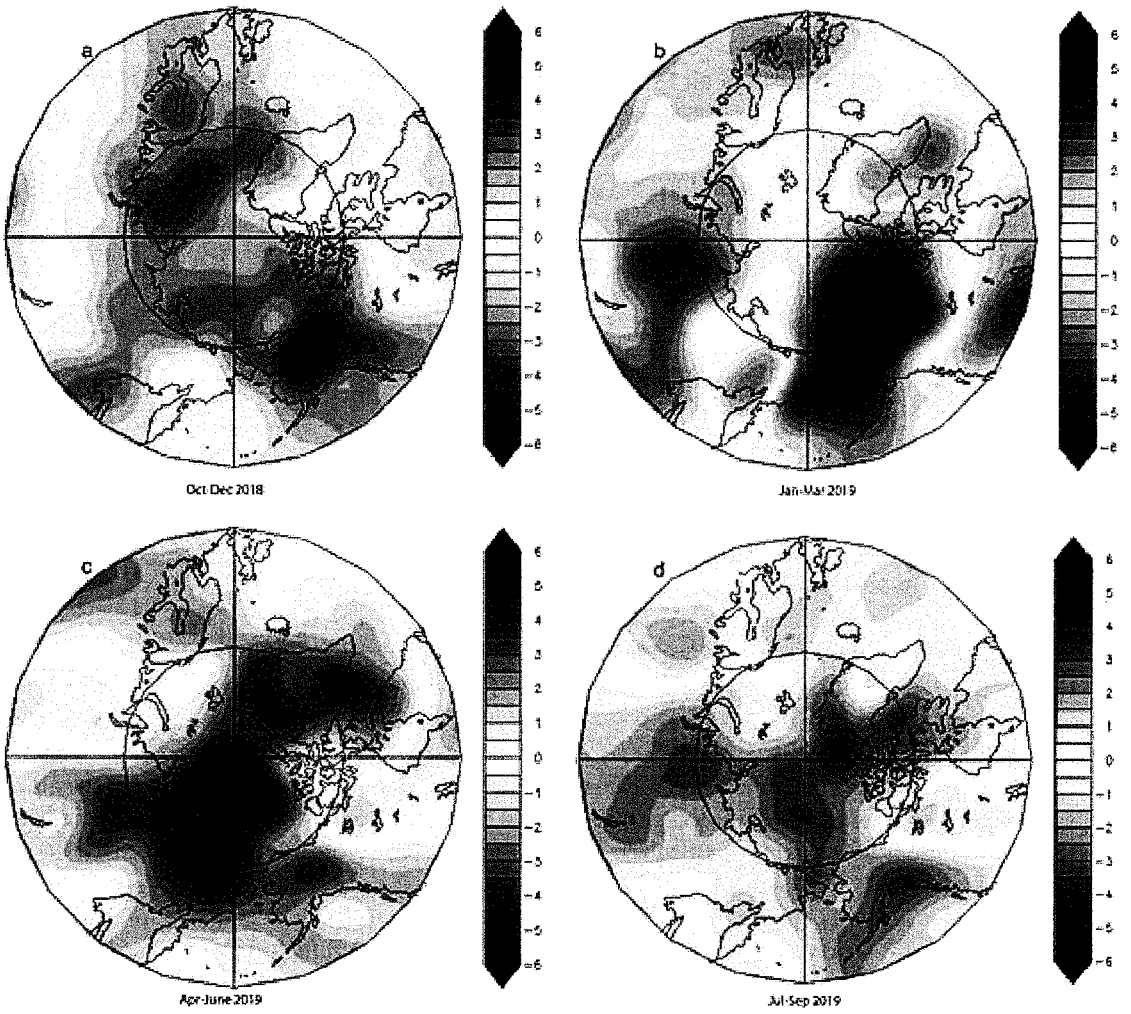

Fig. 2. Seasonal anomaly patterns for near-surface air temperatures (in °C) relative to the baseline period 1981-2010 in autumn 2018 (a), winter 2019 (b), spring 2019 (c), and summer 2019 (d). Temperature anomalies are from slightly above the surface layer (at 925 hPa level) to emphasize large spatial patterns rather than local features. Data accessed from NOAA/ESRL, Boulder, CO, at https://www.esrl.noaa.gov/psd/.

Autumn, spring, and summer seasons showed warm central Arctic temperatures of +2°C above the long-term average (1981-2010). However, 2018/19 regional temperature anomalies were not as extreme as the more than +4°C anomalies of 2017/18 (see Arctic Report Card 2018). Details of the seasonal air temperature variations in 2018/19 are provided below. Atmospheric temperatures and pressures in 2019 did not show major examples of Arctic/mid-latitude weather connections as in 2018.

Autumn 2018 (OND). The largest temperature anomalies (+2°C) stretched across the central Arctic (Fig. 2a). The warmest temperatures were over central Alaska and in the marginal ice zones of the Barents and Chukchi Seas. This sustained warming pattern and associated delayed autumn sea ice freeze-up were associated with winds from the southwest (Fig.3a; see essay *Sea Ice*). Over land, the Eurasian coast was warmer than normal. Finland observed a new record-high daily October temperature of 20.5°C in Ylivieska (central Finland) on 14 October 2018 (https://www.rcinet.ca/eye-on-the-arctic/2018/10/15/finland-weather-record-heat-october-autumn-ylivieska-global-warming/). Like autumn 2017, Svalbard experienced extreme warmth, where the December average for Svalbard Airport

was 5.5°C above the 1981-2010 average. Eastern Asia in autumn 2018 did not experience extensive spells of cold weather as in 2017.

Winter 2018 (JFM). A major Arctic warming event in winter (Fig. 2b) was observed in Alaska and adjacent seas, where monthly temperature anomalies were 4°C above normal. The northern Bering Sea was particularly warm, and contributed to low sea ice extent and ecological impacts to fisheries and marine mammals (see essay *Recent Warming in the Bering Sea*). This rare event was a repetition of the southerly winds and low sea ice coverage in 2018. March was exceptionally warm over much of Alaska, the Yukon, and western Northwest Territory, where most places set all-time record high monthly means, in some cases 3°C warmer than any previous March.

In February and March 2019 (Fig 3b), strong, warm winds from the south over the Bering Sea greatly retarded sea ice advances (see essay *Sea Ice*) and moved warm air northward along the international date line into the central Arctic, as in winter 2018. The lower atmospheric wind pattern (Fig. 3b) was connected to patterns higher in the atmosphere (the polar vortex; Fig. 3d) that contributed to the persistence of the wind pattern over Alaska and the remainder of North America.

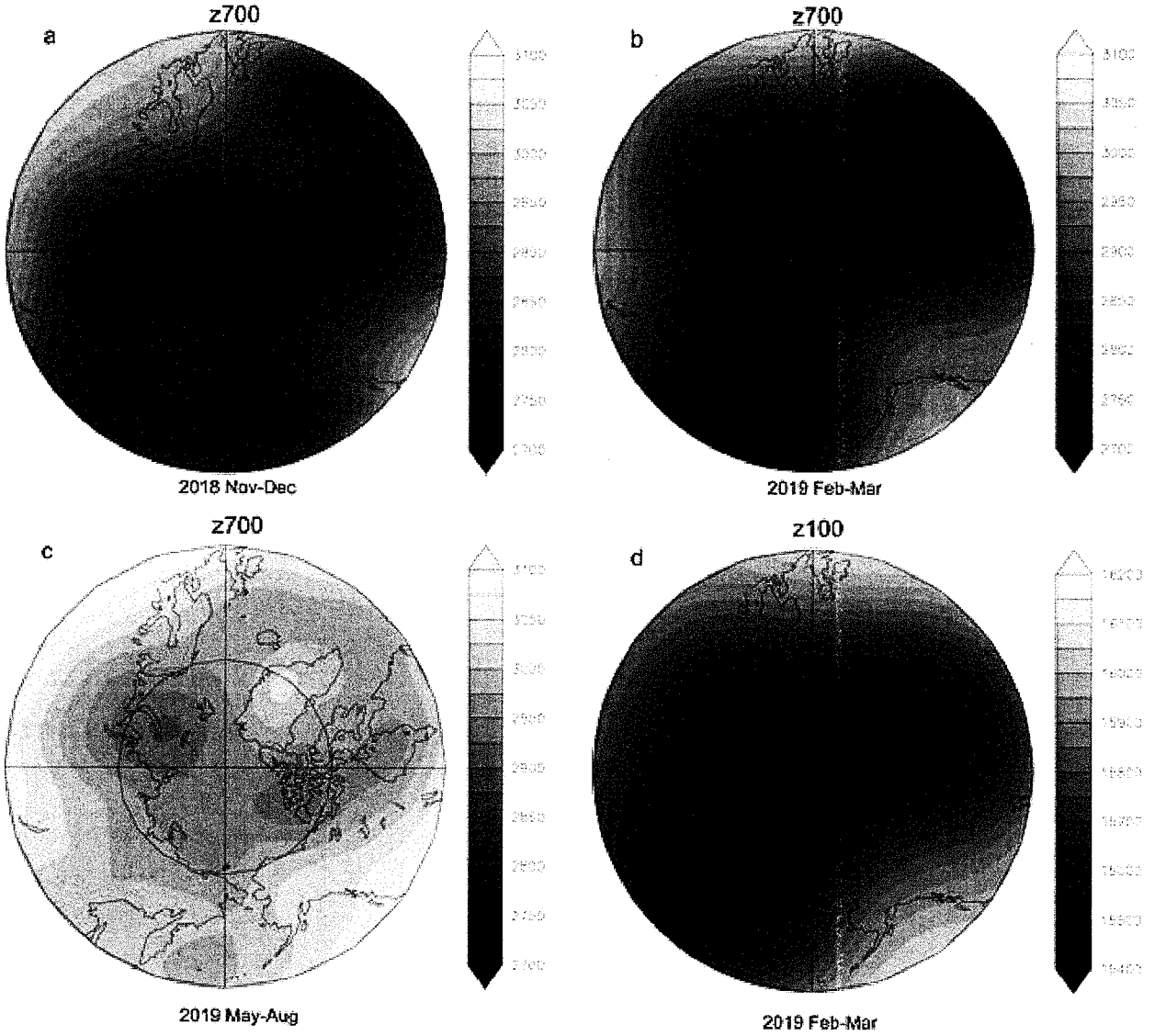

Fig. 3. The geopotential height pattern at 700 hPa for selected 2018-19 months that represent Arctic-wide wind patterns. (700 hPa geopotential height field is used to characterize atmospheric wind circulation about 1/3 of the way up in the troposphere; winds tend to follow the contours of geopotential heights anticlockwise around low values). (a) November-December 2018 showing warm air advection over Alaska and north of Norway, (b) February-March 2019 with southerly flow from the Pacific to Bering Sea, which contributed to the warm anomalies there, (c) low geopotential heights over the Arctic Ocean (centered near Kara Sea) and high heights over Greenland characterized late spring and summer (May to August). There were persistent southerly winds over the Bering Sea and to the west of Greenland. (d) the polar vortex at 100 hPa in February-March 2019, which supported the winter wind pattern shown in Fig 3b. Data accessed from NOAA/ESRL, Boulder, CO, at https://www.esrl.noaa.gov/psd/.

Spring 2018 (AMJ). Spring (Fig. 2c) showed warm temperature anomalies, especially in the East Siberian Sea related to offshore winds, as also seen during 2017 and 2018. In April, record warm temperatures occurred at several sites in Scandinavia and in many parts of Iceland. Localized extreme temperatures off the west coast of Greenland triggered an extensive spring-summer melt season and early snow melt (see essays *Terrestrial Snow Cover* and *Greenland Ice Sheet*). The Greenland coast, especially the west (including northwest) coast, had near-record high temperature maxima of 22-24°C in June-August. The warm temperatures resulted from localized southerly winds (Fig. 3c).

Summer 2018 (JAS). Unlike summers 2016, 2017, and 2018, summer 2019 returned to the warm conditions observed in much of the previous decade (Fig. 2d). Low surface pressures, which often counter extensive summer sea ice melt, actually supported melt in 2019 during the early summer with advection of warm temperatures from the south (see essay *Sea Ice*). While spring and early summer weather indicated possible record-low sea ice coverage (similar to 2012), late summer weather was historically not unusual and conditions were not supportive of a record sea ice minimum for 2019 (see essay *Sea Ice*). June and especially July were very warm over much of Alaska and the southern Yukon Territory. At Anchorage, all three months were the warmest on record relative to the last 69 years' mean. July was the warmest calendar month on record in Reykjavik, Iceland (Trausti Jónsson, Icelandic Met. Office, personal communication).

References

Acosta Navarro, J. C., V. Varma, I. Riipinen, Ø. Seland, A. Kirkevåg, H. Struthers, T. Iversen, H. -C. Hansson, and A. M. L. Ekman, 2016: Amplification of Arctic warming by past air pollution reductions in Europe. *Nat. Geosci.*, **9**, 277-281.

Dufour, A., O. Zolina, and S. K. Gulev, 2016: Atmospheric moisture transport to the Arctic. *J. Climate*, **29**, 5061-5081.

Kim, B. -M., J. -Y. Hong, S. -Y. Jun, X. Zhang, H. Kwon, S. -J. Kim, J. -H. Kim, S. -W. Kim, and H. -K. Kim, 2017: Major cause of unprecedented Arctic warming in January 2016: Critical role of Atlantic windstorm. *Sci. Rep.*, **7**, 40051, https://doi.org/10.1038/srep40051.

Mahlstein, I., and R. Knutti, 2012: September Arctic sea ice predicted to disappear near 2°C global warming above present. *J. Geophys. Res. Atmos.*, **117**, D06104, https://doi.org/10.1029/2011JD016709.

Notz, D., and J. Stroeve, 2016: Observed Arctic sea-ice loss directly follows anthropogenic CO_2 emission. *Science*, **354**, 747-750, https://doi.org/10.1126/science.aag2345.

Overland, J. E., 2009: The case for global warming in the Arctic. *Influence of Climate Change on the Changing Arctic and Sub-Arctic Conditions*, J. C. J. Nihoul and A. G. Kostianoy, Eds., Springer, 13-23.

Pithan, F., and T. Mauritsen, 2014: Arctic amplification dominated by temperature feedbacks in contemporary climate models. *Nat. Geosci.*, **7**, 181-184, https://doi.org/10.1038/ngeo2071.

Stuecker, M. F., C. M. Bitz, K. C. Armour, C. Proistosescu, S. M. Kang, S. -P. Xie, D. Kim, S. McGregor, W. Zhang, S. Zhao, W. Cai, Y. Dong, and F. -F. Jin, 2018: Polar amplification dominated by local forcing and feedbacks. *Nat. Climate Change*, **8**, 1076-1081, https://doi.org/10.1038/s41558-018-0339-y.

December 6, 2019

Terrestrial Snow Cover

L. Mudryk[1], R. Brown[1], C. Derksen[1], K. Luojus[2], B. Decharme[3], and S. Helfrich[4]

[1]Climate Research Division, Environment and Climate Change Canada, Ottawa, ON, Canada
[2]Arctic Research Centre, Finnish Meteorological Institute, Helsinki, Finland
[3]Centre National de Recherches Météorologiques, Toulouse, France
[4]Center for Satellite Applications and Research, NESDIS, NOAA, College Park, MD, USA

Highlights

- After two years of above or near-average anomalies, the 2019 spring saw a return to below-average Arctic snow cover extent (SCE) anomalies, which were predominant over the 2005-16 time period. North American Arctic SCE anomalies in May and June were the 5th and 3rd lowest, respectively, in the 53-year record.
- Long-term trends for SCE remain negative across the Arctic: -3.4%/decade and -15.2%/decade for May and June, respectively (1981-2019).
- Exceptionally early snow melt occurred in March over the northwestern Canadian Arctic and Alaska, contributing to below-average April snow water equivalent and snow depth. Earlier than normal snow melt also occurred across the eastern Canadian Arctic driven by warm temperature anomalies.
- Winter season snow accumulation was near normal over Eurasia.

Snow covers the Arctic land surface (land areas north of 60° N) for up to 9 months each year, and influences the surface energy budget, ground thermal regime, and freshwater budget of the Arctic (Brown et al. 2017). Snow also interacts with vegetation, affects biogeochemical activity, and influences migration and access to forage for wildlife, which impacts terrestrial and aquatic ecosystems (Callaghan et al. 2011). The assessment provided here is based on an ensemble of datasets derived from satellite observations and reconstructions of snow cover from snowpack models driven by atmospheric reanalyses. Collectively, this basis provides a consistent picture of Arctic snow cover variability over the last five decades.

Snow across the Arctic land surface can be characterized by three variables: how much area is covered by snow (snow cover extent - SCE), how long snow continuously remains on the land surface (snow cover duration - SCD), and how much water is stored in solid form by the snowpack (a function of the snow depth and density, commonly expressed as snow water equivalent - SWE). We examine each of these variables in turn for the 2018/19 Arctic snow season.

SCE anomalies (relative to the 1981-2010 climatology) for the Arctic in spring 2019 were computed separately for the North American and Eurasian sectors of the Arctic. Anomalies were derived from the NOAA snow chart climate data record, which extends from 1967 to present (maintained at Rutgers University; Estilow et al. 2015; http://climate.rutgers.edu/snowcover/; Fig. 1a,b). Eurasian Arctic spring SCE anomalies in 2019 were below average in both May and June. SCE anomalies over the North American Arctic were strongly negative in May and June, resulting in the 5th lowest and 3rd lowest, respectively, in the entire record.

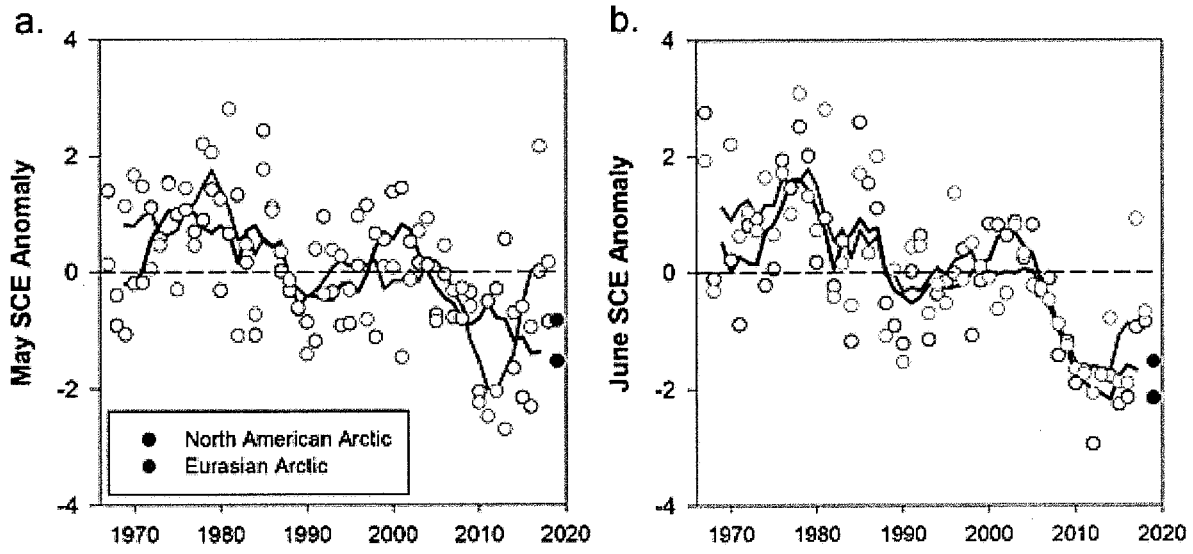

Fig. 1. Monthly snow cover extent (SCE) for Arctic land areas (>60° N) for (a) May and (b) June from 1967 to 2019, a 53-yr record. Anomalies are relative to the average for 1981-2010 and standardized (each observation differenced from the mean and divided by the standard deviation and thus unitless). Solid black and red lines depict 5-yr running means for North America and Eurasia, respectively. Filled circles are used to highlight 2019 anomalies. Source: NOAA snow chart Climate Data Record (CDR).

The spatial pattern of SCD anomalies across the Arctic region in the 2018/19 snow season (Fig. 2) was derived from the NOAA daily Interactive Multisensor Snow and Ice Mapping System (IMS) snow cover product (Helfrich et al. 2007), produced at 24-km resolution since 1998. Snow cover onset (Fig. 2a) was earlier than normal over the eastern Canadian Arctic and later than normal over the Eurasian Arctic and Alaska. These differences corresponded to a pattern of warm surface temperature anomalies over Eurasia and cold anomalies over eastern Canada during September and October, associated with observed atmospheric circulation patterns (see essay *Surface Air Temperature*). Snow-off dates (Fig. 2b) were near normal over most of the Eurasian Arctic. Over North America, earlier than usual melt occurred in March across extensive areas of northwestern Canada and Alaska and also in May over northeastern Canada (Baffin Island and northern Quebec), linked to persistent warm air advection over the Pacific and North Atlantic, respectively. The melt in May over Baffin Island and northern Quebec was also responsible for an early start to the Greenland melt season and contributed to near-record breaking mass loss from the ice sheet and led to substantial sea ice loss in the region as well (see essays *Surface Air Temperature*, *Greenland Ice Sheet*, and *Sea Ice*).

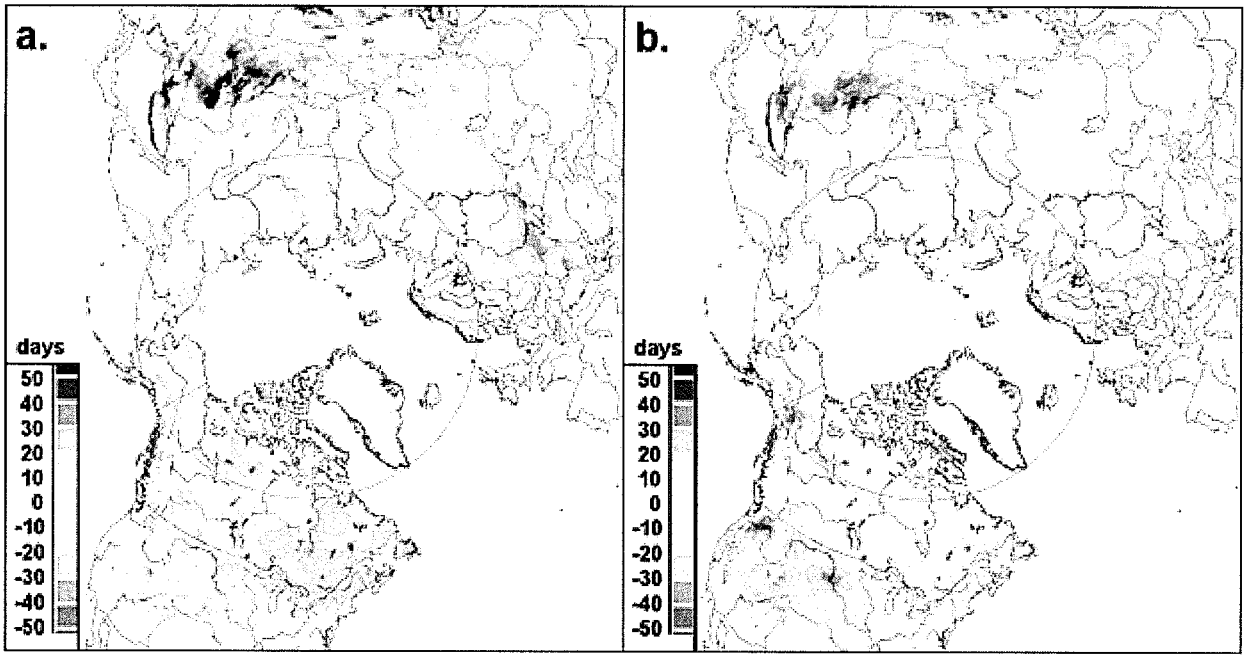

Fig. 2. Snow cover duration (SCD in days) anomalies (difference from 1998-2017 mean; red = shorter SCD than average; blue = longer SCD than average) for the 2018/19 snow year: (a) snow onset (Aug-Jan); and (b) snow melt (Feb-Jul). The grey circle marks the latitude 60° N; land north of this defines Arctic land areas considered in this study. Source: NOAA IMS data record.

Snow depth anomalies (Fig. 3) were derived from the Canadian Meteorological Centre (CMC) daily gridded global snow depth analysis (Brasnett 1999), which combines air temperature and precipitation analyses with the assimilation of surface snow depth observations. This approach is required to obtain hemispheric estimates of snow depth because in situ observations alone are too spatially sparse to be representative. Snow depth over the 2018/19 season was near normal over Eurasia. Over North America, unusually rapid snowmelt, driven by warm temperatures in March over northwestern Canada and Alaska, resulted in reduced March snow depths over the region. Snow depths were even more below average by April (typically the month of maximum SWE across the Arctic)—a pattern that continued through to June, consistent with the shorter than average snow cover duration observed in the region (Fig. 2). The warm May and June temperature anomalies and early snow melt over Baffin Island and Northern Quebec (Fig. 2) are consistent with the lower than normal snow depths observed in these regions (Fig. 3c,d).

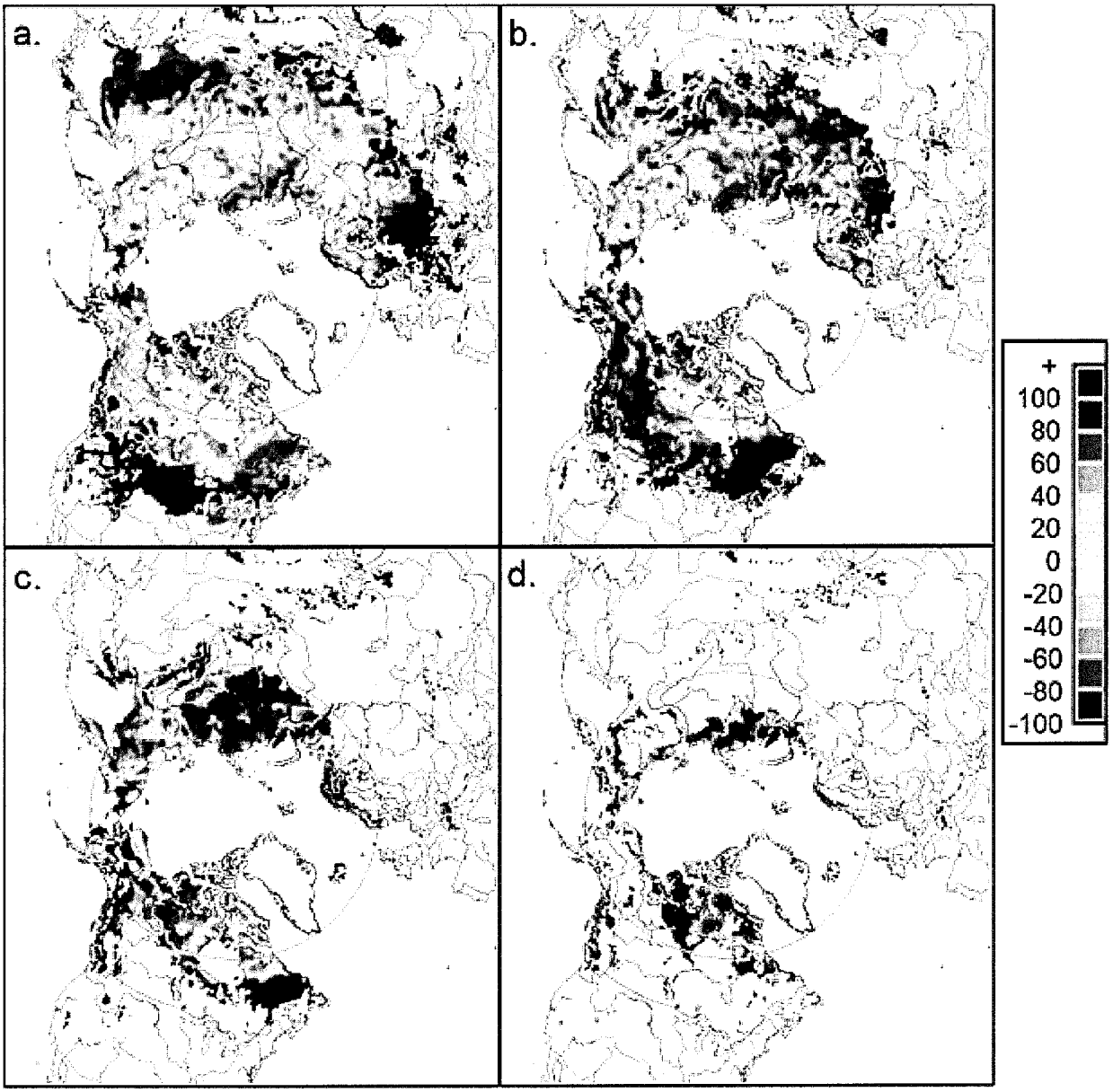

Fig. 3. Snow depth anomalies (% of the 1999-2017 average) in 2019 for (a) March, (b) April, (c) May, and (d) June. The grey circle marks the latitude 60° N. Source: CMC snow depth analysis.

Four products were utilized to generate a multi-dataset SWE anomaly time series (1981-2019) for April (Fig. 4): (1) modern atmospheric reanalysis (The Modern-Era Retrospective Analysis for Research and Applications version 2; MERRA-2; Reichle et al. 2017); (2) reconstructed snow accumulation driven by ERA-interim meteorology with the temperature index model described by Brown et al. (2003); (3) the physical snowpack model Crocus (Brun et al. 2013); and (4) the European Space Agency GlobSnow product derived through a combination of satellite passive microwave data and climate station observations (Takala et al. 2011). The use of multiple SWE products facilitates the determination of inter-product spread through the time series. SWE estimates for 2019 (which don't include Crocus due to data availability) indicate near-normal snow accumulation over the Eurasian Arctic but lower than normal SWE through April across the North American Arctic (consistent with negative snow depth anomalies in March and April; Fig. 3). Note that snow conditions over the North American Arctic were in

contrast to an unusually deep March snowpack with associated longer snow cover duration observed in the midlatitudes (Fig. 3a).

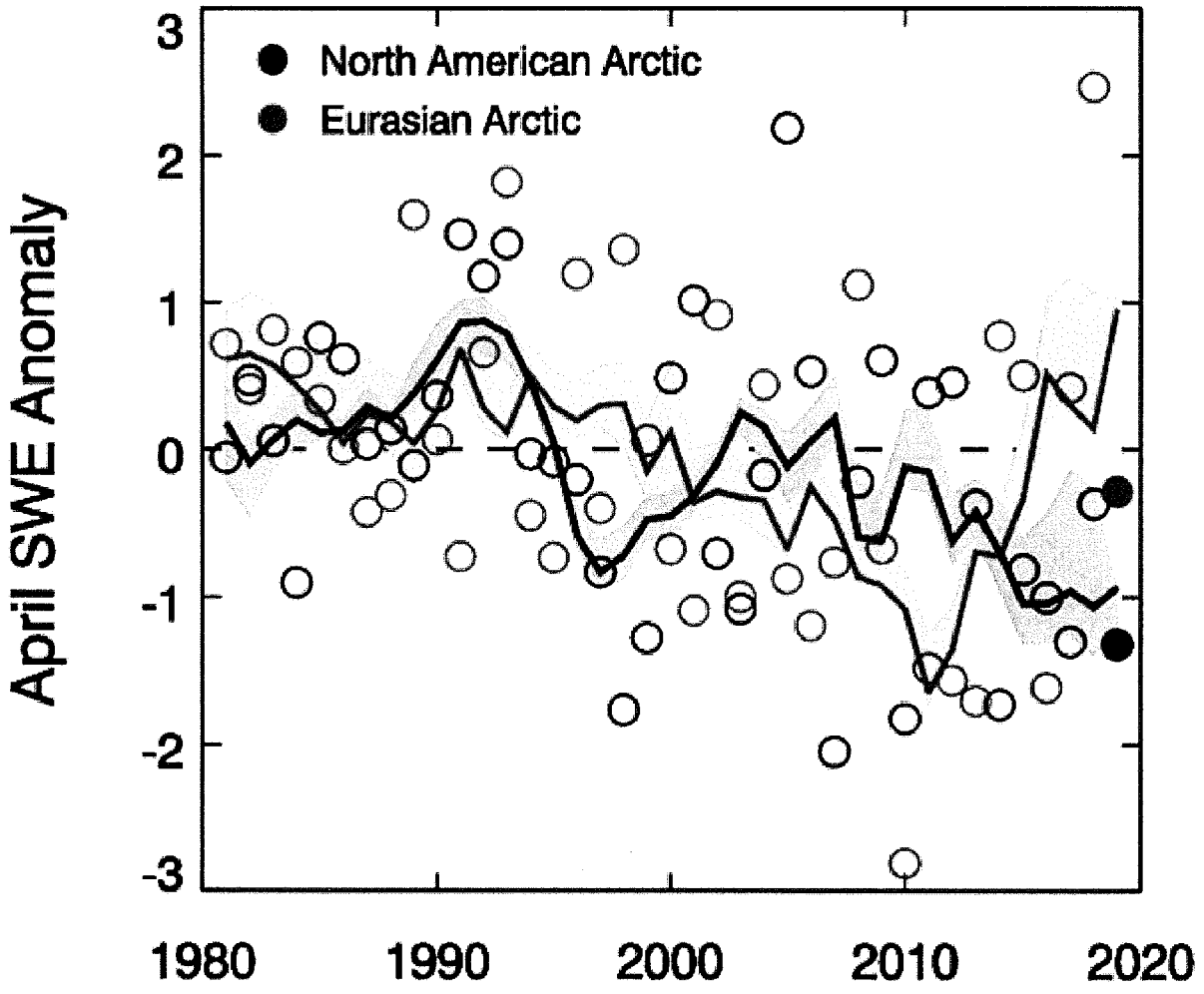

Fig. 4. Mean April SWE anomalies for Arctic land areas calculated for North American (black) and Eurasian (red) sectors of the Arctic. Anomalies are relative to the average for 1981-2010 and standardized (each observation differenced from the mean and divided by the standard deviation and thus unitless). Filled circles are used to highlight 2019 anomalies. Solid black and red lines depict 5-yr running means for North America and Eurasia, respectively; the spread among the running means for individual datasets is shown in shading. Source: suite of four independent snow analyses as described in text.

In summary, snow accumulation during the 2018/19 winter was close to normal over the Eurasian Arctic. Over the North American Arctic, earlier than normal snow melt in northwestern Canada and Alaska resulted in below-average April SWE and below-average snow depth from March through June. Earlier than normal snow melt also occurred over Baffin Island during May and June. These anomalies over the western and eastern sectors of the North American Arctic combined to cause the 5th and 3rd lowest SCE in May and June, respectively, since 1967.

Long-term trends for SCE remain negative across the Arctic: 3.4 ± 2.1%/decade and 15.2 ± 6.4%/decade for May and June, respectively (1981-2019). The April trend in Arctic SWE over the 1981-2019 period is -2.7 ± 2.0%/decade yielding a decrease of more than 10% over the entire Arctic since 1981.

References

Brasnett, B., 1999: A global analysis of snow depth for numerical weather prediction. *J. Appl. Meteor.*, **38**, 726-740.

Brown, R., B. Brasnett, and D. Robinson, 2003: Gridded North American monthly snow depth and snow water equivalent for GCM evaluation. *Atmos.-Ocean.*, **41**, 1-14.

Brown, R., D. Vikhamar Schuler, O. Bulygina, C. Derksen, K. Luojus, L. Mudryk, L. Wang, and D. Yang, 2017: Arctic terrestrial snow cover. *Snow, Water, Ice and Permafrost in the Arctic (SWIPA) 2017*, Arctic Monitoring and Assessment Programme (AMAP), Oslo, Norway, 25-64.

Brun, E., V. Vionnet, A. Boone, B. Decharme, Y. Peings, R. Valette, F. Karbou, and S. Morin, 2013: Simulation of Northern Eurasian local snow depth, mass, and density using a detailed snowpack model and meteorological reanalyses. *J. Hydrometeor.*, **14**, 203-219, https://doi.org/10.1175/JHM-D-12-012.1.

Callaghan, T., M. Johansson, R. Brown, P. Groisman, N. Labba, V. Radionov, R. Barry, O. Bulygina, R. Essery, D Frolov, V. Golubev, T. Grenfell, M. Petrushina, V. Razuvaev, D. Robinson, P. Romanov, D. Shindell, A. Shmakin, S. Sokratov, S. Warren, and D. Yang, 2011: The changing face of Arctic snow cover: A synthesis of observed and projected changes. *Ambio*, **40**, 17-31.

Estilow, T. W., A. H. Young, and D. A. Robinson, 2015: A long-term Northern Hemisphere snow cover extent data record for climate studies and monitoring. *Earth Sys. Sci. Data*, **7**(1), 137-142.

Helfrich, S., D. McNamara, B. Ramsay, T. Baldwin, and T. Kasheta, 2007: Enhancements to, and forthcoming developments in the Interactive Multisensor Snow and Ice Mapping System (IMS). *Hydrol. Process.*, **21**, 1576-1586.

Reichle, R., C. Draper, Q. Liu, M. Girotto, S. Mahanama, R. Koster, and G. De Lannoy, 2017: Assessment of MERRA-2 land surface hydrology estimates. *J. Climate*, **30**(8), 2937–2960, https://doi.org/10.1175/JCLI-D-16-0720.1.

Takala, M., K. Luojus, J. Pulliainen, C. Derksen, J. Lemmetyinen, J-P Kärnä, and J. Koskinen, 2011: Estimating Northern Hemisphere snow water equivalent for climate research through assimilation of space-borne radiometer data and ground-based measurements. *Remote Sens. Environ.*, **115**, 3517-3529.

November 19, 2019

Greenland Ice Sheet

M. Tedesco[1,2], T. Moon[3], J. K. Andersen[3,4], J. E. Box[5], J. Cappelen[6], R. S. Fausto[5], X. Fettweis[7], B. Loomis[8], K. D. Mankoff[5], T. Mote[9], C. J. P. P. Smeets[10], D. van As[5], and R. S. W. van de Wal[4,10]

[1]Lamont Doherty Earth Observatory of Columbia University, Palisades, NY, USA
[2]Goddard Institute of Space Studies, NASA, New York, NY, USA
[3]National Snow and Ice Data Center, Boulder, CO, USA
[4]Institute for Marine and Atmospheric Research Utrecht, Utrecht University, Utrecht, The Netherlands
[5]Geological Survey of Denmark and Greenland, Copenhagen, Denmark
[6]Danish Meteorological Institute, Copenhagen, Denmark
[7]University of Liege, Liege, Belgium
[8]Goddard Space Flight Center, NASA, Greenbelt, MD, USA
[9]Department of Geography, University of Georgia, Athens, GA, USA
[10]Department of Physical Geography, Utrecht University, Utrecht, The Netherlands

Highlights

- Melting in 2019 started early, in April, exceeding the 1981-2010 median during most of June, July, and the first half of August and covering roughly 95% of the ice sheet.
- Surface air temperatures for the 2018/19 winter and the 2019 spring and summer periods were above or near the 1981-2010 average temperatures.
- The updated trend for total mass loss obtained from the GRACE and GRACE-FO satellites estimates for the period May 2002-May 2019 is -267 ± 3 Gt yr^{-1}, which is equal to roughly 0.7 mm yr^{-1} of global average sea level rise.
- Indicative of extensive melting, the surface albedo in summer 2019 was 77.7%, the second lowest value (after 2012) recorded during the 20-year MODIS period (2000-19).
- Ice discharge from most regions has been approximately steady or declining for the past decade, including 2019.

Introduction

The Greenland ice sheet sits atop the largest island in the world and, as the second largest ice sheet on the Earth, contains the equivalent of roughly 7.4 m of global mean sea level rise (Morlighem et al. 2017). While the ice sheet was likely in balance (i.e., ice mass gain was balancing ice mass loss) during the 1970s, 1980s, and early 1990s (Mouginot et al. 2019), it began to lose mass in earnest beginning in the mid- to late 1990s. Continued observations and measurements of the Greenland ice sheet are critical to understanding whether ice mass loss will continue to accelerate and the full implications of this anticipated change. As Greenland loses ice, the additional cold freshwater to the ocean not only changes sea levels, but also impacts ocean properties and circulation locally and regionally (e.g., Luo et al. 2016), alters nutrient and sediment fluxes (e.g., Overeem et al. 2017; Cape et al. 2019), and changes local ecosystems (e.g., Hopwood et al. 2018). Changes at the ice sheet surface also feedback to influence future melt (e.g., Ryan et al. 2019).

Direct observations of the Greenland ice sheet from fall 2018 through 2019 reveal another year of dramatic ice loss. The extent and magnitude of ice loss rival 2012, the previous record year of ice loss. This rapid, ongoing change across Greenland is evident in observations of surface melt area, total ice loss, surface albedo (similar to reflectivity), and motion and ice loss via marine-terminating glaciers.

Surface melting

Roughly 95% of the Greenland ice sheet surface underwent melting during the 2019 summer. Observations derived from brightness temperatures measured by the Special Sensor Microwave Imager/Sounder (SSMIS) passive microwave radiometer (e.g., Mote 2007; Tedesco et al. 2013) indicate that surface melt started early in 2019, around mid-April, 6 to 8 weeks before the long-term average (1981-2010 baseline, Fig. 1a). Similar conditions occurred in 2012, the record melt year, when melting also started at the beginning of April. Melt extent in 2019 exceeded the 1981-2010 median during most of June, July, and the first half of August (Fig. 1a).

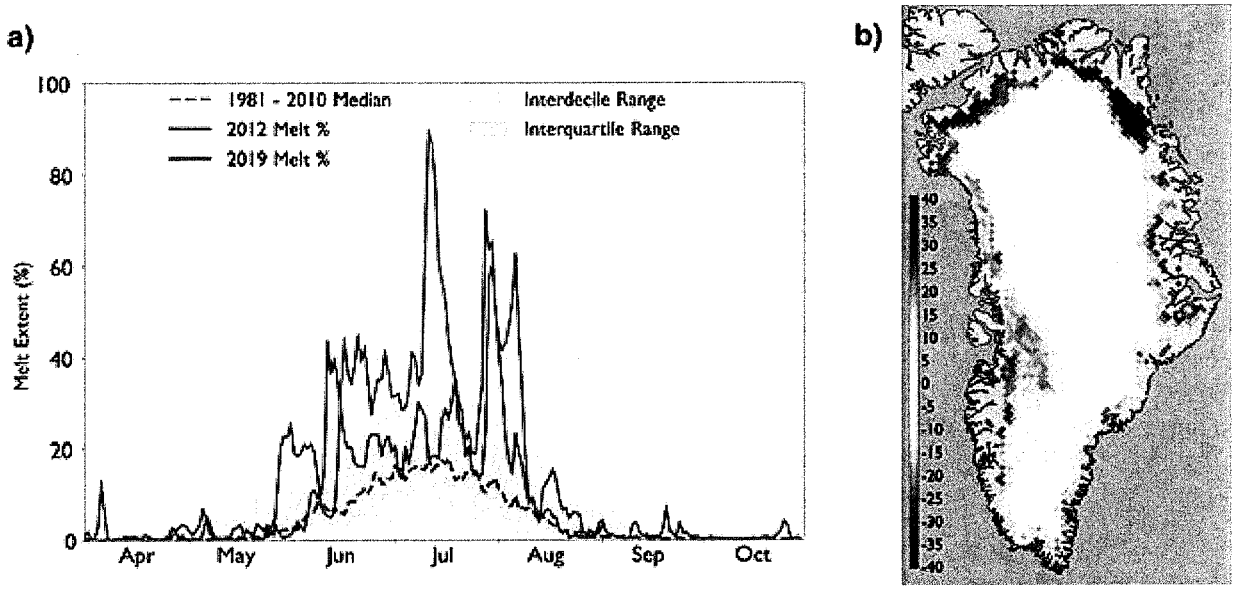

Fig. 1. (a) SSMIS-derived surface melt area as a percentage of the ice sheet area during 2019 (solid red) and 2012 (solid purple), in addition to the 1981-2010 median (dashed blue) and interdecile and interquartile ranges (shaded). (b) Summer 2019 melt anomaly (in number of melting days) with respect to the 1981-2010 period, estimated from spaceborne passive microwave observations.

In 2019, the maximum daily extent of ice sheet surface melt was 60.3% (the maximum daily value exceeding 90% in 2012), occurring on 31 July. In comparison, the average maximum daily extent for the same day (i.e., 31 July) during 1981-2010 is 39.8%. When considering the overall melt extent (i.e., areas that underwent melting at any time during summer), 2019 matched the values reached in 2012, with ~95% of the ice sheet surface experiencing melt. To put this in context, the 1981-2010 averaged value for the total area of the Greenland ice sheet undergoing melting (at any time) during summer is ~64%.

Melt duration in 2019 exceeded the 1981-2010 mean for most of the ice sheet ablation zone. The entire northern periphery of the ice sheet had at least 20 more days with melt compared to the mean (Fig. 1b). The exception was a thin strip of the southeast, where melt duration was below the 1981-2010 mean. The magnitude and timing of 2019 surface melt were consistent with persistent, high-pressure conditions occurring over Greenland during summer. These high-pressure conditions reached their peak

at the end of July, when the seasonal melt extent maximum was established. The persistence of the high-pressure systems promoted an increase in incoming solar radiation associated with reduced cloud cover and, consequently, below-normal summer snowfall.

Surface mass balance

Net ice ablation in 2019 at all 18 PROMICE weather station sites (https://www.promice.dk/) in the ablation area around the Greenland ice sheet was above the 12-year PROMICE 2008-19 average. At lower elevations along the ice sheet margin net ablation recorded by PROMICE stations exceeded the 2008-19 average by 49% in the southwest (KAN), 44% in the northwest (THU), and 39% in the northeast (KPC). Ablation at the ice sheet margin also exceeded the 1981-2010 average (re-referenced following van As et al. 2016) at all sites, most being well beyond uncertainty and, again, most notably again in the southwest (79 ± 20%), northwest (117 ± 45%), and northeast (70 ± 30%) (Fig. 2a).

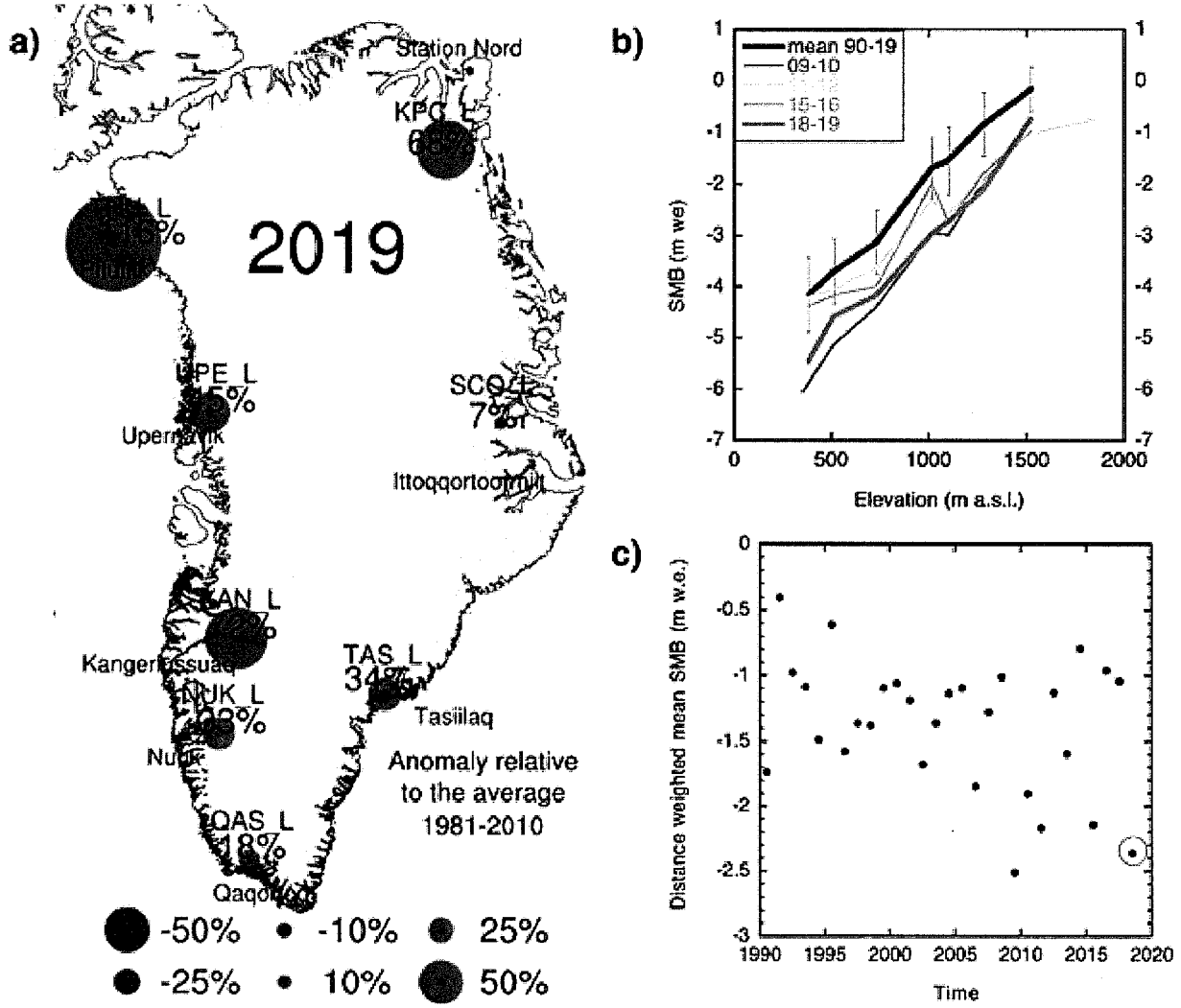

Fig. 2. (a) Ablation anomalies for 2019 ablation area at the lower ("L") PROMICE sites referenced to the period 1981-2010 (van As et al. 2016). (b) The surface mass balance (SMB in meters of water equivalent, m w.e.) as a function of elevation along the K-transect. The error bars show the interannual spread (standard deviation) over the period 1990-2019. (c) Average mass balance along the K-transect based on spatially weighted station data (e.g., weighted using the relative position of the station within the K-transect). Summer 2019 (highlighted by an orange circle) shows the second largest measured ablation rate (after 2009/10).

Consistent with PROMICE data, summer 2019 had high ablation rates along the K-transect (67° N, western ablation zone). Figure 2b shows the K-transect 2018/19 mass balance profile with respect to the average over the entire 29-year measurement period. Comparing 2018/19 to previous years, only the 2009/10 mass balance year had slightly more ablation, particularly near the ice sheet margin. Figure 2c shows the distance-weighted (e.g., scaled by the relative position of each station within the K-transect) average surface mass balance as a function of time along the transect, indicating a relatively large interannual variability. The 2018/19 mass balance gradient in the K-transect area was 3.9 mm w.e./m yr (w.e. = water equivalent), one standard deviation above the average over the last 29 years. The equilibrium line altitude (i.e., the elevation where mass loss is balanced by mass gain) has risen at a rate of around 5 meters per year over the last 29 years.

Total mass balance

The GRACE (2002-17, https://www.nasa.gov/mission_pages/Grace/index.html) and GRACE Follow-On (GRACE-FO, 2018-present, https://gracefo.jpl.nasa.gov/mission/overview/) satellite missions have revolutionized our ability to monitor ice loss by providing estimates of monthly changes in the total mass of the Greenland ice sheet. The GRACE-FO mission was launched on 22 May 2018, creating a gap from October 2017 through May 2018 between the GRACE and GRACE-FO measurements. The GRACE and GRACE-FO time series (Fig. 3) is determined using techniques described in Wahr et al. (1998), Luthcke et al. (2013), and Loomis et al. (2019a,b). The updated total ice mass loss trend for the GRACE period (May 2002-October 2017) is -282 ± 15 Gt yr^{-1}. The trend for the GRACE-FO period (May 2018-May 2019) is -166 ± 46 Gt yr^{-1} (note this period does not include summer of 2019, when losses occur). The larger GRACE-FO trend uncertainty is due to the much shorter data record length. Even with this large uncertainty, we do observe a statistically significant reduction in the rate of mass loss during the first 11 GRACE-FO months, as compared to the full GRACE data span. The updated mass loss trend for the combined GRACE and GRACE-FO periods (May 2002-May 2019) is -267 ± 3 Gt yr^{-1}, which is equal to roughly 0.7 mm yr^{-1} of global average sea level rise. To put this value in context, while GRACE measurements do not exist prior to 2002, the latest study of Greenland mass loss covering 1972-2000 suggests that decadal mass change rates during this time ranged from +47 ± 21 Gt yr^{-1} gain during 1972-80 to 51 ± 17 Gt yr^{-1} mass loss during 1980-90 (Mouginot et al. 2019).

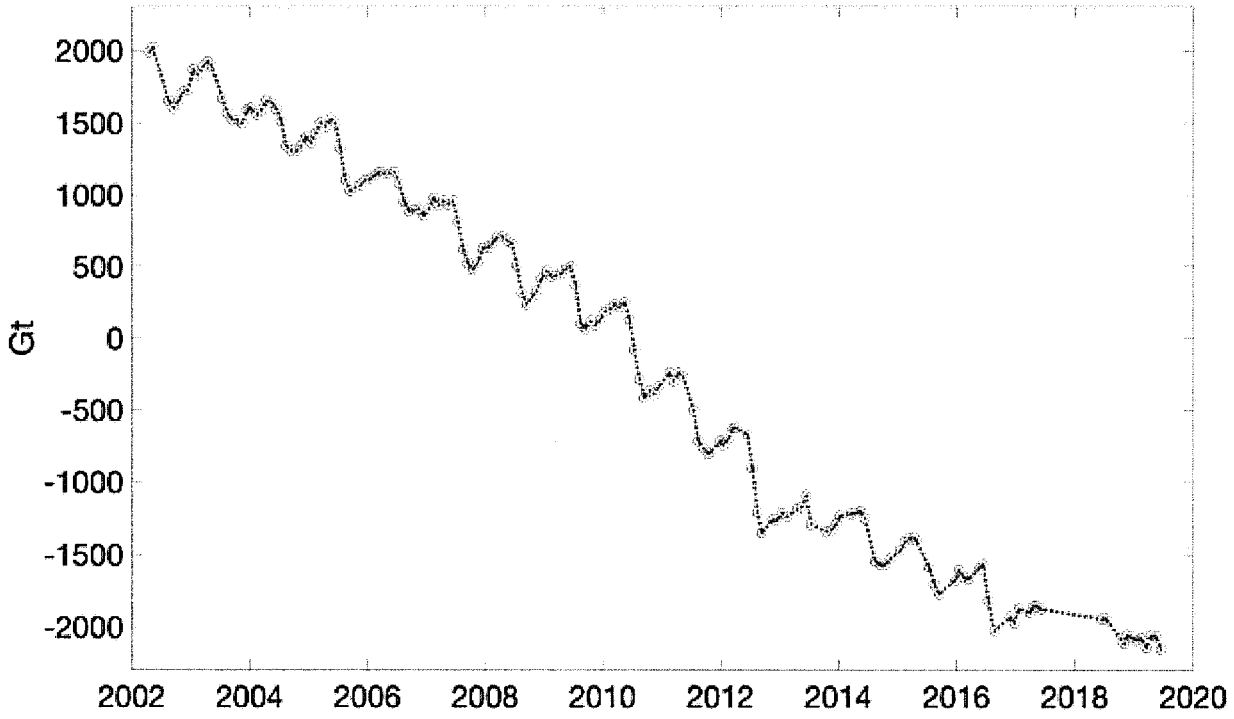

Fig. 3. Total mass change (in Gigatonnes, Gt) of the Greenland ice sheet between April 2002 and April 2019, estimated from GRACE (2002-17) and GRACE-FO (2018/19).

Albedo

The surface albedo can be interpreted as the fraction of incident sunlight reflected by a surface. Summer 2019 (June through August, JJA) surface broadband albedo, estimated from the Moderate Resolution Imaging Spectroradiometer (MODIS; after Box et al. 2017) and averaged over the Greenland ice sheet was 77.7% (Fig. 4a). This is the second lowest value of the 20-year record (2000-19), with a value similar to 2010. The record low for surface broadband albedo was set in 2012 (76.0%). The spatial distribution of albedo anomalies (Fig. 4b) is consistent with the thin snow cover observed along the western ice sheet and the early onset and strong melting in 2019. The 2000-19 trend for summer broadband albedo from MODIS is -1.0% ± 1.0 per year.

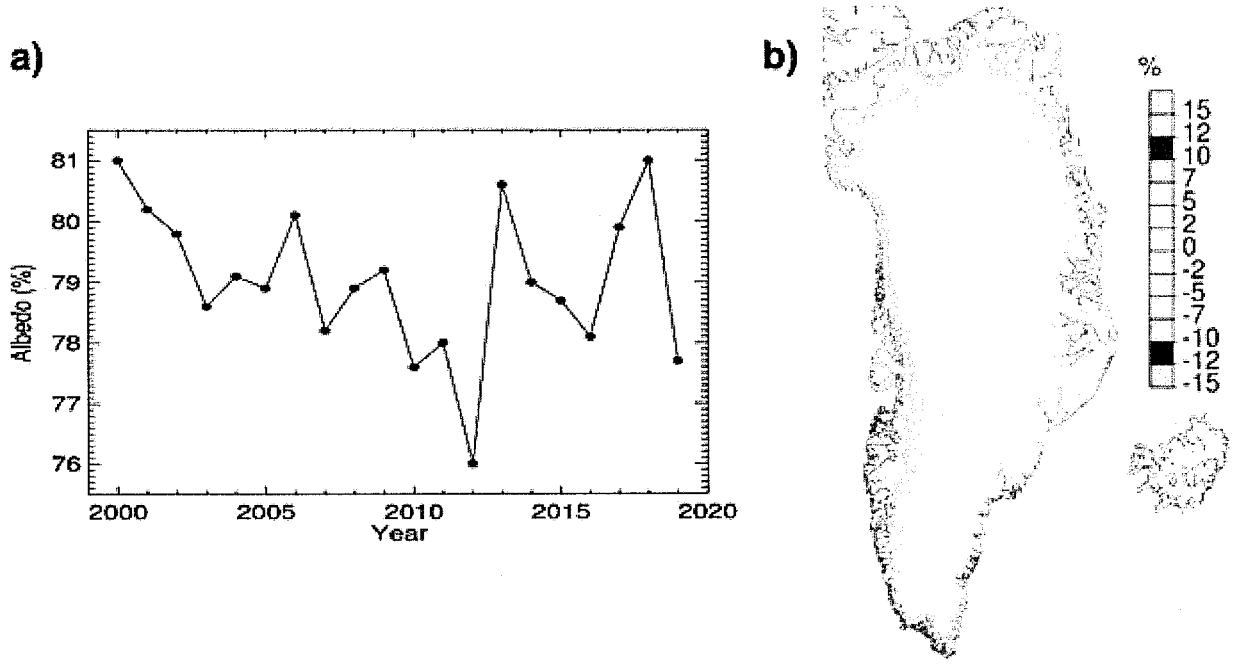

Fig. 4. (a) Time series of summer MODIS albedo (%) and (b) Map of the summer MODIS (JJA) albedo anomaly relative to a 2000-09 reference period.

Surface air temperature

Measurements at 20 Danish Meteorological Institute (DMI) weather stations indicate widespread above or near average air temperatures (1981-2010 baseline) for winter 2018/19 (December through February, DJF), spring 2019 (March through May, MAM) and summer 2019 (JJA). The 2018 autumn season (September through November, SON) had colder or near-average surface temperatures in the western and southern parts of Greenland and warmer or near-average values in the northern and eastern portions. At DMI Summit, in the interior of the ice sheet, autumn 2018 and winter 2018/19 were colder than average, but spring and summer were warmer than average. A record low was set for October 2018 at DMI Summit, including a new record-breaking cold temperature of -55.4°C on 26 October (previous record was -55.2°C).

Consistent with net ablation observations, summer temperatures in 2019 were above the 2008-19 average by more than one standard deviation at all PROMICE measurement sites along the northern, northwestern, and northeastern slopes (stations above 65° N). Out of all January-August 2019 DMI station-months (n=180), 24% of monthly temperatures were more than one standard deviation above average, and only 10% were one standard deviation below average.

Ice discharge and glaciers

Along with losing mass via surface melt, Greenland also loses mass via the direct loss—or calving—of solid ice (i.e., icebergs) into the ocean. Solid ice discharge occurs where marine-terminating glaciers meet the ocean. PROMICE estimates for the Greenland ice sheet, following Mankoff et al. (2019), indicate that as of August 2019 solid ice discharge has averaged 497 ± 50 Gt yr^{-1}. As a comparison, the discharge for the period 1986-2010 was 462 ± 46 Gt yr^{-1}. Figure 5 (a,b) illustrates that the southeast marine-terminating glaciers are responsible for 30-34% of ice-sheet wide discharge (139-167 Gt yr^{-1})

over the 1986 to 2019 period. By comparison, the glaciers in the north, northeast, and southwest regions, which are predominantly land-terminating, together were responsible for ~31% of ice-sheet wide discharge (131-168 Gt yr^{-1}) during this same period. The discharge from most regions has been approximately steady or declining for the past decade. The northwest is the only region exhibiting a persistent increase in discharge from ~89 to 113 Gt yr^{-1} (21% increase) over the 1998-2019 period. The largest contributing region is the southeast, discharging a high of 166 ± 19 Gt in 2005 and dropping to 146 ± 18 Gt in 2016. However, discharge in the southeast region has increased its contributions in the last couple of years, reaching 155 ± 16 Gt during the last year. The discharge in the central west, which is dominated by Sermeq Kujalleq (Jakobshavn Isbræ), has seen an almost 20% decrease in discharge over the past two years. Central west area discharge has remained steady during the past year at 77 Gt.

Marine-terminating glacier front annual area change measurements from Sentinel-2, LANDSAT, and ASTER satellite optical imagery since 1999 (Andersen et al. 2019) indicate that the 2019 net area change of seven major glaciers from across the ice sheet relative to the previous year (2018) was -71.2 ± 1.4 km^2 (i.e., glacier retreat, Fig. 5c). The 2018/19 annual change stands out as the largest area loss since a 2013-18 period of relative stability. Understanding the reasons behind the observed decline in the rate of ice loss in recent years across the Greenland ice sheet is an area of active research (e.g., Mankoff et al. 2019). The individual discharge rates of the seven glaciers used to document the net area change are among the largest observed via satellite.

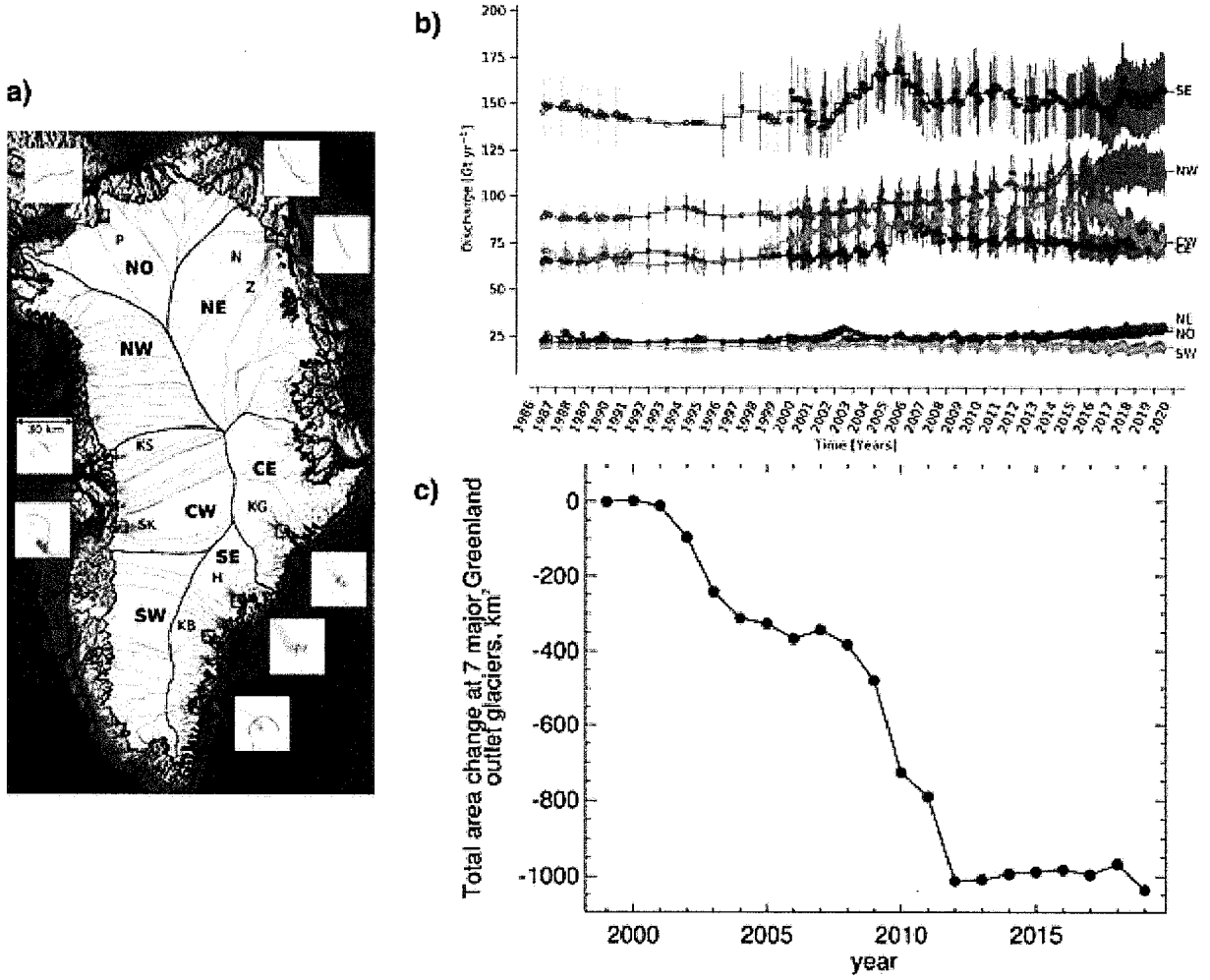

Fig. 5. (a) Overview showing fast-flowing ice (orange, greater than 100 m yr^{-1}) and the flux measurement gates for

eight major discharging glaciers. Gates are shown as black lines in inset images. Each inset is 30 × 30 km with the same color scaling, but different than the main map. Insets pair with the nearest label and box. On the main map, regions as defined by Mouginot et al. (2019) are designated by thicker black lines and large bold labels. Smaller sectors are delineated with thinner gray lines, and the top discharging glaciers are labeled with smaller font. H = Helheim Gletsjer, KB = (Køge Bugt), KG = Kangerlussuaq Gletsjer, KS = Kangilliup Sermia (Rink Isbræ), N = (Nioghalvfjerdsbræ), P = Petermann Gletsjer, SK = Sermeq Kujalleq (Jakobshavn Isbræ), and Z = Zachariae Isstrøm. Basemap terrain (gray), ocean bathymetry (blues), and ice mask (white) are from BedMachine3. (b) Time series of ice discharge from the Greenland ice sheet. Dots represent when observations occurred. Gray bars show ±10% uncertainty range. (c) Cumulative annual net glacier area change (km^2) at seven major marine-terminating glacier outlets of the Greenland ice sheet from 1999/2000 to 2018/19 (after Andersen et al. 2019). Note: The 7 out of 8 glaciers are identical, except Køge bugt, which is not included in the glacier area change product.

Acknowledgments

M. Tedesco would like to acknowledge financial support by the National Science Foundation (PLR-1603331, PLR-1713072), NASA (NNX17AH04G, 80NSSC17K0351) and the Heising-Simons foundation. Financial support for measurements along the K-transect was received from the Dutch Polar Program of NWO. Data from the Programme for Monitoring of the Greenland Ice Sheet (PROMICE) and the Greenland Analogue Project (GAP) were provided by the Geological Survey of Denmark and Greenland (GEUS) at http://www.promice.dk.

References

Andersen, J. K., R. S. Fausto, K. Hansen, J. E. Box, S. B. Andersen, A. P. Ahlstrøm, D. van As, M. Citterio, W. Colgan, N. B. Karlsson, K. K. Kjeldsen, N. J. Korsgaard, S. H. Larsen, K. D. Mankoff, A. Ø. Pedersen, C. L. Shields, A. Solgaard, and B. Vandecrux, 2019: Update of annual calving front lines for 47 marine terminating outlet glaciers in Greenland (1999-2018). *Geol. Surv. Den. Greenl.*, **43**, e2019430202, https://doi.org/10.34194/GEUSB-201943-02-02.

Box, J. E., D. van As, and K. Steffen, 2017: Greenland, Canadian and Icelandic land ice albedo grids (2000-2016). *Geol. Surv. Den. Greenl.*, **38**, 53-56.

Cape, M. R., F. Straneo, N. Beaird, R. M. Bundy, and M. A. Charette, 2019: Nutrient release to oceans from buoyancy-driven upwelling at Greenland tidewater glaciers. *Nat. Geosci.*, **12**, 34–39, https://doi.org/10.1038/s41561-018-0268-4.

Hopwood, M. J., D. Carroll, T. J. Browning, L. Meire, J. Mortensen, S. Krisch, and E. P. Achterberg, 2018: Non-linear response of summertime marine productivity to increased meltwater discharge around Greenland. *Nat. Commun.*, **9**, 3256, https://doi.org/10.1038/s41467-018-05488-8.

Loomis, B. D., S. B. Luthcke, and T. J. Sabaka, 2019a: Regularization and error characterization of GRACE mascons. *J. Geodesy*, **93**(9), 1381-1398, https://doi.org/10.1007/s00190-019-01252-y.

Loomis, B. D., K. E. Rachlin, and S. B. Luthcke, 2019b: Improved Earth oblateness rate reveals increased ice sheet losses and mass-driven sea level rise. *Geophys. Res. Lett.*, **46**, 6910- 6917, https://doi.org/10.1029/2019GL082929.

Luo, H., R. M. Castelao, A. K. Rennermalm, M. Tedesco, A. Bracco, P. L. Yager, and T. L. Mote, 2016: Oceanic transport of surface meltwater from the southern Greenland ice sheet. *Nat. Geosci.*, **9**(7), 528-532, https://doi.org/10.1038/ngeo2708.

Luthcke, S. B., T. J. Sabaka, B. D. Loomis, A. A. Arendt, J. J. McCarthy, and J. Camp, 2013: Antarctica, Greenland and Gulf of Alaska land ice evolution from an iterated GRACE global mascon solution. *J. Glaciol.*, **59**(216), 613-631, https://doi.org/10.3189/2013JoG12J147.

Mankoff, K. D., W. Colgan, A. Solgaard, N. B. Karlsson, A. P. Ahlstrøm, D. van As, J. E. Box, S. A. Khan, K. K. Kjeldsen, J. Mouginot, and R. S. Fausto, 2019: Greenland Ice Sheet solid ice discharge from 1986 through 2017. *Earth Syst. Sci. Data*, **11**, 769-786, https://doi.org/10.5194/essd-11-769-2019. Data product updated through 2019-08-16 at http://promice.org.

Morlighem, M., and Coauthors, 2017: BedMachine v3: Complete bed topography and ocean bathymetry mapping of Greenland from multibeam echo sounding combined with mass conservation. *Geophys. Res. Lett.*, **44**(21), 11051-11061, https://doi.org/10.1002/2017GL074954.

Mote, T., 2007: Greenland surface melt trends 1973-2007: Evidence of a large increase in 2007. *Geophys. Res. Lett.*, **34**, L22507.

Mouginot, J., E. Rignot, A. A. Bjørk, M. van den Broeke, R. Millan, M. Morlighem, B. Noël, B. Scheuchl, and M. Wood, 2019: Forty-six years of Greenland Ice Sheet mass balance from 1972 to 2018. *P. Natl. Acad. Sci. USA*, **116**(19), 9239-9244, https://doi.org/10.1073/pnas.1904242116.

Overeem, I., B. D. Hudson, J. P. M. Syvitski, A. B. Mikkelsen, B. Hasholt, M. R. Van Den Broeke, B. P. Y. Noël, and M. Morlighem, 2017: Substantial export of suspended sediment to the global oceans from glacial erosion in Greenland. *Nat. Geosci.*, **10**(11), 859-863, https://doi.org/10.1038/ngeo3046.

Ryan, J. C., L. C. Smith, D. van As, S. W. Cooley, M. G. Cooper, L. H. Pitcher, and A. Hubbard, 2019: Greenland Ice Sheet surface melt amplified by snowline migration and bare ice exposure. *Sci Adv.*, **5**(3), eaav3738, https://doi.org/10.1126/sciadv.aav3738.

Tedesco, M., X. Fettweis, T. Mote, J. Wahr, P. Alexander, J. Box, and B. Wouters, 2013: Evidence and analysis of 2012 Greenland records from spaceborne observations, a regional climate model and reanalysis data. *Cryosphere*, **7**, 615-630.

van As, D., R. S. Fausto, J. Cappelen, R. S. van de Wal, R. J. Braithwaite, and H. Machguth, 2016: Placing Greenland ice sheet ablation measurements in a multi-decadal context. *Geol. Surv. Den. Greenl.*, **35**, 71-74.

Wahr, J., M. Molenaar, and F. Bryan, 1998: Time variability of the Earth's gravity field: Hydrological and oceanic effects and their possible detection using GRACE. *J. Geophys. Res.*, **103**(B12), 30205- 30229, https://doi.org/10.1029/98JB02844.

November 26, 2019

Sea Ice

D. Perovich[1], W. Meier[2], M. Tschudi[3], S. Farrell[4], S. Hendricks[5], S. Gerland[6], L. Kaleschke[5], R. Ricker[5], X. Tian-Kunze[5], M. Webster[7], and K. Wood[8,9]

[1]Thayer School of Engineering, Dartmouth College, Hanover, NH, USA
[2]National Snow and Ice Data Center, Cooperative Institute for Research in Environment Sciences at the University of Colorado, Boulder, CO, USA
[3]Aerospace Engineering Sciences, University of Colorado, Boulder, CO, USA
[4]NOAA Earth System Science Interdisciplinary Center, University of Maryland, College Park, MD, USA
[5]Alfred Wegener Institute, Helmholtz Centre for Polar and Marine Research, Bremerhaven, Germany
[6]Norwegian Polar Institute, Fram Centre, Tromsø, Norway
[7]Geophysical Institute, University of Alaska Fairbanks, Fairbanks, AK, USA
[8]Joint Institute for the Study of the Atmosphere and Ocean, University of Washington, Seattle, WA, USA
[9]Pacific Marine Environmental Laboratory, NOAA, Seattle, WA, USA

Highlights

- The Arctic sea ice cover continues the declining trends in the summer minimum and winter maximum extents. In 2019, the end of summer extent was tied with 2007 and 2016 as the 2nd lowest and the end of winter extent was the 7th lowest in the satellite record (1979-2019).
- As in the previous year (2017/18), the Bering Sea had little ice during most of the 2018/19 winter and 2019 spring seasons.
- The Chukchi Sea experienced very early melt onset and rapid ice loss in spring 2019, and by the end of summer 2019 reached one of the lowest ice extents in the satellite record for the region.
- Despite low extents, sea ice volume was higher over much of the central Arctic compared to the average since Cryosat-2 measurements began in 2011.

Sea ice extent

Sea ice is an important element of the Arctic system because it (1) acts as a barrier between the underlying ocean and the atmosphere, (2) limits the amount of absorbed solar energy during the summer due to its high albedo, (3) provides a habitat for biological activity, (4) limits human access to the Arctic Ocean, and (5) serves as a platform for Indigenous community hunting and travel. Arctic sea ice cover varies substantially during the year, with end-of-winter ice cover generally being two to three times as large as at the end of summer. Sea ice extent has been continuously monitored by passive microwave instruments on satellite platforms since 1979, providing a consistent long-term perspective on changing coverage over the last four decades.

The sea ice extent estimates used here are based on products from the National Snow and Ice Data Center (NSIDC) Sea Ice Index (Fetterer et al. 2017), derived from NASA gridded sea ice concentration fields (Cavalieri et al. 1996; Maslanik and Stroeve 1999). Other similar products exist and, while absolute numbers vary, they all show general consistency in trends and variability.

The months of March and September are of particular interest in sea ice time series because they represent typical Arctic sea ice maximum and minimum extents, respectively. Figure 1 shows monthly

average ice extents in March and September 2019. The sea ice cover reached a winter maximum extent of 14.78 million km^2 on 13 March 2019. This was tied with 2007 as the 7th lowest maximum extent in the 41-year satellite record and was 5.9% below the 1981-2010 average. The previous four years (2015-18) are the four lowest years in the record. However, these losses are not evenly distributed, with some marginal seas near normal, such as the Sea of Okhotsk for example, while the Bering Sea was 70-80% lower than normal.

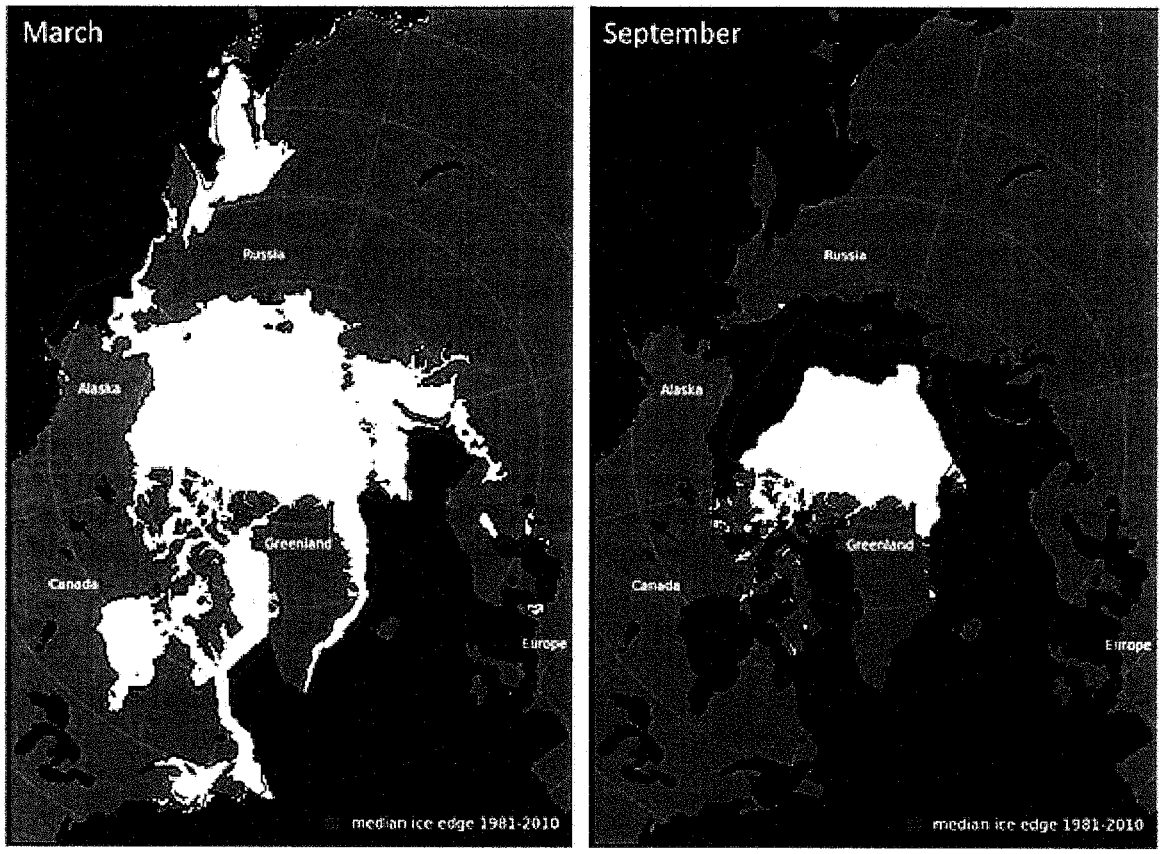

Fig. 1. Average monthly sea ice extent in March 2019 (left) and September 2019 (right) illustrate the respective winter maximum and summer minimum extents. The magenta line indicates the median ice extents in March and September, respectively, during the period 1981-2010. Maps are from NSIDC at http://nsidc.org/data/seaice_index/ (Fetterer et al. 2017).

The sea ice cover reached a minimum summer extent of 4.15 million km^2 on 18 September 2019. This was tied with 2007 and 2016 as the 2nd lowest extent of the satellite record and was 2.04 million km^2 (33%) less than the 1981-2010 average minimum ice extent. The September ice extent has not returned to pre-2007 levels; the 13 lowest extents in the satellite record having all occurred in the last 13 years (2007-19).

Observations of Arctic sea ice extent have shown decreasing trends in all months and virtually all regions (Meier et al. 2014). The September monthly average trend for the entire Arctic Ocean is now -12.9 ± 2.2% per decade relative to the 1981-2010 average (Fig. 2), statistically significant at the 99% confidence level. Trends are smaller during March (-2.7% per decade), but the decrease is statistically significant. In

2019, 10.63 million km^2 of ice was lost between the March maximum and September minimum extent, the fourth greatest difference between maximum and minimum extents in the satellite record.

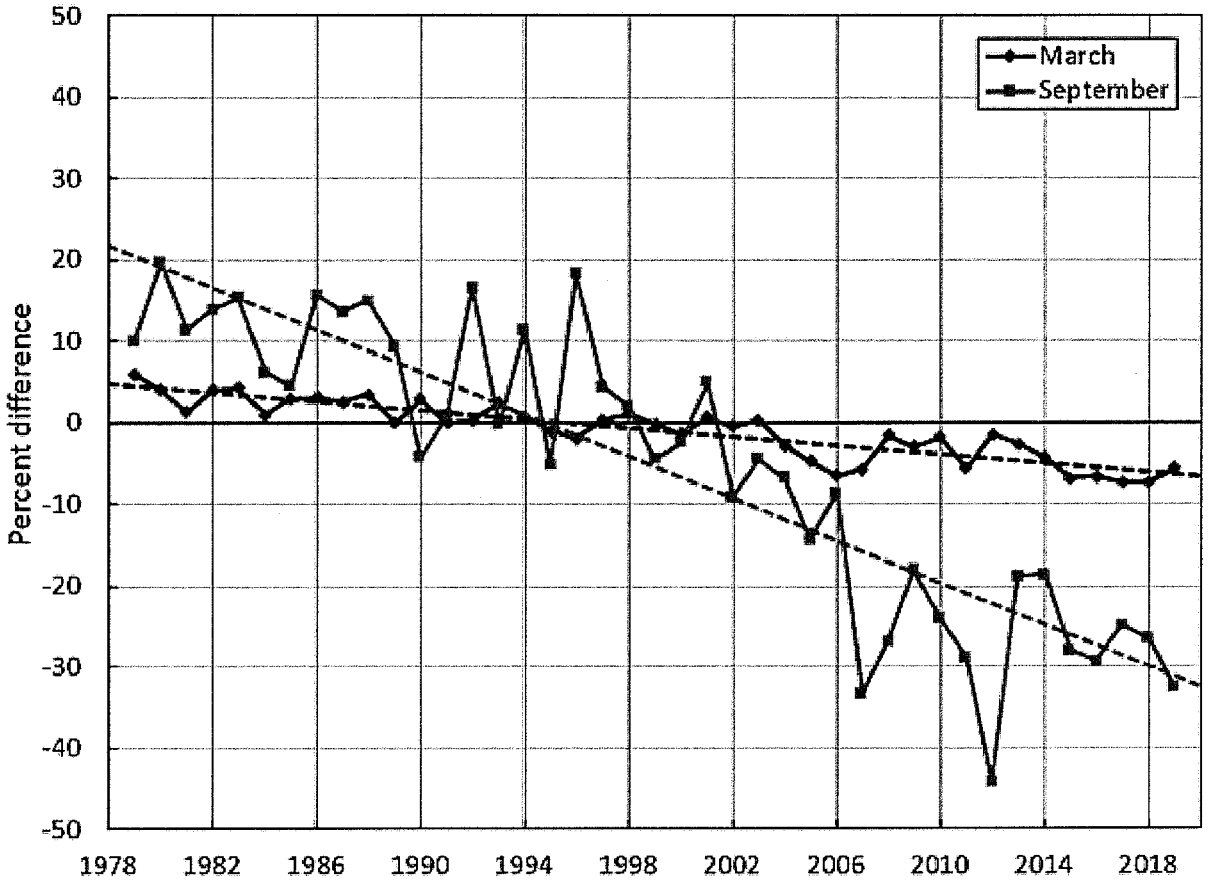

Fig. 2. Time series of ice extent anomalies in March (the month of maximum ice extent, in black) and September (the month of minimum ice extent, in red). The anomaly value for each year is the difference (in %) in ice extent relative to the mean values for the period 1981-2010. The black and red lines are least-squares linear regression lines. The slopes of these lines indicate ice losses of -2.7 ± 0.4% and -12.9 ± 2.2% per decade in March and September, respectively. Both trends are significant at the 99% confidence level. Data are from the NSIDC Sea Ice Index (Fetterer et al. 2017).

The 2019 melt season started fairly slowly relative to recent years, with ice extent loss rates near normal despite the lack of winter/spring ice in the Bering Sea (see essay *Recent Warming in the Bering Sea* for further information about sea ice conditions in the Bering Sea). However, in late June and July the loss rate accelerated considerably such that by mid-July ice extent was below that of mid-July 2012, the year the current record low minimum extent occurred. Starting in mid-August 2019, the loss rate slowed considerably through early September, falling well off the 2012 pace. September had two brief periods of further ice loss in the first half of the month with essentially no change or increasing extent during the rest of the month.

Age of the sea ice

The age of sea ice is also a key descriptor of the state of the sea ice cover. It serves as an indicator for ice physical properties, including snow cover, surface roughness, optical properties, melt pond coverage,

salinity, and thickness (Tschudi et al. 2016). Older ice tends to be thicker and thus more resilient to changes in atmospheric and oceanic forcing compared to younger ice. The age of the ice has been determined using satellite observations and drifting buoy records to track ice parcels over several years (Tschudi et al. 2010; Maslanik et al. 2011). This method has been used to provide a record of the age of the ice since the early 1980s (Tschudi et al. 2019 a,b).

The oldest ice (>4 years old), which once dominated within the Arctic Ocean, now makes up just a small fraction of the Arctic Ocean ice pack in March, when the sea ice cover is at its maximum extent (Fig. 3). In 1985, 33% of the ice pack was very old ice (>4 years), but by March 2019 old ice only constituted 1.2% of the ice pack within the Arctic Ocean. The total extent of the oldest ice declined from 2.52 million km^2 in March 1985 to 0.09 million km^2 in March 2019. Note that previous Arctic Report Cards calculated age percentages based on all ice-covered regions. This year the percentages are relative to ice in the Arctic Ocean region (Fig. 3, bottom inset); areas outside of this region have little or no older ice and thus do not show any change over time.

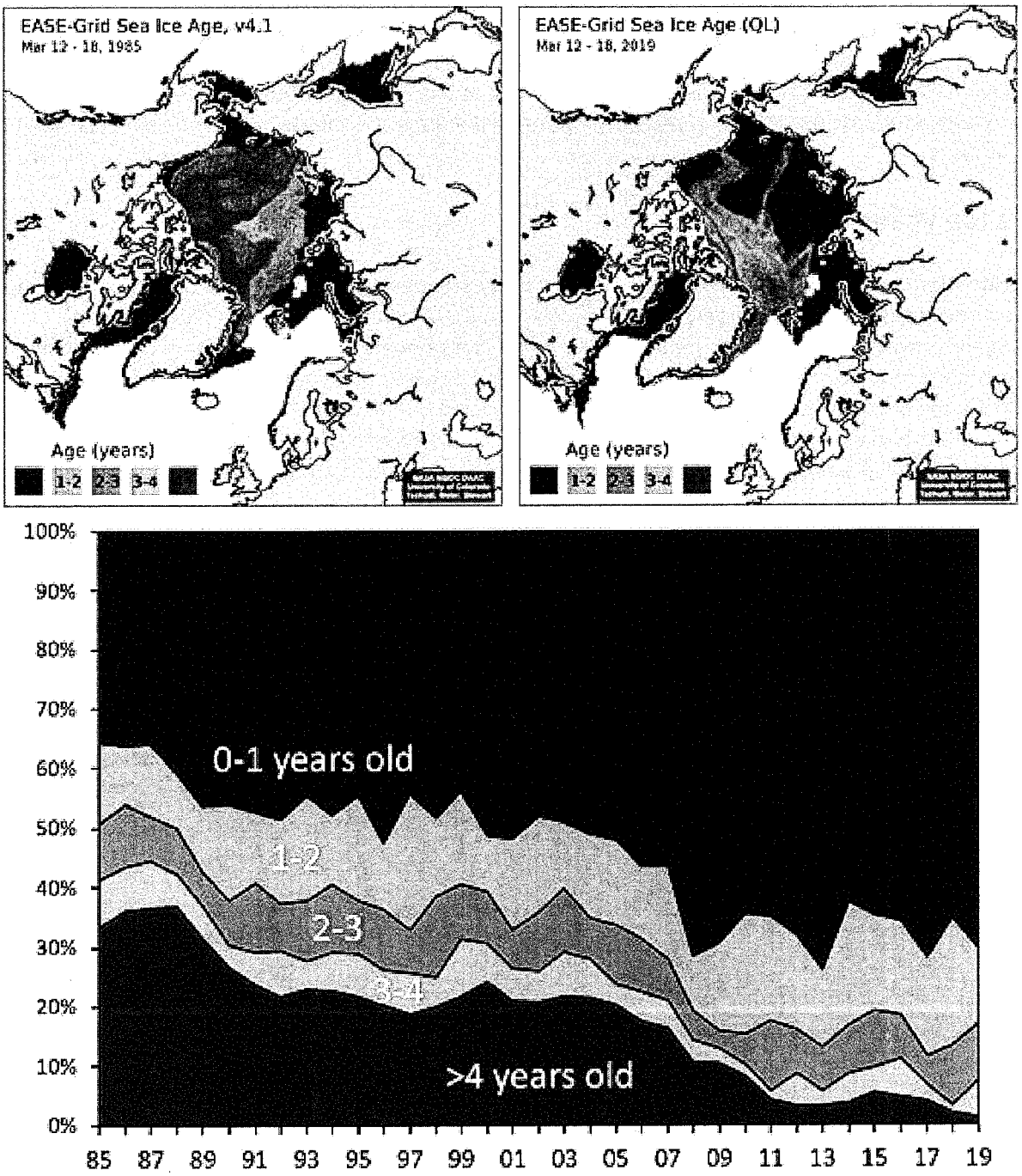

Fig. 3. Late winter sea ice age coverage map for the week of 12-18 March 1985 (upper left) and 12-18 March 2019 (upper right). Bottom: Sea ice age percentage within the Arctic Ocean region (purple shaded region in inset image) for the week of 12-18 March 1985-2019. Data are from NSIDC (Tschudi et al. 2019a,b).

First-year ice now dominates the sea ice cover, comprising ~70% of the March 2019 ice pack, compared to approximately 35-50% in the 1980s. Given that older ice tends to be thicker, the sea ice cover has transformed from a strong, thick ice mass in the 1980s to a younger, more fragile, and thinner ice mass in recent years. First-year ice is therefore more vulnerable to melting out in summer, thereby increasing the likelihood of lower minimum ice extents.

The distribution of ice age in March 2019 was generally similar to that in March of the previous year. The largest changes were a decrease in second-year ice (1-2 years old) coverage, from 21.4% in March 2018 to 12.8% in March 2019, and an increase in 3-4 year old ice from 1.3% to 6.3%. The increase in the 3-4 year old ice results as ice survives the summer melt season and ages. This could replenish the >4 year old ice category, but in recent years, ice has tended to be lost either by melt or be advection out of the Arctic.

Sea ice volume

Satellite remote sensing and airborne survey programs extended the observational data record of Arctic sea ice thickness (SIT) and volume in 2019. The ESA CryoSat-2 radar altimeter and SMOS L-Band radiometer missions have each completed their ninth year of operation. The data from both satellites have been combined in a multi-sensor SIT analysis based on an optimal interpolation scheme (Ricker et al. 2017) and are available on a weekly basis; the analyses cover all sea ice in the Northern Hemisphere during autumn to early spring (mid-October to mid-April). Combined with sea ice concentration, the CryoSat-2/SMOS product evaluates change and variability of sea ice volume (SIV) over the past nine winter seasons.

The weekly SIV time series from November 2010 to April 2019 is shown in the upper panel of Fig. 4. The Northern Hemisphere gained 12,524 km^3 of sea ice between October 2018 and April 2019. The gain is essentially the same as the mean volume gain of 12,559 km^3 in the CryoSat-2/SMOS data record. The 2018/19 SIV was higher than average for the entire season, indicated by a positive SIV anomaly (lower panel in Fig. 4).

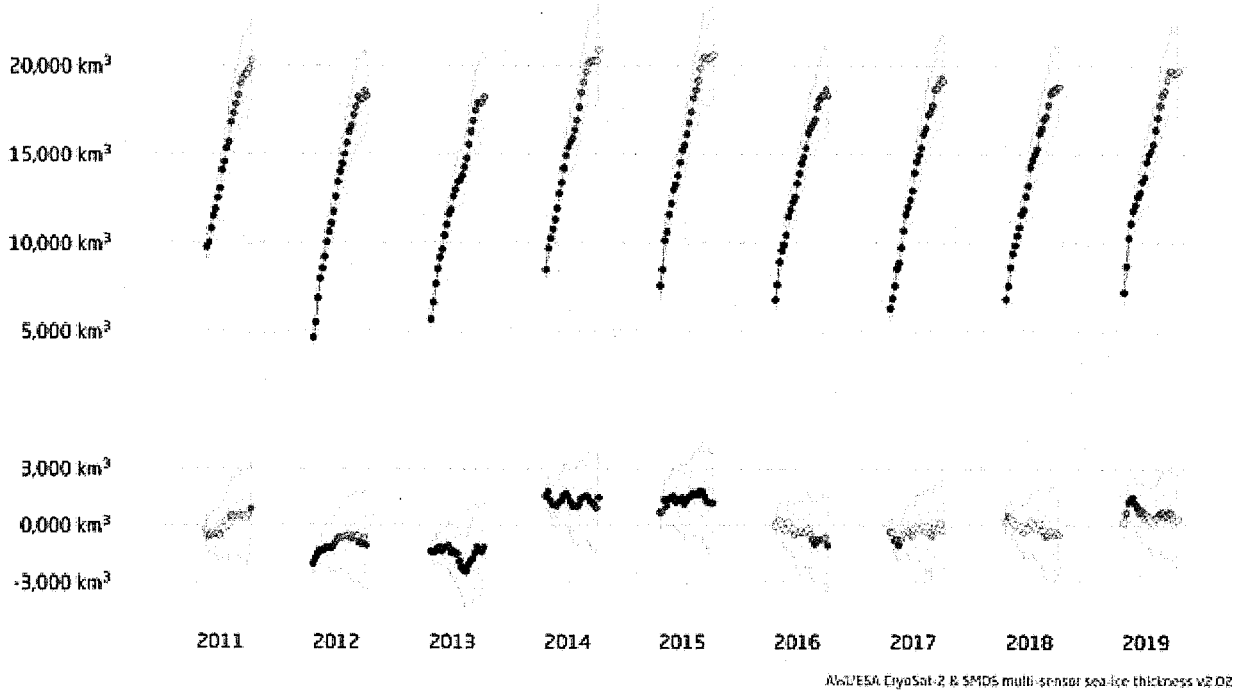

Fig. 4. Time series of sea ice volume (SIV) in the Northern Hemisphere for winter (mid-October to mid-April) from multi-sensor analysis of CryoSat-2 and SMOS SIT data (upper panel). Sea ice volume anomaly with respect to mean winter SIV evolution in the CryoSat-2/SMOS data period (November 2010-April 2019) (lower panel).(Data source: AWI/ESA CryoSat-2 & SMOS multi-sensor sea ice thickness v2.02, ftp://ftp.awi.de/sea_ice/product/cryosat2_smos/, based on Ricker et al. 2017).

The above-average SIV in the Northern Hemisphere was driven by above-average SIT in the central Arctic Basin, rather than by increased sea ice extent. Figure 5 shows the regional distribution of SIT in mid-April 2019 and its difference from the mean of the previous years. A significant portion of the central Arctic Basin shows a positive thickness anomaly, with a mean SIT of 2.04 m that is 0.09 (+4.6%) above the average SIT of the eight previous winters. Above-average SIT in the central Arctic Basin mitigated the impact of sea ice area loss on SIV in the short observation period of the past 9 winters seasons, notwithstanding the long-term loss of SIV in the Northern Hemisphere (Kwok 2018). The above-average thickness in the central Arctic Basin, however, adds to the resilience of sea ice with respect to summer melt.

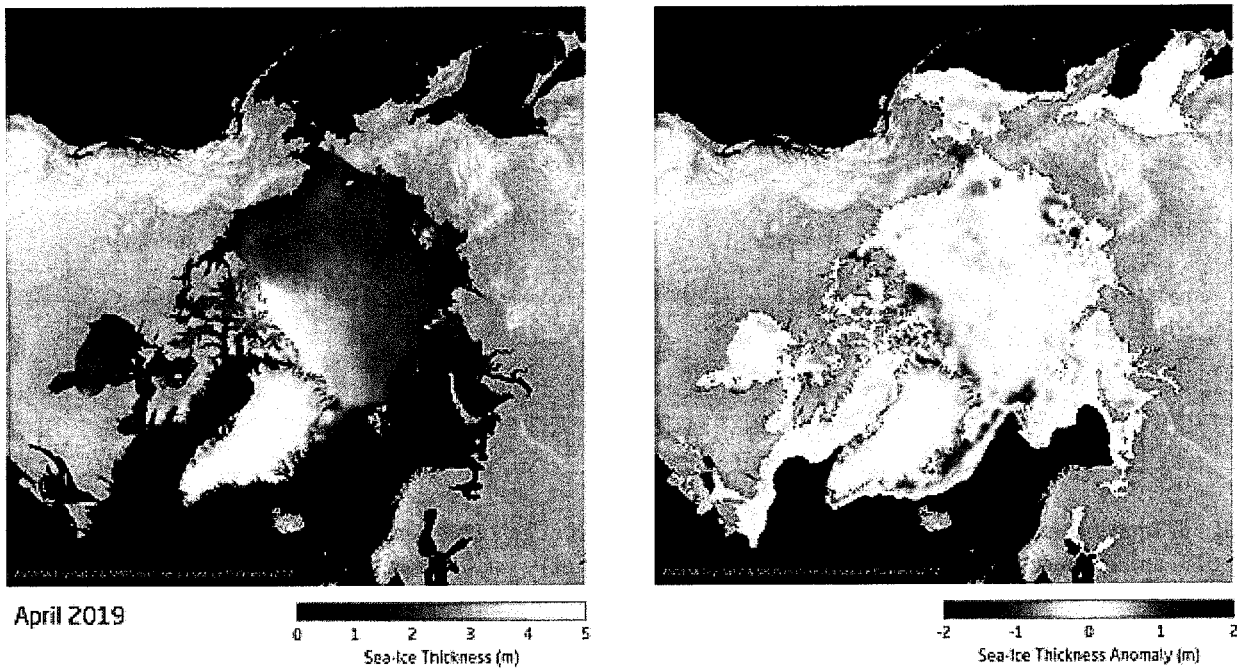

Fig. 5. Sea ice thickness (SIT) in mid-April 2019 from multi-sensor analysis of CryoSat-2 and SMOS SIT data (left). Sea ice thickness anomaly in mid-April 2019 with respect to the 2011-18 mid-April average from CryoSat-2/SMOS data (right). The anomaly in regions without sea ice coverage in April 2019 has been set to the negative mean thickness of values from 2011-18. (Data source: AWI/ESA CryoSat-2 & SMOS multi-sensor sea ice thickness v2.02, ftp://ftp.awi.de/sea_ice/product/cryosat2_smos/, based on Ricker et al. 2017).

Chukchi Sea

The Chukchi Sea has experienced large changes in sea ice coverage. The September 2018 Arctic sea ice minimum extent was characterized by profound sea ice loss in the Chukchi Sea (Fig. 6). The dearth of sea ice continued into the autumn season, accompanied by anomalously warm air temperatures of 3-8°C above the 1981-2010 average. Progressing into October and November 2018, a high-pressure system over the Bering Sea expanded into the Chukchi and Beaufort Seas, sustaining warm conditions and, as a consequence, slowed the autumn advance of the sea ice cover. Sea ice extent in the Chukchi Sea remained well below average until the end of December 2018, when it reached near-average coverage (Fig. 6). Throughout the winter and spring, air temperatures continued to be 1-4°C warmer than the 1981-2010 average, which likely contributed to the low sea ice concentrations.

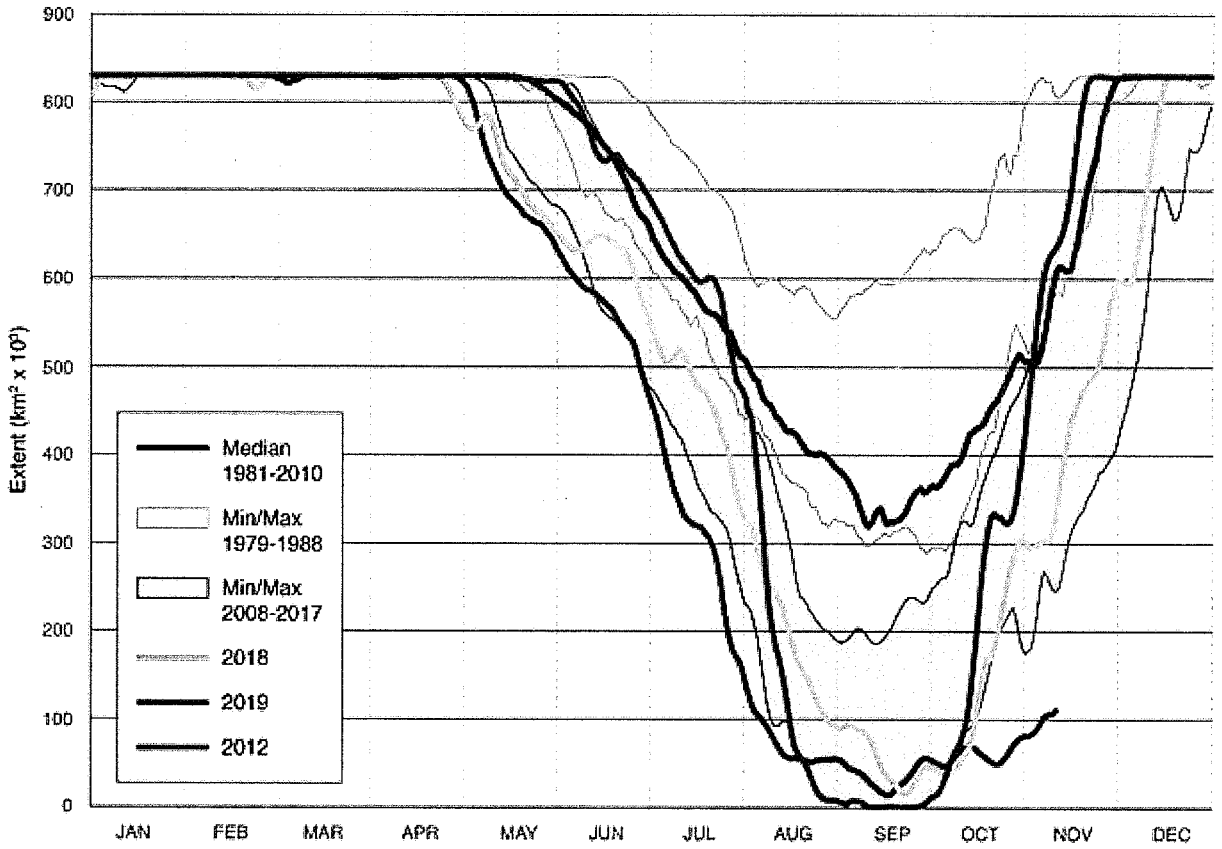

Fig. 6. Time series of 2019 sea ice extent in the Chukchi Sea through 12 November compared to the previous year (2018) and the record minimum year (2012), derived from satellite passive-microwave data. The grey shaded areas show the maximum range of variability of sea ice extent for the first decade of the satellite era (1979-88) and the recent decade (2008-17), illustrating the long-term change in sea ice extent over the entire period since 1979. Data are from the NSIDC Sea Ice Index, Version 3 (Fetterer et al. 2017).

In spring 2019, melt onset across the Chukchi Sea occurred 20-35 days earlier than the 1981-2010 average. Sea ice began a rapid and accelerating retreat from the south in early May, leading to a record low sea ice extent that lasted until early August, with negative sea ice concentration anomalies of 50%. A combination of anomalously warm air temperatures (1-5°C above the 1981-2010 average) and southerly winds promoted this precipitous loss ice. As the sea ice retreated northward, exposed open water areas warmed, leading to anomalous sea surface temperatures greater than 5°C above average. By mid-September, sea ice coverage in the Chukchi Sea remained far below the 1981-2010 average. This reduction in sea ice coverage has continued far into the freeze-up period, with ice extent only one-third of the previous record minimum. Consistent with the long-term record of Arctic-wide ice loss, most characteristics of the sea ice in the Chukchi Sea, including the length of the melt season and area of open water subject to rapid warming in summer, are now entirely different compared to the first decade (1979-88) of the satellite record.

References

Cavalieri, D. J., C. L. Parkinson, P. Gloersen, and H. J. Zwally, 1996, updated yearly: Sea Ice Concentrations from Nimbus-7 SMMR and DMSP SSM/I-SSMIS Passive Microwave Data, Version 1. NASA National Snow and Ice Data Center Distributed Active Archive Center, Boulder, CO, USA, https://doi.org/10.5067/8GQ8LZQVL0VL.

Fetterer, F., K. Knowles, W. N. Meier, M. Savoie, and A. K. Windnagel, 2017 (updated daily): Sea Ice Index, Version 3: Regional Daily Data. National Snow and Ice Data Center (NSIDC), Boulder, CO, USA, https://doi.org/10.7265/N5K072F8.

Kwok, R., 2018: Arctic sea ice thickness, volume, and multiyear ice coverage: Losses and coupled variability (1958 - 2018). *Environ. Res. Lett.*, **13** (2018), 105005, https://doi.org/10.1088/1748-9326/aae3ec.

Maslanik, J., and J. Stroeve, 1999: Near-Real-Time DMSP SSMIS Daily Polar Gridded Sea Ice Concentrations, Version 1. NASA National Snow and Ice Data Center Distributed Active Archive Center, Boulder, CO, USA, https://doi.org/10.5067/U8C09DWVX9LM.

Maslanik, J., J. Stroeve, C. Fowler, and W. Emery, 2011: Distribution and trends in Arctic sea ice age through spring 2011. *Geophys. Res. Lett.*, **38**(13), L13502, https://doi.org/10.1029/2011GL047735.

Meier, W. N., G. Hovelsrud, B. van Oort, J. Key, K. Kovacs, C. Michel, M. Granskog, S. Gerland, D. Perovich, A. P. Makshtas, and J. Reist, 2014: Arctic sea ice in transformation: A review of recent observed changes and impacts on biology and human activity. *Rev. Geophys.*, **52**(3), 185-217, https://doi.org/10.1002/2013RG000431.

NSIDC, March 2019: Arctic Sea Ice News and Analysis. Arctic sea ice maximum ties for seventh lowest in satellite record. http://nsidc.org/arcticseaicenews/2019/03/.

Ricker, R., S. Hendricks, L. Kaleschke, X. Tian-Kunze, J. King, and C. Haas, 2017: A weekly Arctic sea-ice thickness data record from merged CryoSat-2 and SMOS satellite data. *Cryosphere*, **11**, 1607-1623, https://doi.org/10.5194/tc-11-1607-2017.

Tschudi, M., W. N. Meier, J. S. Stewart, C. Fowler, and J. Maslanik, 2019a: EASE-Grid Sea Ice Age, Version 4. Boulder, Colorado USA. NASA National Snow and Ice Data Center Distributed Active Archive Center. https://doi.org/10.5067/UTAV7490FEPB.

Tschudi, M., W. N. Meier, and J. S. Stewart, 2019b: Quicklook Arctic Weekly EASE-Grid Sea Ice Age, Version 1. Boulder, Colorado USA. NASA National Snow and Ice Data Center Distributed Active Archive Center. https://doi.org/10.5067/2XXGZY3DUGNQ.

Tschudi, M. A., C. Fowler, J. A. Maslanik, and J. A. Stroeve, 2010: Tracking the movement and changing surface characteristics of Arctic sea ice. *IEEE J. Sel. Top. Appl. Earth Observ. Remote Sens.*, **3**(4), 536-540, https://doi.org/10.1109/JSTARS.2010.2048305.

Tschudi, M. A., J. C. Stroeve, and J. S. Stewart, 2016: Relating the age of Arctic sea ice to its thickness, as measured during NASA's ICESat and IceBridge Campaigns. *Remote Sens.*, **8**(6), 457, https://doi.org/10.3390/rs8060457.

November 22, 2019

Sea Surface Temperature

M. -L. Timmermans[1] and C. Ladd[2]

[1]Yale University, New Haven, CT, USA
[2]Pacific Marine Environmental Laboratory, NOAA, Seattle, WA, USA

Highlights

- August mean sea surface temperatures (SSTs) in 2019 were ~1-7°C warmer than the 1982-2010 August mean in the Beaufort, Chukchi, and Laptev Seas and Baffin Bay, and ~0.5-2°C cooler in the Barents Sea region.
- August mean SSTs show statistically significant warming trends for 1982-2019 in most regions of the Arctic Ocean that are ice-free in August.
- Northern Barents Sea August mean SSTs show statistically significant cooling trends for 1982-2019.

Summer sea surface temperatures (SST) in the Arctic Ocean are driven mainly by the amount of incoming solar radiation absorbed by the sea surface. Solar warming of the Arctic surface ocean is influenced by the distribution of sea ice (with greater warming occurring in ice-free regions), cloud cover, ocean optical properties, and upper-ocean stratification. In the Barents and Chukchi Seas, there is an additional source of ocean heat contributed by the advection of warm water from the North Atlantic and North Pacific Oceans, respectively. Arctic SSTs are an essential indicator of the role of the ice-albedo feedback mechanism in any given summer melt season. As the area of sea-ice cover decreases, more incoming solar radiation is absorbed by the ocean and, in turn, the warmer ocean melts more sea ice. In addition, marine ecosystems are influenced by SST, which affects the timing and development of primary and secondary production cycles as well as available habitat for individual species (see essay *Arctic Ocean Primary Productivity*).

SST data presented here are from the NOAA Optimum Interpolation (OI) SST Version 2 product (OISSTv2), which is a blend of in situ and satellite measurements from December 1981 to present (Reynolds et al. 2002, 2007). Compared to purely in situ temperature measurements, the OISSTv2 product has explained about 80% of the variance, with an overall tendency to underestimate SST by -0.02°C, i.e., a cold bias (Stroh et al. 2015). The OISSTv2 product uses a linear relationship with sea-ice concentration to infer SST, with SST constrained to -1.8°C (the freezing point of seawater with a salinity of 33 PSU at the sea surface) where ice cover is 100% (Reynolds et al. 2007). Variations in freezing temperature as a result of variations in sea-surface salinity (not accounted for in the algorithm) imply that SSTs under sea ice can be too cool by up to 0.2°C, with the highest errors in the fresher surface waters of the Canada Basin (see Timmermans and Proshutinsky 2015). August mean SSTs provide the most appropriate representation of Arctic Ocean summer SSTs because they are not affected by the cooling and subsequent sea-ice growth that typically takes place in the latter half of September. The period 1982-2010 is taken as a climatological reference mean.

August 2019 mean SSTs ranged from 8 to 9°C in the southern Chukchi and Barents Seas to approximately 1°C in the interior Arctic Ocean near the mean sea-ice edge for that month (Fig. 1). August 2019 mean SSTs were around 1-7°C warmer than the 1982-2010 August mean in the Beaufort, Chukchi, and Laptev Seas and Baffin Bay (Fig. 2a). The anomalously warm SSTs in the vicinity of the

August 2019 mean sea-ice edge are linked to anomalously low sea-ice extent, which allowed for direct solar heating of the exposed surface waters (Fig. 2a). Conversely, the entire Barents Sea region was marked by anomalously cool August 2019 SSTs around 0.5-2°C cooler than the 1982-2010 mean. The interplay between sea-ice cover, solar absorption, and lateral ocean heat transport that results in cooler August SSTs in the Barents Sea region requires further study. Relative to August 2018, August 2019 exhibited SSTs up to 4°C warmer in the Beaufort Sea and Baffin Bay, while SSTs were a few degrees cooler in the Barents Sea in August 2019 compared to August 2018 (Fig. 2b).

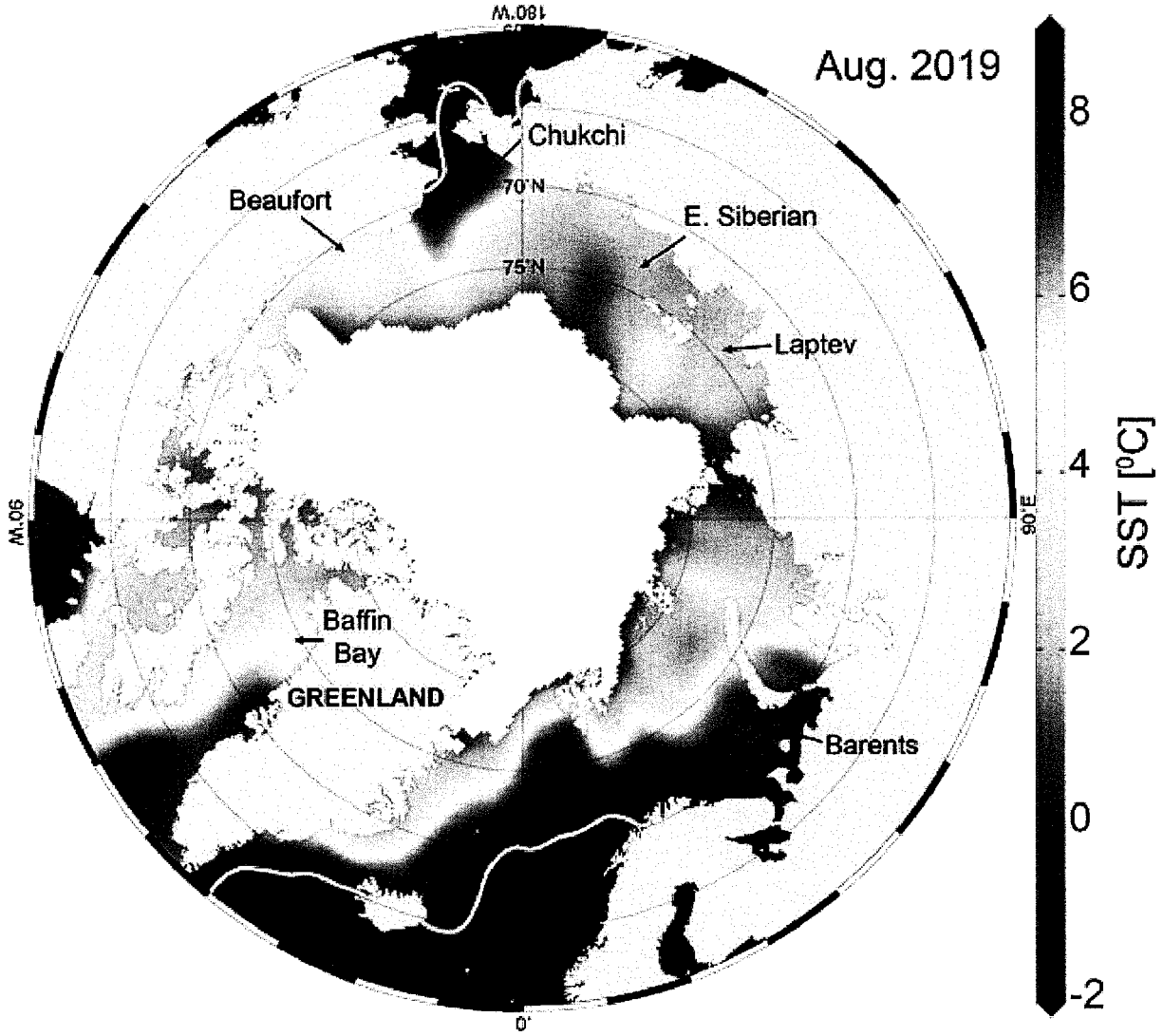

Fig. 1. Mean SST (°C) in August 2019. White shading is the August 2019 mean sea-ice extent, and gray contours indicate the 10°C SST isotherm. (Sources: SST data are from the NOAA OISSTv2; sea-ice extent data are from NSIDC Sea Ice Index, Version 3, Fetterer et al. 2017.)

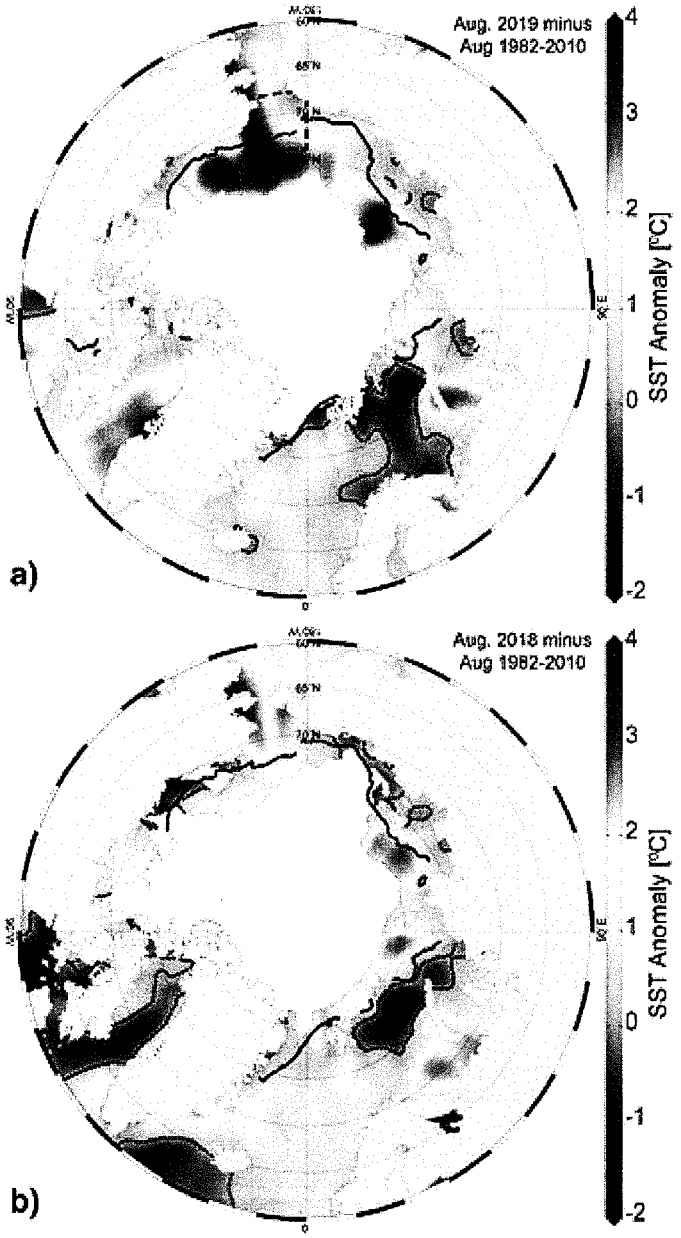

Fig. 2. SST anomalies (°C) in (a) August 2019 and (b) August 2018 relative to the August 1982-2010 mean (the dotted black contour indicates zero anomaly). The black line indicates the median ice edge for August 1982-2010 and white shading indicates the August 2019 (a) and August 2018 (b) mean sea-ice extent. The two regions marked by black dashed lines in (a) relate to data presented in Fig 4. (Sources: SST data are from the NOAA OISSTv2; sea-ice extent and ice-edge data are from NSIDC Sea Ice Index, Version 3, Fetterer et al. 2017.)

Mean August SSTs from 1982 to 2019 show warming trends over much of the Arctic Ocean, with statistically significant (at the 95% confidence interval) linear warming trends of up to +1°C per decade (Fig. 3). The Chukchi Sea region continues to warm significantly, with August 2019 mean SSTs in the region being the second highest on record (Fig. 4). A marked exception to the prevalent August SST warming trend is the cooling trend (-0.06 ± 0.03°C/yr) in the northern Barents Sea (Fig. 3; Fig. 4). In line with this trend, most of the Barents Sea exhibited August 2019 SSTs around 0.3-2°C cooler than the 1982-2010 average (Fig. 2a) and parts of the southern Barents Sea were a few degrees cooler than in August 2018 (Fig. 2). The statistically significant northern Barents Sea cooling trend is not observed in all

months; annually-averaged northern Barents Sea SSTs exhibit a warming trend, which has been attributed to changes in Atlantic Water influence in the region (see e.g., Barton et al. 2018).

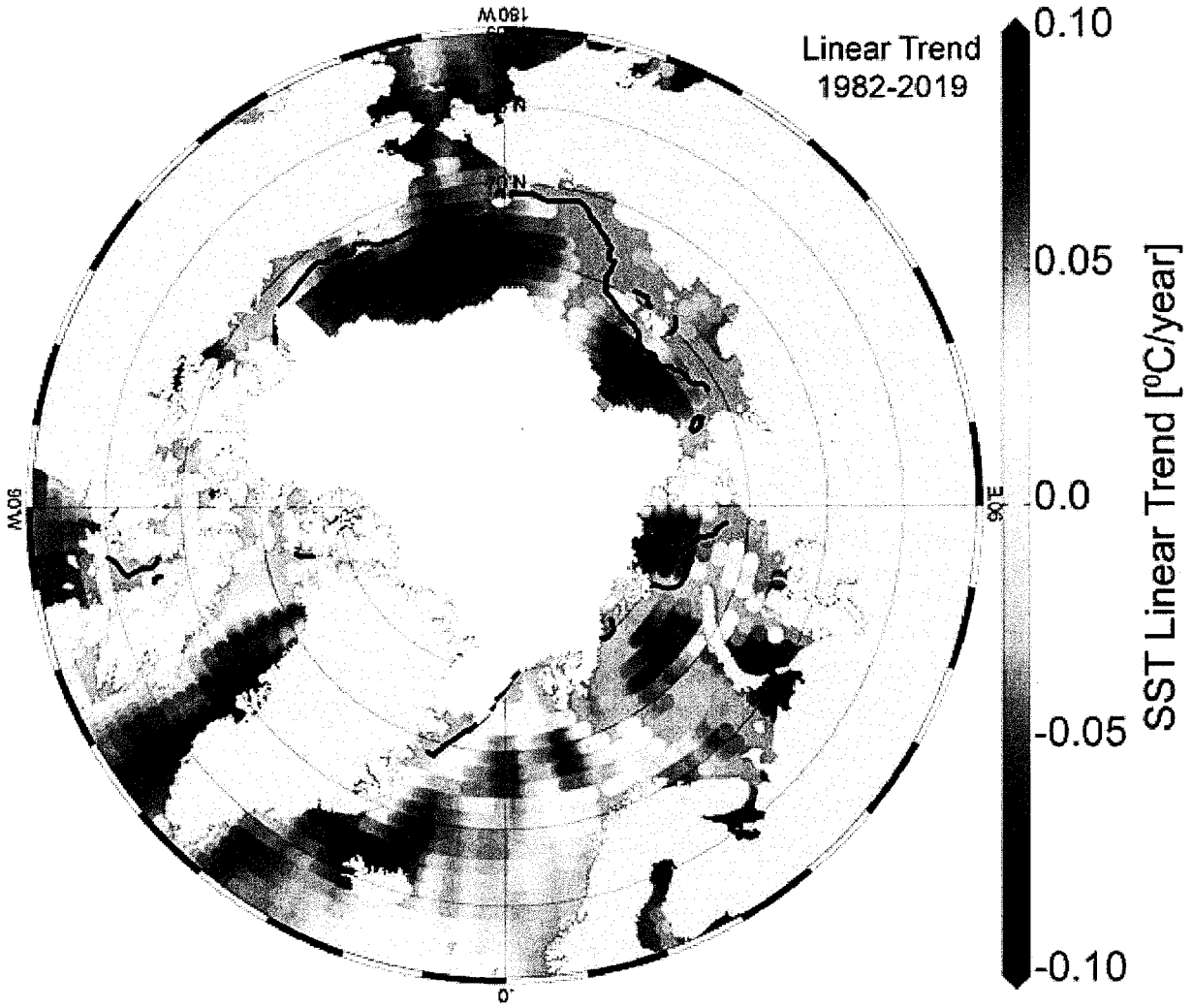

Fig. 3. Linear SST trend (°C yr^{-1}) for August of each year from 1982 to 2019. The trend is only shown for values that are significant at the 95% confidence interval; the region is grey otherwise. The black line indicates the median ice edge for August 1982-2010. White shading is the August 2019 mean sea-ice extent. (Sources: SST data are from the NOAA OISSTv2; sea-ice extent and ice-edge data are from NSIDC Sea Ice Index, Version 3, Fetterer et al. 2017.)

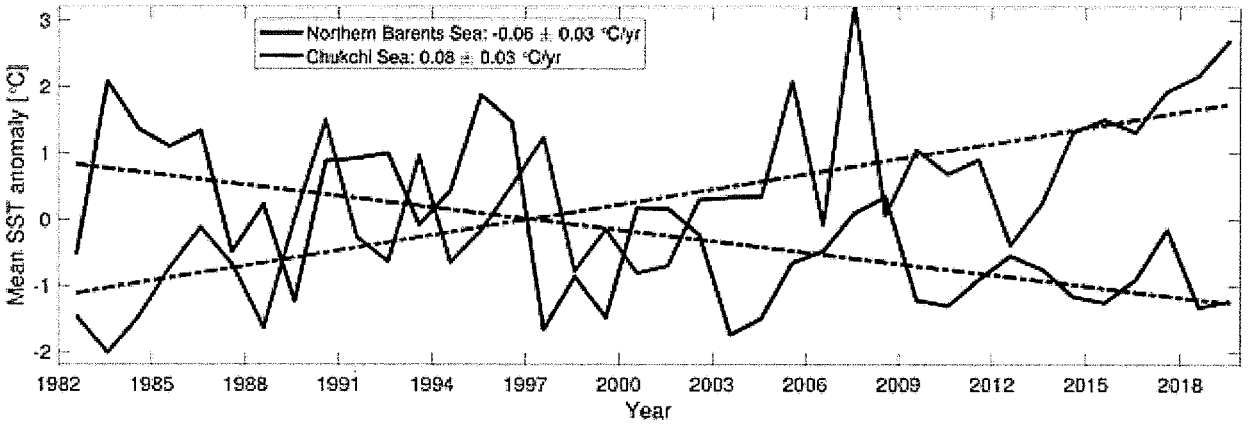

Fig. 4. Area-averaged SST anomalies (°C) for August of each year relative to the 1982-2010 August mean (regions are shown by black dashed lines in Fig. 2a). The dashed lines show the linear SST anomaly trends over the period shown. Numbers in the legend correspond to linear trends in °C year^{-1} (with 95% confidence intervals).

References

Barton, B. I., Y. Lenn, and C. Lique, 2018: Observed Atlantification of the Barents Sea causes the Polar Front to limit the expansion of winter sea ice. *J. Phys. Oceanogr.*, **48**, 1849-1866, https://doi.org/10.1175/JPO-D-18-0003.1.

Fetterer, F., K. Knowles, W. N. Meier, M. Savoie, and A. K. Windnagel, 2017 (updated daily): Sea Ice Index, Version 3: Regional Daily Data. National Snow and Ice Data Center (NSIDC), Boulder, CO, USA, https://doi.org/10.7265/N5K072F8.

Reynolds, R. W., N. A. Rayner, T. M. Smith, D. C. Stokes, and W. Wang, 2002: An improved in situ and satellite SST analysis for climate. *J. Climate*, **15**, 1609-1625.

Reynolds, R. W., T. M. Smith, C. Liu, D. B. Chelton, K. S. Casey, and M. G. Schlax, 2007: Daily high-resolution-blended analyses for sea surface temperature. *J. Climate*, **20**, 5473-5496, and see http://www.esrl.noaa.gov/psd/data/gridded/data.noaa.oisst.v2.html.

Stroh, J. N., G. Panteleev, S. Kirillov, M. Makhotin, and N. Shakhova, 2015: Sea-surface temperature and salinity product comparison against external in situ data in the Arctic Ocean. *J. Geophys. Res. Oceans*, **120**, 7223-7236, https://doi.org/0.1002/2015JC011005.

Timmermans, M. -L., and A. Proshutinsky, 2015. The Arctic: Sea surface temperature [in "State of the Climate in 2014"]. *Bull. Amer. Meteor. Soc.*, **96**(7), S147-S148.

November 19, 2019

Arctic Ocean Primary Productivity: The Response of Marine Algae to Climate Warming and Sea Ice Decline

K. E. Frey[1], J. C. Comiso[2], L. W. Cooper[3], J. M. Grebmeier[3], and L. V. Stock[2]

[1]Graduate School of Geography, Clark University, Worcester, MA, USA
[2]Cryospheric Sciences Laboratory, Goddard Space Flight Center, NASA, Greenbelt, MD, USA
[3]Chesapeake Biological Laboratory, University of Maryland Center for Environmental Science, Solomons, MD, USA

Highlights

- Satellite estimates of ocean primary productivity (i.e., the rate at which marine algae transform dissolved inorganic carbon into organic material) showed higher values for 2019 (relative to the 2003-18 mean) for seven of the nine investigated regions (with the Barents Sea and North Atlantic the only regions showing lower than average values).
- All regions continue to exhibit positive trends over the 2003-19 period, with the strongest trends in the Eurasian Arctic, Barents Sea, and Greenland Sea.
- During May 2019, a ~1500 km long region along the sea ice edge in the Greenland Sea showed on average ~18 times higher chlorophyll-*a* concentrations than the same month of the previous years (2003-18) on record.
- Unprecedented declines of sea ice in the Bering Sea in late winter 2018 and 2019 have been associated with shifts in the timing and intensity of phytoplankton blooms. Both years showed increases in chlorophyll biomass in March in the St. Lawrence Island Polynya region, associated with earlier spring break-up of sea ice. However, 2019 (unlike 2018) showed a more characteristic phytoplankton bloom in May, which may be associated with the resurgence of ice cover in April 2019.

Introduction

Autotrophic single-celled algae living in sea ice (ice algae) and water column (phytoplankton) are the main primary producers in the Arctic Ocean. Through photosynthesis, they transform dissolved inorganic carbon into organic material. Consequently, primary production provides a key ecosystem service by providing energy to the entire food web in the oceans. Primary productivity is strongly dependent upon light availability and the presence of nutrients, and thus is highly seasonal in the Arctic. In particular, the melting and retreat of sea ice during spring are strong drivers of primary production in the Arctic Ocean and its adjacent shelf seas, owing to enhanced light availability and stratification (Barber et al. 2015; Leu et al. 2015; Ardyna et al. 2017). Recent declines in Arctic sea ice extent (see essay *Sea Ice*) have contributed substantially to shifts in primary productivity throughout the Arctic Ocean. However, the response of primary production to sea ice loss has been both seasonally and spatially variable (e.g., Tremblay et al. 2015; Hill et al. 2018).

Here we present satellite-based estimates of algal chlorophyll-*a* (occurring in all species of phytoplankton), based on the color of the ocean, and subsequently provide calculated primary production estimates. These results are shown for ocean areas with less than 15% sea ice concentration and, therefore, do not include production by sea ice algae or under-ice phytoplankton blooms.

Chlorophyll-*a*

Measurements of the algal pigment chlorophyll (e.g., chlorophyll-*a*) serve as a proxy for the amount of algal biomass present as well as overall plant health. The complete, updated MODIS-Aqua satellite chlorophyll-*a* record for the northern polar region for the years 2003-19 can serve as a time series against which individual years can be compared. For this reporting, a reference period of 2003-18 was chosen to calculate the 2019 anomalies to maximize the length of the satellite-based time series.

The 2019 data show a distribution of both positive and negative anomalies in chlorophyll-*a* concentrations in a number of locations across the Arctic Ocean region, where patterns are spatially and temporally heterogeneous (Fig. 1). These patterns are often associated with the timing of the seasonal break-up and retreat of the sea ice cover (Fig. 2): positive anomalies tend to occur in regions where the break-up is relatively early, while negative anomalies tend to occur in regions where the break-up is delayed. The most notable positive anomalies in 2019 occurred during May, with high concentrations of chlorophyll-*a* occurring along the ice edge in the Greenland Sea (Figs. 1a and 3). In particular, this regional positive anomaly of chlorophyll-*a* concentrations extended nearly 1500 km in length from Svalbard at ~80° N southward to central East Greenland at 70° N and exhibited on average ~18 times higher concentrations than previous years on record (Fig. 3b). Before this observed anomaly, the highest concentration in chlorophyll-*a* for this region had been in June 2007 (Fig. 3b), but it was only two-thirds as high as in 2019. Furthermore, not only was the intensity of the spring bloom unprecedented in 2019, but also the timing: peak seasonal phytoplankton blooms in this region typically occur in June (Fig. 3b) but were shifted one month earlier to May in 2019. Additional widespread positive anomalies occurred in the Bering Sea in May, June, and July, which are discussed in greater detail below. Some of the strongest negative anomalies in chlorophyll-*a* concentrations (i.e., low primary productivity) occurred in the Barents Sea in May (Fig. 1a) and in the Beaufort Sea in July (Fig. 1c). The relatively low chlorophyll-*a* concentrations in the Barents Sea in May are associated with increases in sea ice cover in that region throughout the season (Fig. 2a-c).

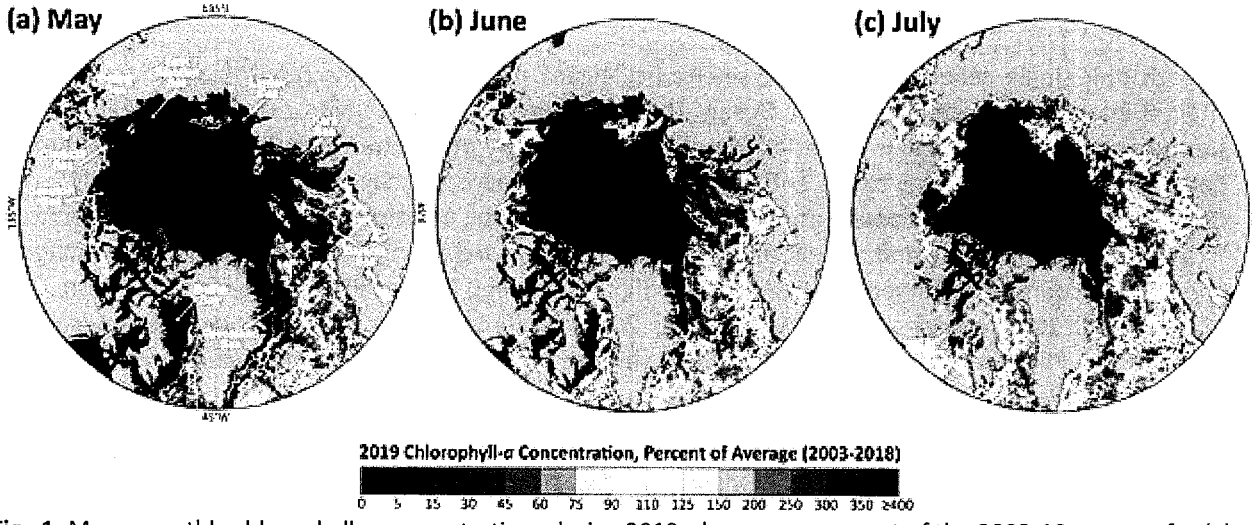

Fig. 1. Mean monthly chlorophyll-*a* concentrations during 2019, shown as a percent of the 2003-18 average for (a)

May, (b) June, and (c) July. The black regions represent areas where no data are available (either owing to >15% sea ice concentrations or cloud cover). Satellite-based chlorophyll-*a* data across the pan-Arctic region were derived using the MODIS-Aqua Reprocessing 2018.0, OCx algorithm: http://oceancolor.gsfc.nasa.gov/.

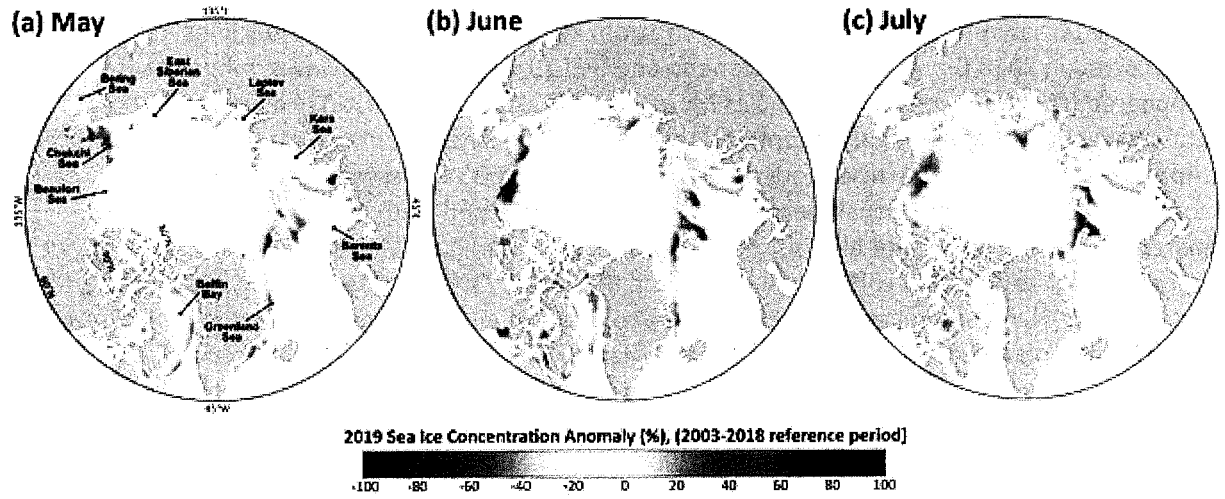

Fig. 2. Sea ice concentration anomalies (%) in 2019 (compared to a 2003-18 mean reference period) for (a) May, (b) June, and (c) July. Satellite-based sea ice concentrations were derived from the Special Sensor Microwave/Imager (SSM/I) and Special Sensor Microwave Imager/Sounder (SSMIS) passive microwave instruments, calculated using the Goddard Bootstrap (SB2) algorithm (Comiso et al. 2017a,b).

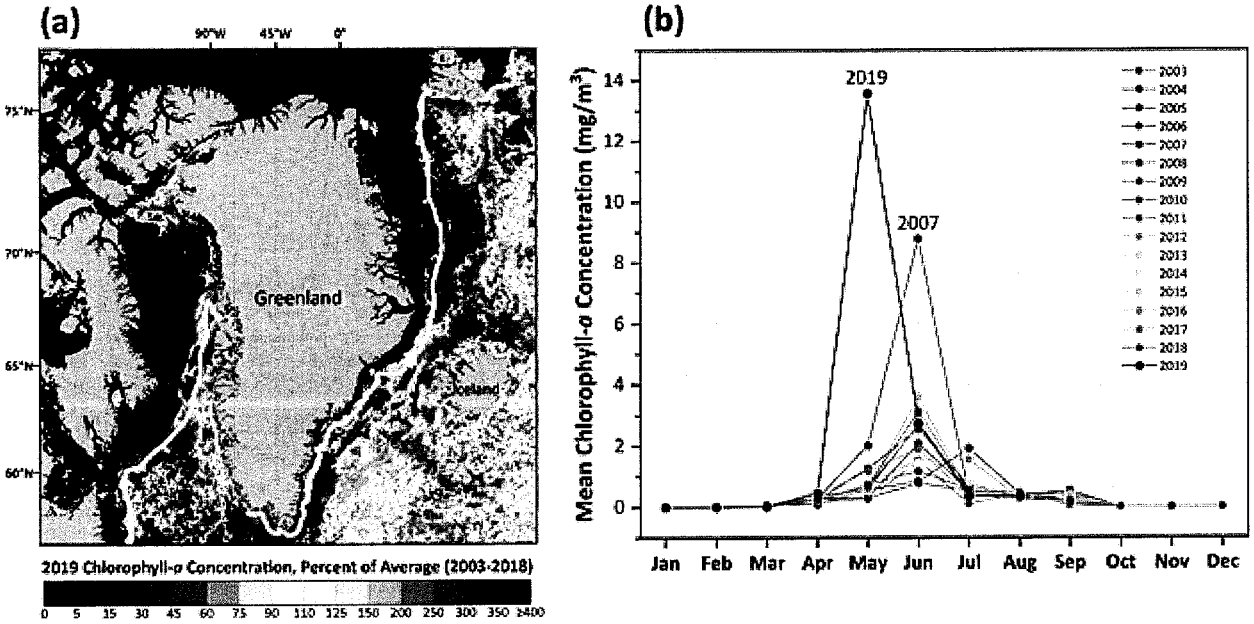

Fig. 3. (a) Mean chlorophyll-*a* anomalies surrounding Greenland in May 2019, shown as a percent of the 2003-18 average. The white line denotes the mean sea ice extent (i.e., sea ice concentration at 15%) for May 2019. The red box denotes the area along the sea ice edge in the Greenland Sea for which data are shown in (b). (b) Mean chlorophyll-*a* concentrations for the region in the Greenland Sea highlighted in (a) from 2003-19, where May 2019 showed on average ~18 times higher concentrations than previous years on record. Phytoplankton blooms are distinctly seasonal in high-latitude seas, with peak production occurring once light levels and stratification are sufficient (with melting snow and the break-up of sea ice) and then dissipate once nutrients in the water column are depleted.

As noted above, some of the largest positive anomalies in chlorophyll-*a* concentrations observed in 2019 occurred over the shelf region of the Bering Sea during May and June (Fig. 1a,b). During July, these positive anomalies extended more widely across the northern Bering Sea and into the Chukchi Sea (Fig. 1c). In particular, focusing on the Distributed Biological Observatory Site 1 (DBO1; Moore and Grebmeier 2018) in the St. Lawrence Island Polynya (SLIP) region, 2019 experienced similar declines in sea ice that also occurred in 2018 (Frey et al. 2018; Stabeno and Bell 2019) (Fig. 4a). However, while sea ice had disappeared from this region by the end of March in both 2018 and 2019, 2019 in contrast showed a slight resurgence of ice during the month of April before it declined again a few weeks later by the end of April. These general patterns of early sea ice break-up at DBO1 are associated with upticks in March chlorophyll-*a* concentrations that were observed in both 2018 and 2019 (Fig. 4b). In 2018, it was apparent that the typical large blooms that are produced in April and May did not occur; instead, we observed a redistribution of chlorophyll biomass in March (~275% increase over the 2003-17 average) and June (~500% increase over the 2003-17 average) (Frey et al. 2018). In contrast, the typical seasonal bloom of phytoplankton occurred as expected in May 2019 (Fig. 4b), which may be associated with the resurgence of sea ice cover in the region in April. In particular, May 2019 showed a ~360% increase in chlorophyll-*a* concentrations over the 2003-18 average, with similar percentage increases persisting through the season including ~140% (June), ~200% (July), and ~220% (August) (Fig. 4b).

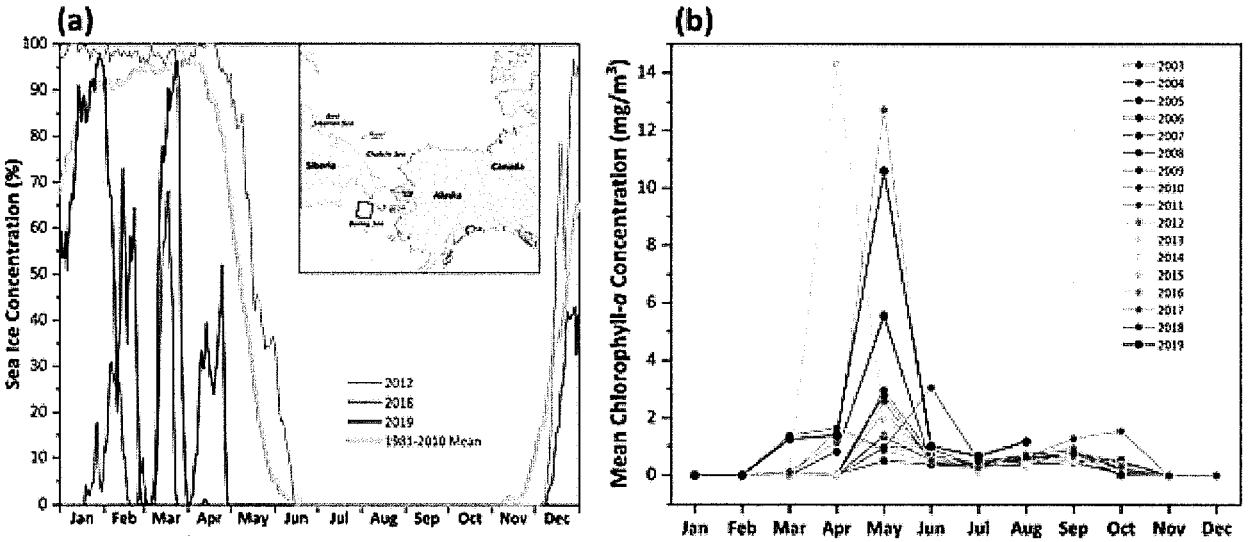

Fig. 4. (a) Daily time series of sea ice concentration in the Bering Sea region at the DBO1/SLIP region (red square within the map inset), highlighting the 1981-2010 mean, 2012 (one of the highest winters/springs of sea ice cover on record), and 2018 and 2019 (the lowest winters/springs of sea ice cover on record). (b) Mean chlorophyll-*a* concentrations for the DBO1/SLIP region from 2003-19.

Having knowledge of how regions experience changes in chlorophyll-*a* concentrations alongside dramatic losses of sea ice cover provides insight into what to expect with future sea ice declines. While many of these observed patterns are directly linked to sea ice variability (and therefore light availability), it is important to note that there are other dominant factors at play that add to the complexity of observed chlorophyll-*a* concentrations such as the distribution and availability of nutrients (e.g., Giesbrecht et al. 2019). The impacts of sea ice decline on specific water column phytoplankton properties, such as community composition and carbon biomass (Neeley et al. 2018), as well as broader ecosystem responses (Duffy-Anderson et al. 2019), are critical to continue to monitor.

Primary production

Chlorophyll-*a* concentrations give an estimate of the total standing stock of algal biomass. However, rates of primary production (i.e., the production of organic carbon via photosynthesis) provide a different perspective since not all algae present in the water column are necessarily actively producing, and can be estimated by combining remotely sensed chlorophyll-*a* concentrations with sea surface temperatures, incident solar irradiance, and mixed layer depths (see Fig. 5 for references to details of the method for estimation). Estimates of ocean primary productivity for nine regions (and the average of these nine regions) across the Arctic, relative to the 2003-18 reference period, indicate above-average primary productivity for 2019 in all regions except for the Barents Sea and North Atlantic (Fig. 5, Table 1). In the longer term, positive trends in primary productivity occurred in all regions during the period 2003-19 (Fig. 5, Table 1). Statistically significant positive trends occurred in the Eurasian Arctic, Barents Sea, Greenland Sea, Baffin Bay/Labrador Sea, North Atlantic, and for the average of the nine regions. The steepest trends were found for the Eurasian Arctic (12.85 g $C/m^2/yr/dec$, or a ~35.5% increase), the Barents Sea (10.62 g $C/m^2/yr/dec$, or a ~22.7% increase), and the Greenland Sea (7.33 g $C/m^2/yr/dec$, or a ~20.5% increase).

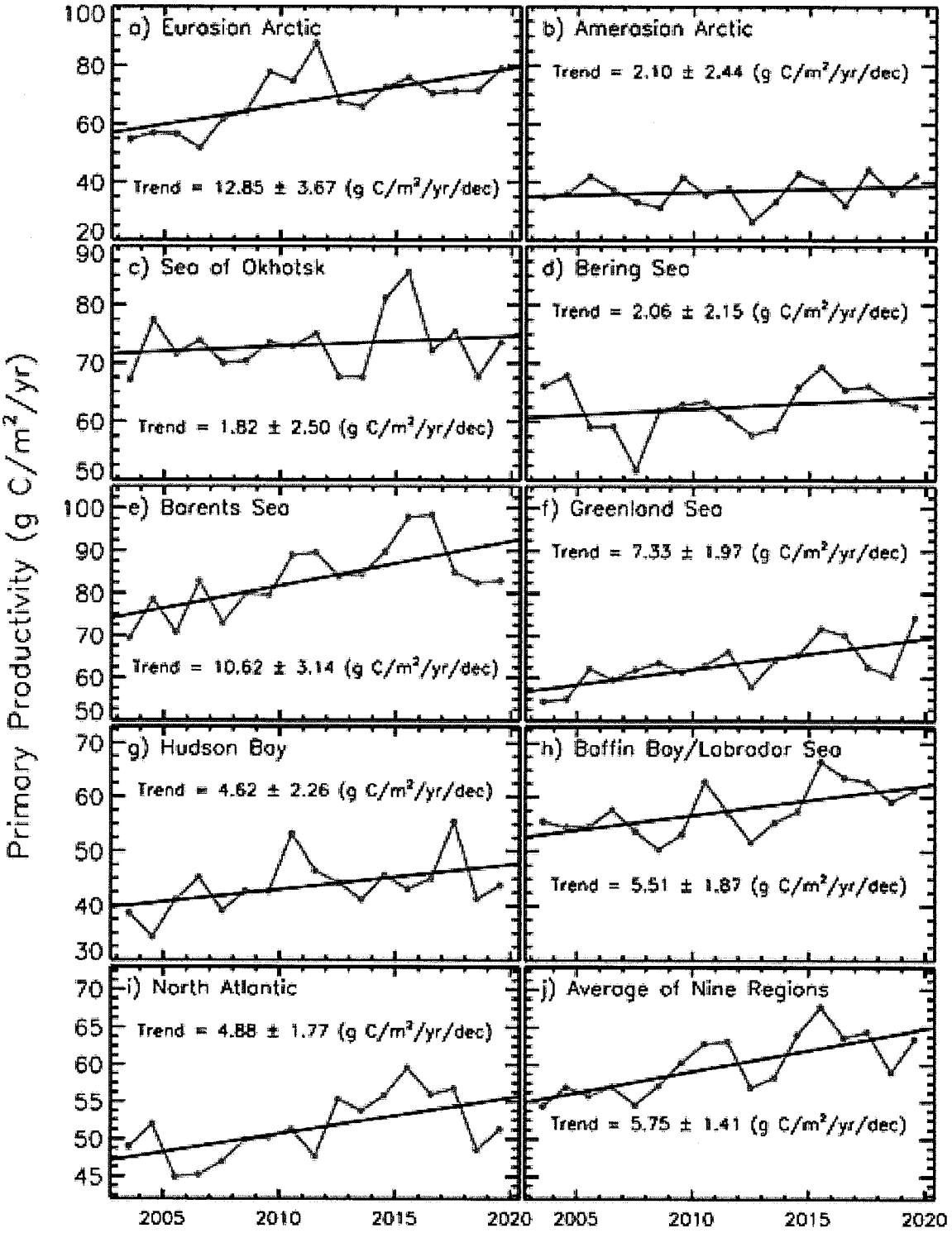

Fig. 5. Primary productivity (2003-19, March-September only) in nine different regions of the Northern Hemisphere (for a definition of the regions see Comiso 2015), as well as the average of these nine regions, derived using chlorophyll-*a* concentrations from MODIS-Aqua data, the NOAA 1/4° daily Optimum Interpolation Sea Surface Temperature dataset (or daily OISST) that uses satellite sea surface temperatures from AVHRR, and additional parameters. Values are calculated based on the techniques described by Behrenfield and Falkowski (1997) and represent net primary productivity (NPP). Additional information regarding these data can be found in Table 1.

Table 1. Linear trends, statistical significance, percent change and primary productivity anomalies in 2019 (March-September) in the nine regions (and overall average) as shown in Fig. 5. Utilizing the Mann-Kendall test for trend, values in **bold** are significant at the 95% confidence level. The percent change was estimated from the linear regression of the 17-year time series.

Region	Trend, 2003-19 (g C/m^2/yr/decade)	Mann-Kendall *p* -value	% Change	2019 Anomaly (g C/m^2/yr) from a 2003-18 base period	2019 Primary Productivity (% of the 2003-18 average)
Eurasian Arctic	**12.85**	0.003	35.5	11.32	116.8
Amerasian Arctic	2.10	0.349	9.5	5.78	115.8
Sea of Okhotsk	1.82	0.490	4.1	0.44	100.6
Bering Sea	2.06	0.490	5.4	0.07	100.1
Barents Sea	**10.62**	0.002	22.7	-0.45	99.5
Greenland Sea	**7.33**	0.005	20.5	11.80	118.9
Hudson Bay	4.62	0.052	18.5	0.09	100.2
Baffin Bay/Labrador	**5.51**	0.042	16.6	4.11	107.2
North Atlantic	**4.88**	0.006	16.5	-0.11	99.8
Average of nine regions	**5.75**	0.000	16.6	3.67	106.1

References

Ardyna, M., M. Babin, E. Devred, A. Forest, M. Gosselin, P. Raimbault, and J. -É. Tremblay, 2017: Shelf-basin gradients shape ecological phytoplankton niches and community composition in the coastal Arctic Ocean (Beaufort Sea). *Limnol. Oceanogr.*, **62**, 2113-2132, https://doi.org/10.1002/lno.10554.

Barber, D. G., H. Hop, C. J. Mundy, B. Else, I. A. Dmitrenko, J. -É. Tremblay, J. K. Ehn, P. Assmy, M. Daase, L. M. Candlish, and S. Rysgaard, 2015: Selected physical, biological and biogeochemical implications of a rapidly changing Arctic Marginal Ice Zone. *Prog. Oceanogr.*, **139**, 122-150, https://doi.org/10.1016/j.pocean.2015.09.003.

Behrenfeld, M. J., and P. G. Falkowski, 1997: Photosynthetic rates derived from satellite-based chlorophyll concentration. *Limnol. Oceanogr.*, **42**(1), 1-20.

Comiso, J. C., 2015: Variability and trends of the global sea ice covers and sea levels: Effects on physicochemical parameters. *Climate and Fresh Water Toxins*, L. M. Botana, M. Carmen Lauzao, and N. Vilarino, Eds., De Gruyter, Berlin, Germany.

Comiso, J. C., R. Gersten, L. Stock, J. Turner, G. Perez, and K. Cho, 2017a: Positive trends in the Antarctic sea ice cover and associated changes in surface temperature. *J. Climate*, **30**, 2251-2267, https://doi.org/10.1175/JCLI-D-0408.1.

Comiso, J. C., W. N. Meier, and R. Gersten, 2017b: Variability and trends in the Arctic Sea ice cover: Results from different techniques. *J. Geophys. Res. Oceans*, **122**, 6883-6900, https://doi.org/10.1002/2017JC012768.

Duffy-Anderson, J. T., P. Stabeno, A. G. Andrews III, K. Cieciel, A. Dreary, E. Farley, C. Fugate, C. Harpold, R. Heintz, D. Kimmel, K. Kuletz, J. Lamb, M. Paquin, S. Porter, L. Rogers, A. Spear, and E. Yasumiishi, 2019: Responses of the northern Bering Sea and southeastern Bering Sea pelagic ecosystems following record-breaking low winter sea ice. *Geophys. Res. Lett.*, **46**(16), 9833-9842, https://doi.org/10.1029/2019GL083396.

Frey, K. E., J. C. Comiso, L. W. Cooper, J. M. Grebmeier, and L. V. Stock, 2018: Arctic Ocean primary productivity: The response of marine algae to climate warming and sea ice decline. *Arctic Report Card 2018*, E. Osborne, J. Richter-Menge, and M. Jeffries, Eds., https://www.arctic.noaa.gov/Report-Card.

Giesbrecht, K. E., D. E. Varela, J. Wiktor, J. M. Grebmeier, B. Kelly, and J. E. Long, 2019: A decade of summertime measurements of phytoplankton biomass, productivity and assemblage composition in the Pacific Arctic Region from 2006 to 2016. *Deep-Sea Res. Pt. II*, **162**, 93-113, https://doi.org/10.1016/j.dsr2.2018.06.010.

Hill, V., M. Ardyna, S. H. Lee, and D. E. Varela, 2018: Decadal trends in phytoplankton production in the Pacific Arctic Region from 1950 to 2012. *Deep-Sea Res. Pt. II*, **152**, 82-94, https://doi.org/10.1016/j.dsr2.2016.12.015.

Leu, E., C. J. Mundy, P. Assmy, K. Campbell, T. M. Gabrielsen, M. Gosselin, T. Juul-Pedersen, and R. Gradinger, 2015: Arctic spring awakening - Steering principles behind the phenology of vernal ice algal blooms. *Prog. Oceanogr.*, **139**, 151-170, https://doi.org/10.1016/j.pocean.2015.07.012.

Moore, S. E., and J. M. Grebmeier, 2018: The distributed biological observatory: Linking physics to biology in the Pacific Arctic region. *Arctic*, **71**(Suppl. 1), 1-7, https://doi.org/10.14430/arctic4606.

Neeley, A. R., L. A. Harris, and K. E. Frey, 2018: Unraveling phytoplankton community dynamics in the northern Chukchi and western Beaufort seas amid climate change. *Geophys. Res. Lett.*, **45**(15), 7663-7671, https://doi.org/10.1029/2018GL077684.

Stabeno, P., and S. W. Bell, 2019: Extreme conditions in the Bering Sea (2017-2018): Record-breaking low sea-ice extent. *Geophys. Res. Lett.*, **46**, 8952-8959, https://doi.org/10.1029/2019GL083816.

Tremblay J. -É., L. G. Anderson, P. Matrai, S. Bélanger, C. Michel, P. Coupel, and M. Reigstad, 2015: Global and regional drivers of nutrient supply, primary production and CO_2 drawdown in the changing Arctic Ocean. *Prog. Oceanogr.*, **139**, 171-196, https://doi.org/10.1016/j.pocean.2015.08.009.

November 20, 2019

Tundra Greenness

G. V. Frost[1], U. S. Bhatt[2], H. E. Epstein[3], D. A. Walker[4], M. K. Raynolds[4], L. T. Berner[5], J. W. Bjerke[6], A. L. Breen[2], B. C. Forbes[7], S. J. Goetz[5], C. M. Iversen[8], M. J. Lara[9], M. J. Macander[1], G. K. Phoenix[10], A. V. Rocha[11], V. G. Salmon[8], P. E. Thornton[8], H. Tømmervik[6], and S. D. Wullschleger[8]

[1]Alaska Biological Research, Inc., Fairbanks, AK, USA
[2]International Arctic Research Center, University of Alaska Fairbanks, Fairbanks, AK, USA
[3]Department of Environmental Sciences, University of Virginia, Charlottesville, VA, USA
[4]Institute of Arctic Biology, University of Alaska Fairbanks, Fairbanks, AK, USA
[5]School of Informatics, Computing, and Cyber Systems, Northern Arizona University, Flagstaff, AZ, USA
[6]Norwegian Institute for Nature Research, FRAM - High North Research Centre for Climate and the Environment, Tromsø, Norway
[7]Arctic Centre, University of Lapland, Rovaniemi, Finland
[8]Environmental Sciences Division and Climate Change Science Institute, Oak Ridge National Laboratory, Oak Ridge, TN, USA
[9]Department of Plant Biology and Department of Geography, University of Illinois at Urbana-Champaign, IL, USA
[10]Department of Animal and Plant Sciences, University of Sheffield, Sheffield, UK
[11]Department of Biological Sciences, University of Notre Dame, Notre Dame, IN, USA

Highlights

- The long-term satellite record (1982-2018) indicates "greening" across most Arctic tundra regions, especially Alaska's North Slope, mainland Canada, and the Russian Far East, but trends are not homogeneous, and some regions instead exhibit no trend or "browning," such as the Canadian Archipelago, southwestern Alaska, and parts of northwestern Siberia.
- In 2018, there were stark contrasts in tundra greenness by continent, with a sharp decline in greenness in North America but a modest increase in Eurasia.
- In North America, tundra productivity for the full growing season was the second lowest on record, concurrent with relatively cool spring and summer temperatures and late snowmelt in the Canadian Archipelago and Greenland.

Arctic lands and seas have experienced dramatic environmental and climatic changes in recent decades. These changes have been reflected in progressive increases in the aboveground quantity of live vegetation across most of the Arctic tundra biome—the treeless environment encircling most of the Arctic Ocean. This trend of increasing biomass is often referred to as "the greening of the Arctic." Trends in tundra productivity, however, have not been uniform in direction or magnitude across the circumpolar region and there has been substantial variability from year to year (Bhatt et al. 2013, 2017; Park et al. 2016; National Academies of Sciences, Engineering, and Medicine 2019). Sources of spatial and temporal variability in tundra greenness arise from complex interactions among the vegetation, atmosphere, sea-ice, seasonal snow cover, ground (soils, permafrost, and topography), disturbance processes, and herbivores of the Arctic system.

Many of the changes being observed in tundra vegetation are producing a cascade of effects on the structure and function of Arctic ecosystems. For example, changes in the height and vigor of tundra plants impact the cycling of carbon and nutrients (Blume-Werry et al. 2019; Hewitt et al. 2019; Mörsdorf et al. 2019; Salmon et al. 2019; Treharne et al. 2019), as well as the exchange of energy between the atmosphere and permafrost soils (Wilcox et al. 2019). The latter has implications for permafrost stability and surface wetness which, coupled with changes in vegetation structure, can strongly alter habitat conditions for wildlife (Cray and Pollard 2018; Tape et al. 2018; Taylor et al. 2018; Ims et al. 2019; Kolari et al. 2019). Continued monitoring of circumpolar Arctic vegetation using Earth-observing satellites and field studies improves our understanding of these complex interactions and their impacts within, and beyond the Arctic.

Since 1982, a constellation of NOAA Earth-observing satellites has continually monitored the productivity of Arctic vegetation using a spectral metric termed the Normalized Difference Vegetation Index (NDVI), which is sensitive to the unique properties of photosynthetically-active vegetation in the Red and Near Infrared wavelengths. NDVI is highly correlated with the quantity of aboveground vegetation, or "greenness," of Arctic tundra (Raynolds et al. 2012). The data reported here come from the Global Inventory Modeling and Mapping Studies 3g V1.1 dataset (GIMMS-3g); it is a biweekly, maximum-value composited dataset of the NDVI with a spatial resolution of 1/12° based on the Advanced Very High Resolution Radiometer (AVHRR) sensor (Pinzon and Tucker 2014). At the time of writing, the GIMMS-3g dataset was available only through the 2018 growing season. We use two metrics based on the NDVI: MaxNDVI and TI-NDVI. MaxNDVI is the peak NDVI value for the year and is related to the annual maximum biomass of aboveground vegetation that is reached in midsummer (typically late July or early August). TI (time-integrated) NDVI is the sum of the biweekly NDVI values for the growing season and is correlated with the total aboveground vegetation productivity. NDVI is generally highest near treeline and declines with increasing latitude. Values for North American tundra average lower than those for Eurasia, because a larger proportion of the North American Arctic lies in the High Arctic and was glaciated much more recently.

The GIMMS-3g record now spans 37 years (1982-2018) and indicates that both MaxNDVI and TI-NDVI have increased across most of the circumpolar Arctic tundra biome (Fig. 1a,b). Regions with the strongest greening include the Alaska's North Slope, the Low Arctic (southern tundra subzones) of mainland Canada, and the Russian Far East. Tundra greenness appears to have declined, however, in western Alaska, the Canadian Archipelago, and parts of northwestern Siberia. Regional "hotspots" of greening and browning, evident as NDVI increases and decreases, respectively, are generally consistent between the two NDVI metrics, but decreases in TI-NDVI have been more widespread than decreases in MaxNDVI. In recent years, similar NDVI datasets have been compiled from other satellites and can be used to corroborate the GIMMS-3g record, albeit with a shorter period-of-record. For example, a recent analysis of the Landsat record indicates widespread increases in MaxNDVI from 1985 to 2018; greening was evident at 47% of sampling sites, but significant browning occurred at only 2% of sampling sites. The remaining 51% of sampling sites showed no deterministic trend over this period (L. Berner, personal communication).

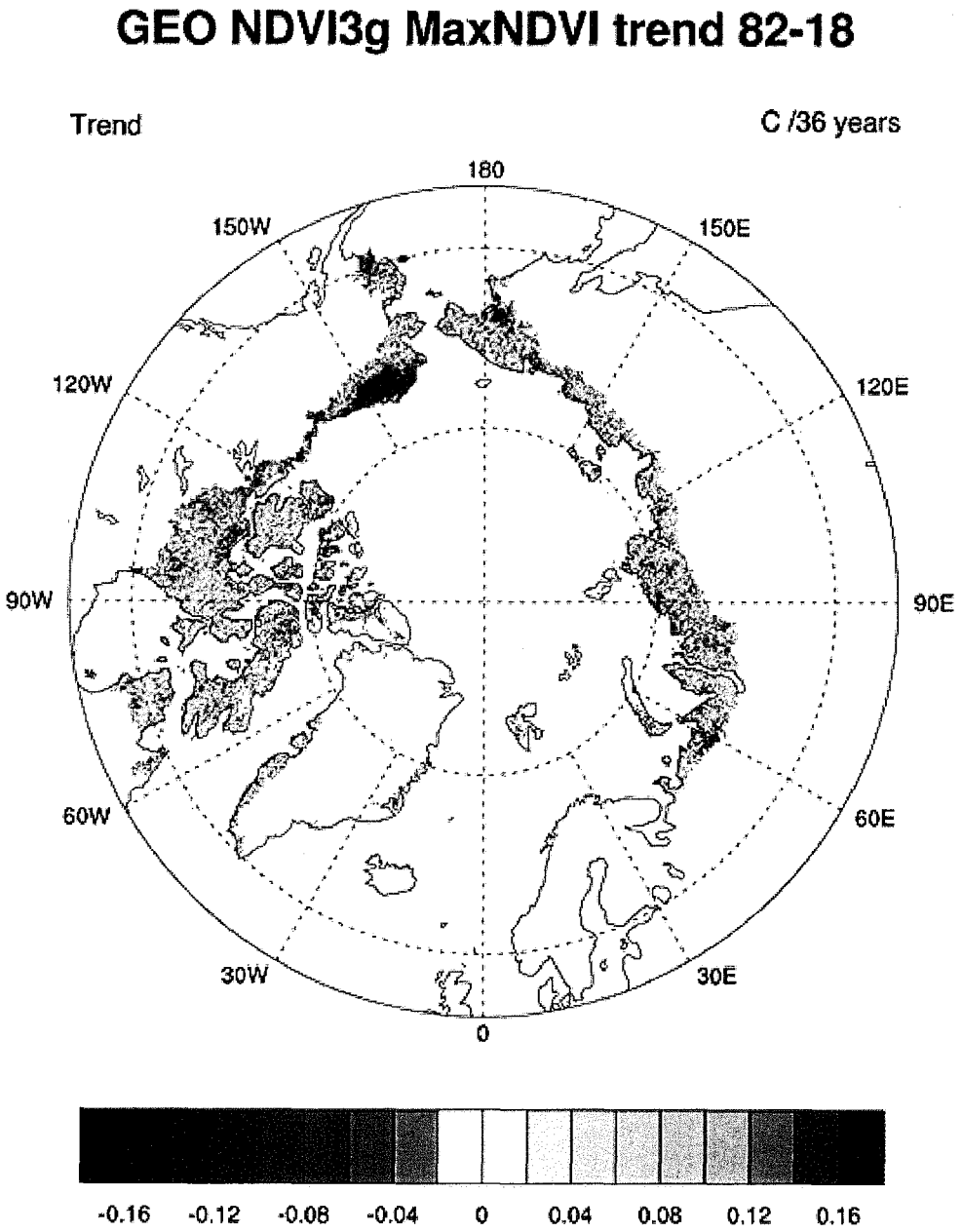

Fig. 1a. Magnitude of the overall trend in MaxNDVI (Maximum Normalized Difference Vegetation Index) for the 37-year period 1982-2018.

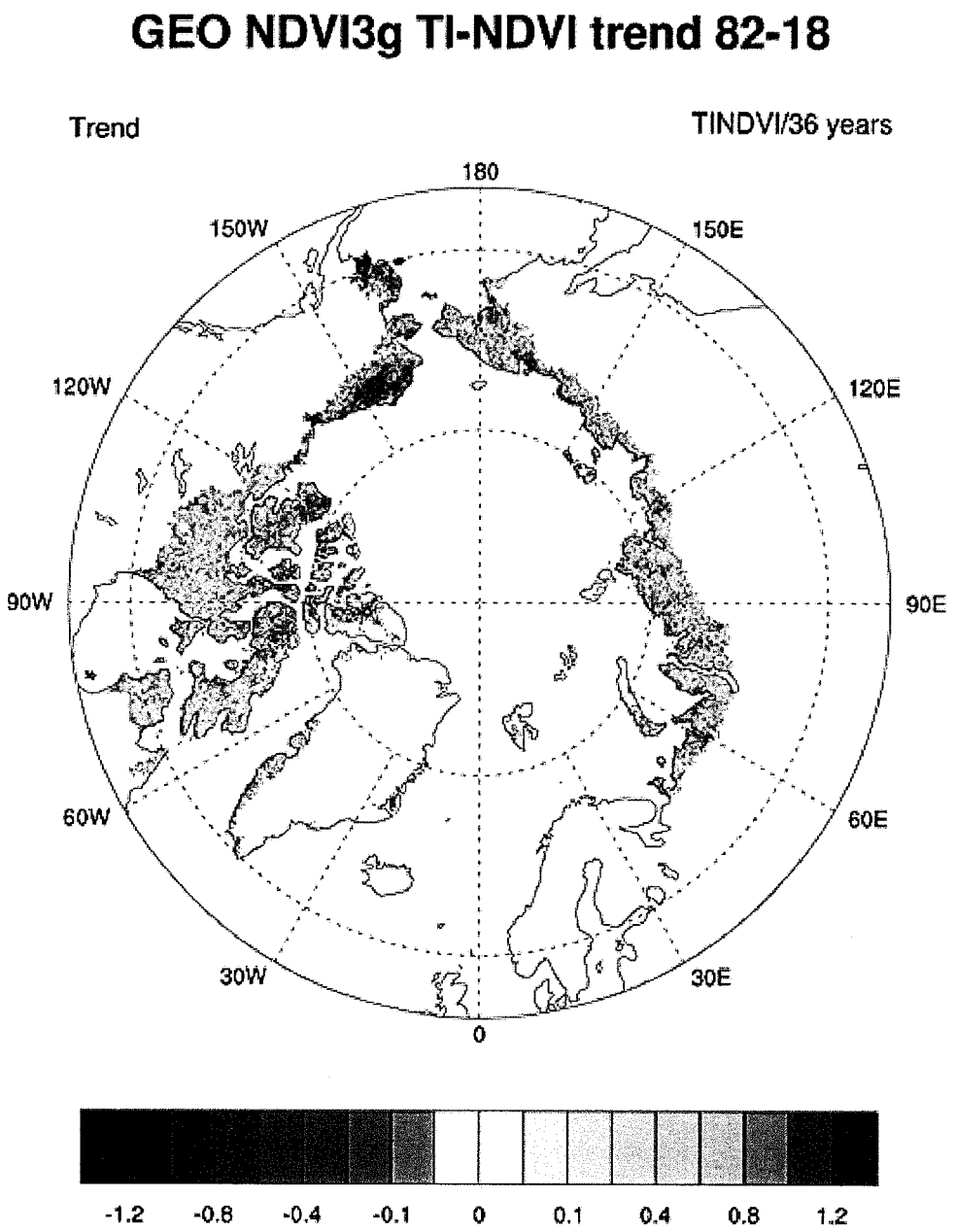

Fig. 1b. Magnitude of the overall trend in TI-NDVI (Time-integrated Normalized Difference Vegetation Index) for the 37-year period 1982-2018.

In 2018, growing season conditions and tundra productivity contrasted starkly between North America and Eurasia. NDVI in the Eurasian Arctic was similar to the previous year, but declined sharply in the North American Arctic (Fig. 2a,b), much of which experienced late snowmelt and relatively cool summer temperatures (Mudryk et al. 2018; Schmidt et al. 2019). Considering the circumpolar Arctic as a whole, NDVI declined for the second straight year; the decline was most obvious for TI-NDVI, for which the highest value in the record occurred in 2016. The 2018 TI-NDVI in North America fell well below the long-term median value and was the second lowest in the entire record behind 1992, when Arctic summer warmth was affected by atmospheric aerosols from the 1991 eruption of Mt. Pinatubo (Lucht 2002). TI-NDVI in North America declined 11.1% from 2017 to 2018, the largest single-year decline in the 37-year record. The year-to-year decline in MaxNDVI in North America was not as sharp (3.0%) and the

2018 value was near the long-term median. In the Eurasian Arctic, however, TI-NDVI increased slightly and MaxNDVI was steady; both values were above the long-term median.

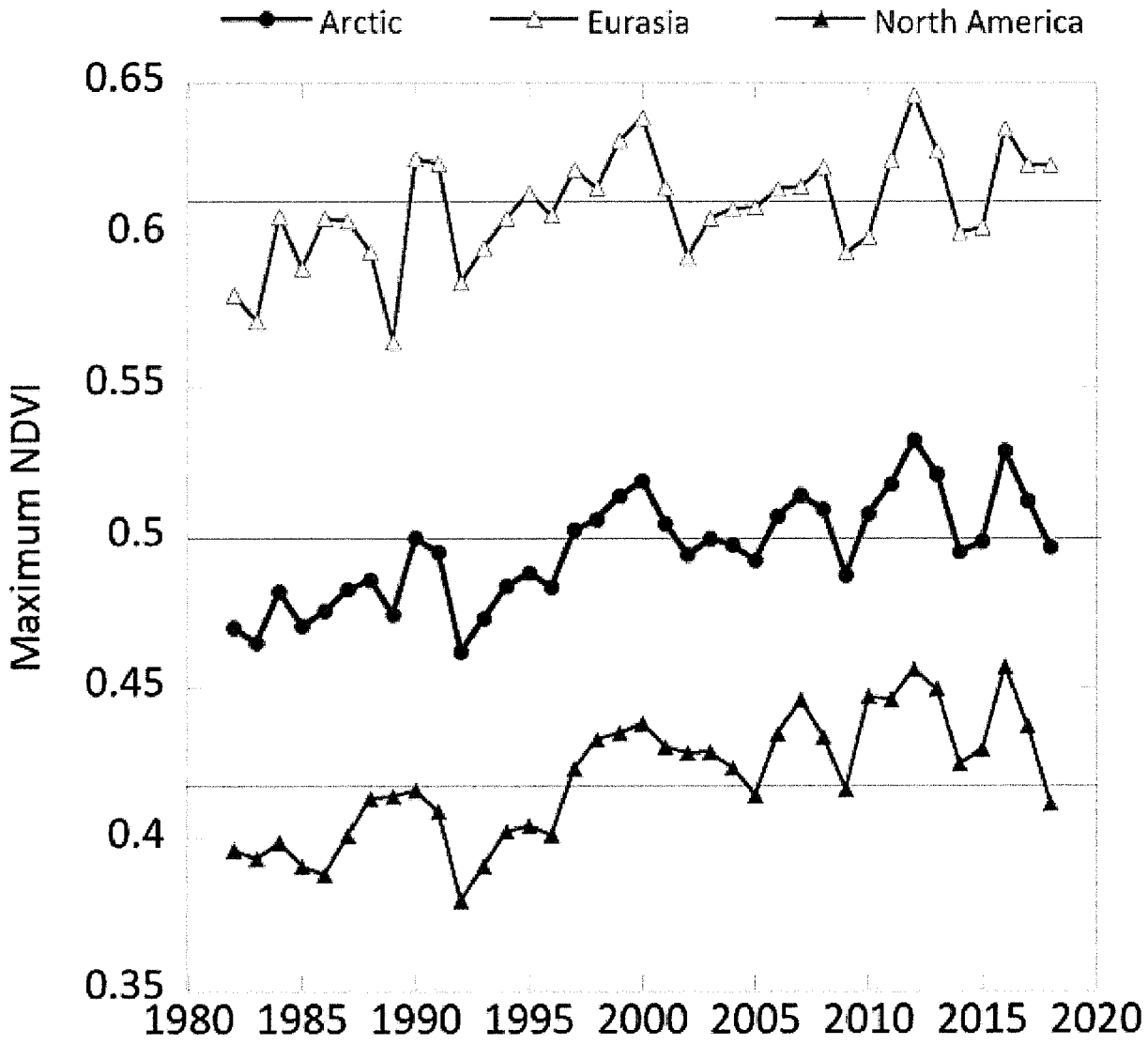

Fig. 2a. MaxNDVI (Maximum Normalized Difference Vegetation Index) during 1982-2018 for the North American Arctic (bottom), Eurasian Arctic (top), and the circumpolar Arctic (middle).

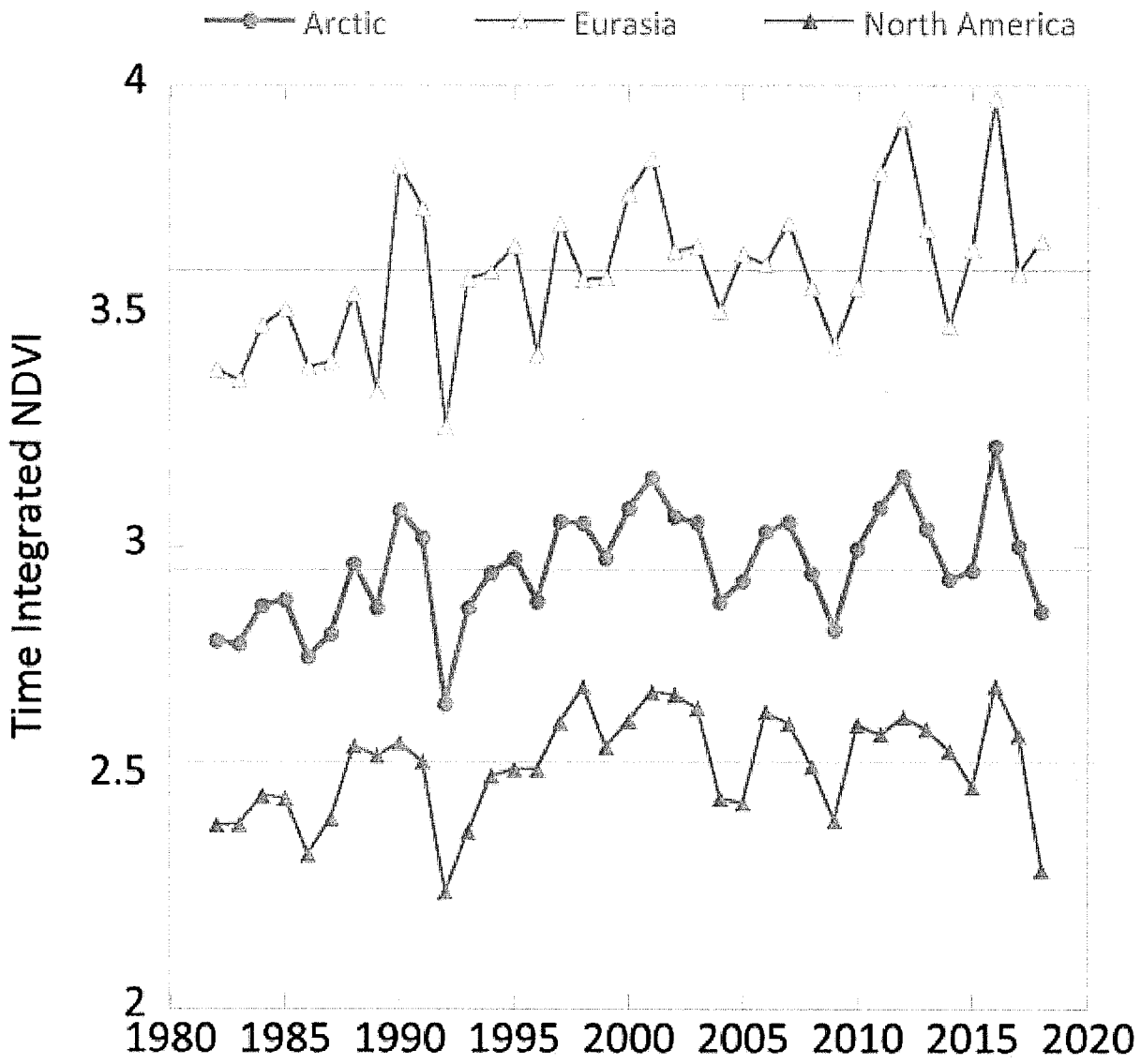

Fig. 2b. TI-NDVI (Time-integrated Normalized Difference Vegetation Index) during 1982-2018 for the North American Arctic (bottom), Eurasian Arctic (top), and the circumpolar Arctic (middle).

Within the 37-year record, MaxNDVI values for 2018 ranked 19th, 9th, and 25th for the circumpolar Arctic, Eurasian Arctic, and North American Arctic, respectively. TI-NDVI values ranked 31st, 11th, and 36th for the circumpolar Arctic, Eurasian Arctic, and North American Arctic respectively. Circumpolar measurements of summer warmth–a key control of NDVI–provide valuable context for understanding the strong contrasts in tundra productivity observed by continent in 2018. The AVHRR sensors that record NDVI values also record the Land Surface Temperature (LST). To evaluate temperature over the entire growing season, we summarize the LST observations as the Summer Warmth Index (SWI), the sum of mean monthly LST for months with mean temperatures above freezing (> 0°C). For the circumpolar Arctic region as a whole, SWI in 2018 was similar to the prior year and was the 6th highest in the record. In Eurasia, SWI increased sharply from the previous year and was the 2nd highest in the 37-year record, second only to 2016. In North America, however, the 2018 SWI declined sharply from 2017 and was the lowest recorded since 2009.

What are the drivers of Arctic vegetation change, and what types of change would be apparent to an observer on the ground? A growing number of long-term field studies have documented changes in vegetation and the physical environment that could account for the trends recorded by satellites (Jorgenson et al. 2015; Pattison et al. 2015; Myers-Smith et al. 2019). The productivity of tundra plants in a given year is influenced by many climatic and environmental factors, but increasing summer air temperature is widely acknowledged as the most influential driver of the long-term greening observed in many Arctic environments (Myers-Smith and Hik 2018; Pastick et al. 2019; see essay *Surface Air Temperature*). Arctic shrub expansion is a well-recognized tundra response to summer warming, particularly in moist habitats of the Low Arctic (Elmendorf et al. 2012; Myers-Smith et al. 2015; Salmon et al. 2019). On the other hand, recent reports show that increased temperatures can have disruptive effects on the phenology and growth of tundra plants (Assmann et al. 2019; Prevéy et al. 2019).

Tundra "browning" has been observed after extreme weather, such as winter thaw events (followed by abrupt cooling and desiccation) and icing (e.g., rain-on-snow); recent work in Norway suggests that such events reduce the capacity of the vegetation to sequester carbon (Treharne et al. 2019). Changes in precipitation, permafrost conditions, and soil moisture also influence tundra vegetation dynamics and are linked to the effects of air temperature changes (Lara et al. 2018; Kemppinen et al. 2019). Increased winter snow cover can also alter vegetation structure and function, in some cases countering the impact of warming (Addis and Bret-Harte 2019; Cooper et al. 2019). Ecological disturbances such as tundra fire can also cause abrupt changes in greenness over large areas (French et al. 2016); at local scales, permafrost thaw and herbivory can create "hotspots" of greening and browning (Lara et al. 2018; Pastick et al. 2019). Disparate vegetation responses to temperature and precipitation are also evident when comparing plant communities along gradients of latitude (Miles et al. 2019), elevation (Verbyla and Kurkowski 2019), soil moisture (Rocha et al. 2018), and human land-use (Chen et al. 2019; Tømmervik et al. 2019). These findings highlight the importance of understanding indirect responses to climate warming that occur at local and regional scales when interpreting Arctic NDVI trends.

References

Addis, C. E., and M. S. Bret-Harte, 2019: The importance of secondary growth to plant responses to snow in the arctic. *Funct. Ecol.*, **33**, 1050-1066.

Assmann, J. J., I. H. Myers-Smith, A. B. Phillimore, A. D. Bjorkman, R. E. Ennos, J. S. Prevéy, G. H. R. Henry, N. M. Schmidt, and R. D. Hollister, 2019: Local snow melt and temperature-but not regional sea ice-explain variation in spring phenology in coastal Arctic tundra. *Glob. Change Biol.*, **25**, 2258–2274, https://doi.org/10.1111/gcb.14639.

Bhatt, U. S., D. A. Walker, M. K. Raynolds, P. A. Bieniek, H. E. Epstein, J. C. Comiso, J. E. Pinzon, C. J. Tucker, M. Steele, W. Ermold, and J. Zhang, 2017: Changing seasonality of panarctic tundra vegetation in relationship to climatic variables. *Environ. Res. Lett.*, **12**, 055003.

Bhatt, U., D. Walker, M. Raynolds, P. Bieniek, H. Epstein, J. Comiso, J. Pinzon, C. Tucker, and I. Polyakov, 2013: Recent declines in warming and vegetation greening trends over Pan-Arctic tundra. *Remote Sens.*, **5**, 4229-4254.

Blume-Werry, G., A. Milbau, L. M. Teuber, M. Johansson, and E. Dorrepaal, 2019: Dwelling in the deep - strongly increased root growth and rooting depth enhance plant interactions with thawing permafrost soil. *New Phytol.*, **223**, 1328-1339.

Chen, C., T. Park, X. Wang, S. Piao, B. Xu, R. K. Chaturvedi, R. Fuchs, V. Brovkin, P. Ciais, R. Fensholt, H. Tømmervik, G. Bala, Z. Zhu, R. R. Nemani, and R. B. Myneni, 2019: China and India lead in greening of the world through land-use management. *Nat. Sustain.*, **2**, 122-129.

Cooper, E. J., C. J. Little, A. K. Pilsbacher, and M. A. Mörsdorf, 2019: Disappearing green: Shrubs decline and bryophytes increase with nine years of increased snow accumulation in the High Arctic. *J. Veg. Sci.*, **30**, 857-867.

Cray, H. A., and W. H. Pollard, 2018: Use of stabilized thaw slumps by Arctic birds and mammals: evidence from Herschel Island, Yukon. *Can. Field Nat.*, **132**, 279-284.

Elmendorf, S. C., G. H. R. Henry, R. D. Hollister, R. G. Björk, N. Boulanger-Lapointe, E. J. Cooper, J. H. C. Cornelissen, T. A. Day, E. Dorrepaal, T. G. Elumeeva, M. Gill, W. A. Gould, J. Harte, D. S. Hik, A. Hofgaard, D. R. Johnson, J. F. Johnstone, I. S. Jónsdóttir, J. C. Jorgenson, K. Klanderud, J. A. Klein, S. Koh, G. Kudo, M. Lara, E. Lévesque, B. Magnússon, J. L. May, J. A. Mercado-Díaz, A. Michelsen, U. Molau, I. H. Myers-Smith, S. F. Oberbauer, V. G. Onipchenko, C. Rixen, N. Martin Schmidt, G. R. Shaver, M. J. Spasojevic, Þ. E. Þórhallsdóttir, A. Tolvanen, T. Troxler, C. E. Tweedie, S. Villareal, C. -H. Wahren, X. Walker, P. J. Webber, J. M. Welker, and S. Wipf, 2012: Plot-scale evidence of tundra vegetation change and links to recent summer warming. *Nat. Climate Change*, **2**, 453-457.

French, N. H. F., M. A. Whitley, and L. K. Jenkins, 2016: Fire disturbance effects on land surface albedo in Alaskan tundra. *J. Geophys.Res.-Biogeosci.*, **12**, 841-854.

Hewitt, R. E., D. L. Taylor, H. Genet, A. D. McGuire, and M. C. Mack, 2019: Below-ground plant traits influence tundra plant acquisition of newly thawed permafrost nitrogen. *J. Ecol.*, **107**, 950-962.

Ims, R. A., J. -A. Henden, M. A. Strømeng, A. V. Thingnes, M. J. Garmo, and J. U. Jepsen, 2019: Arctic greening and bird nest predation risk across tundra ecotones. *Nat. Clim. Change*, **9**, 607-610.

Jorgenson, J. C., M. K. Raynolds, J. H. Reynolds, and A. -M. Benson, 2015: Twenty-five year record of changes in plant cover on tundra of northeastern Alaska. *Arct. Antarct. Alp. Res.*, **47**, 785-806.

Kemppinen, J., P. Niittynen, J. Aalto, P. C. le Roux, and M. Luoto, 2019: Water as a resource, stress and disturbance shaping tundra vegetation. *Oikos*, **128**, 811-822.

Kolari, T. H. M., T. Kumpula, M. Verdonen, B. C. Forbes, and T. Tahvanainen, 2019: Reindeer grazing controls willows but has only minor effects on plant communities in Fennoscandian oroarctic mires. *Arct. Antarct. Alp. Res.*, **51**, 506-520.

Lara, M. J., I. Nitze, G. Grosse, P. Martin, and A. D. McGuire, 2018: Reduced arctic tundra productivity linked with landform and climate change interactions. *Sci. Rep.-UK*, **8**, 2345.

Lucht, W., 2002: Climatic control of the high-latitude vegetation greening trend and Pinatubo effect. *Science*, **296**, 1687-1689.

Miles, M. W., V. V. Miles, and I. Esau, 2019: Varying climate response across the tundra, forest-tundra and boreal forest biomes in northern West Siberia. *Environ. Res. Lett.*, **14**, 075008.

Mörsdorf, M. A., N. S. Baggesen, N. G. Yoccoz, A. Michelsen, B. Elberling, P. L. Ambus, and E. J. Cooper, 2019: Deepened winter snow significantly influences the availability and forms of nitrogen taken up by plants in High Arctic tundra. *Soil Biol. Biochem.*, **135**, 222-234.

Mudryk, L., R. Brown, C. Derksen, K. Luojus, B. Decharme, and S. Helfrich, 2018: Terrestrial snow cover. *Arctic Report Card 2018*, E. Osborne, J. Richter-Menge, and M. Jeffries, Eds., https://www.arctic.noaa.gov/Report-Card.

Myers-Smith, I. H., S. C. Elmendorf, P. S. A. Beck, M. Wilmking, M. Hallinger, D. Blok, K. D. Tape, S. A. Rayback, M. Macias-Fauria, B. C. Forbes, J. D. M. Speed, N. Boulanger-Lapointe, C. Rixen, E. Lévesque, N. M. Schmidt, C. Baittinger, A. J. Trant, L. Hermanutz, L. S. Collier, M. A. Dawes, T. C. Lantz, S. Weijers, R. H. Jørgensen, A. Buchwal, A. Buras, A. T. Naito, V. Ravolainen, G. Schaepman-Strub, J. A. Wheeler, S. Wipf, K. C. Guay, D. S. Hik, and M. Vellend, 2015: Climate sensitivity of shrub growth across the tundra biome. *Nat. Clim. Change*, **5**, 887-891.

Myers-Smith, I. H., M. M. Grabowski, H. J. D. Thomas, S. Angers-Blondin, G. N. Daskalova, A. D. Bjorkman, A. M. Cunliffe, J. J. Assmann, J. S. Boyle, E. McLeod, S. McLeod, R. Joe, P. Lennie, D. Arey, R. R. Gordon, and C. D. Eckert, 2019: Eighteen years of ecological monitoring reveals multiple lines of evidence for tundra vegetation change. *Ecol. Monogr.*, **89**, e01351.

Myers-Smith, I. H., and D. S. Hik, 2018: Climate warming as a driver of tundra shrubline advance. R. Aerts, Ed. *J. Ecol.*, **106**, 547-560.

National Academies of Sciences, Engineering, and Medicine, 2019: Understanding northern latitude vegetation greening and browning: proceedings of a workshop. A. Melvin, Ed. The National Academies Press, Washington, DC.

Park, T., S. Ganguly, H. Tømmervik, E. S. Euskirchen, K. -A. Høgda, S. R. Karlsen, V. Brovkin, R. R. Nemani, and R. B. Myneni, 2016: Changes in growing season duration and productivity of northern vegetation inferred from long-term remote sensing data. *Environ. Res. Lett.*, **11**, 084001.

Pastick, N. J., M. T. Jorgenson, S. J. Goetz, B. M. Jones, B. K. Wylie, B. J. Minsley, H. Genet, J. F. Knight, D. K. Swanson, and J. C. Jorgenson, 2019: Spatiotemporal remote sensing of ecosystem change and causation across Alaska. *Glob. Change Biol.*, **25**, 1171-1189.

Pattison, R. R., J. C. Jorgenson, M. K. Raynolds, and J. M. Welker, 2015: Trends in NDVI and tundra community composition in the arctic of NE Alaska between 1984 and 2009. *Ecosystems*, **18**, 707-719.

Pinzon, J., and C. Tucker, 2014: A Non-stationary 1981-2012 AVHRR NDVI3g time series. *Remote Sens.*, **6**, 6929-6960.

Prevéy, J. S., C. Rixen, N. Rüger, T. T. Høye, A. D. Bjorkman, I. H. Myers-Smith, S. C. Elmendorf, I. W. Ashton, N. Cannone, C. L. Chisholm, K. Clark, E. J. Cooper, B. Elberling, A. M. Fosaa, G. H. R. Henry, R. D. Hollister, I. S. Jónsdóttir, K. Klanderud, C. W. Kopp, E. Lévesque, M. Mauritz, U. Molau, S. M. Natali, Steven. F. Oberbauer, Z. A. Panchen, E. Post, S. B. Rumpf, N. M. Schmidt, E. Schuur, P. R. Semenchuk, J. G. Smith, K. N. Suding, Ø. Totland, T. Troxler, S. Venn, C. -H. Wahren, J. M. Welker, and S. Wipf, 2019: Warming shortens flowering seasons of tundra plant communities. *Nat. Ecol. Evol.*, **3**, 45-52.

Raynolds, M. K., D. A. Walker, H. E. Epstein, J. E. Pinzon, and C. J. Tucker, 2012: A new estimate of tundra-biome phytomass from trans-Arctic field data and AVHRR NDVI. *Remote Sens. Lett.*, **3**, 403-411.

Rocha, A. V., B. Blakely, Y. Jiang, K. S. Wright, and S. R. Curasi, 2018: Is arctic greening consistent with the ecology of tundra? Lessons from an ecologically informed mass balance model. *Environ. Res. Lett.*, **13**, 125007.

Salmon, V. G., A. L. Breen, J. Kumar, M. J. Lara, P. E. Thornton, S. D. Wullschleger, and C. M. Iversen, 2019: Alder distribution and expansion across a tundra hillslope: implications for local N cycling. *Front. Plant Sci.*, **10**, 1099, https://doi.org/10.3389/fpls.2019.01099.

Schmidt, N. M., J. Reneerkens, J. H. Christensen, M. Olesen, and T. Roslin, 2019: An ecosystem-wide reproductive failure with more snow in the Arctic. *PLOS Biol.*, **17**, e3000392.

Tape, K. D., B. M. Jones, C. D. Arp, I. Nitze, and G. Grosse, 2018: Tundra be dammed: Beaver colonization of the Arctic. *Glob. Change Biol.*, **24**, 4478-4488.

Taylor, A. R., R. B. Lanctot, and R. T. Holmes, 2018: An evaluation of 60 years of shorebird response to environmental change at Utqiaġvik (Barrow), Alaska. *Trends and Traditions: Avifaunal Change in Western North America*, W. D. Shuford, R. E. Gill, and C. M. Handel, Eds., Western Field Ornithologists, 312-330, accessed 24 September 2019, http://www.wfopublications.org/Avifaunal_Change/Taylor.

Tømmervik, H., J. W. Bjerke, T. Park, F. Hanssen, and R. B. Myneni, 2019: Legacies of historical exploitation of natural resources are more important than summer warming for recent biomass increases in a boreal-arctic transition region. *Ecosystems*, **22**, 1512, https://doi.org/10.1007/s10021-019-00352-2.

Treharne, R., J. W. Bjerke, H. Tømmervik, L. Stendardi, and G. K. Phoenix, 2019: Arctic browning: Impacts of extreme climatic events on heathland ecosystem CO_2 fluxes. *Glob. Change Biol.*, **25**, 489-503.

Verbyla, D., and T. A. Kurkowski, 2019: NDVI-Climate relationships in high-latitude mountains of Alaska and Yukon Territory. *Arct. Antarct. Alp. Res.*, **51**, 397-411.

Wilcox, E. J., D. Keim, T. de Jong, B. Walker, O. Sonnentag, A. E. Sniderhan, P. Mann, and P. Marsh, 2019: Tundra shrub expansion may amplify permafrost thaw by advancing snowmelt timing. *Arct. Sci.*, https://doi.org/10.1139/as-2018-0028.

November 19, 2019

Permafrost and the Global Carbon Cycle

T. Schuur

Center for Ecosystem Science and Society, Northern Arizona University, Flagstaff, AZ, USA

Highlights

- Northern permafrost region soils contain 1,460-1,600 billion metric tons of organic carbon, about twice as much as currently contained in the atmosphere.
- This pool of organic carbon is climate-sensitive. Warming conditions promote microbial conversion of permafrost carbon into the greenhouse gases carbon dioxide and methane that are released to the atmosphere in an accelerating feedback to climate warming.
- New regional and winter season measurements of ecosystem carbon dioxide flux independently indicate that permafrost region ecosystems are releasing net carbon (potentially 0.3 to 0.6 Pg C per year) to the atmosphere. These observations signify that the feedback to accelerating climate change may already be underway.

Introduction

The Arctic continues to warm at a rate that is currently twice as fast as the global average (see essay *Surface Air Temperature*). Warming is causing perennially-frozen ground (permafrost) to thaw, with permafrost in many locations currently reaching record high temperatures (Biskaborn et al. 2019). Organic carbon contained in soils of the permafrost region represent a climate-sensitive carbon reservoir that is affected by warming air and ground temperatures and permafrost thaw. This permafrost carbon is the remnants of plants, animals, and microbes that have lived and died in tundra and boreal ecosystems, accumulating in frozen soil over hundreds to thousands of years (Schuur et al. 2008). The northern permafrost region holds almost twice as much carbon as is currently in the atmosphere. Additional net releases of carbon dioxide (CO_2) and methane (CH_4) to the atmosphere as a result of warming and faster microbial decomposition of permafrost carbon have the potential to accelerate climate warming. This report details recent advances in quantifying the amount of organic carbon stored in permafrost soils and the current exchange of CO_2 between tundra and boreal ecosystems and the atmosphere. It updates material included in an essay on the terrestrial carbon cycle that appeared in Arctic Report Card 2016 (Schuur and Hugelius, 2016).

Permafrost carbon pools: How much permafrost carbon is available to release into the atmosphere?

The new, best mean estimate of the amount of organic carbon stored in the northern permafrost region is 1,460-1,600 petagrams (Pg; 1 Pg = 1 billion metric tons) (Hugelius et al. 2014; Schuur et al. 2015). Of this inventory, 65-70% (1,035 ± 150 Pg) of the carbon is within the surface layer (0-3 m depth) (Fig. 1). Soils in the top 3 m of the rest of Earth's biomes (excluding Arctic and boreal biomes) contain 2,050 Pg of organic carbon (Jobbagy and Jackson 2000). The soil carbon from the northern circumpolar permafrost region adds another 50% to this 3-m inventory, even though it occupies only 15% of the total global soil area (Schuur et al. 2015).

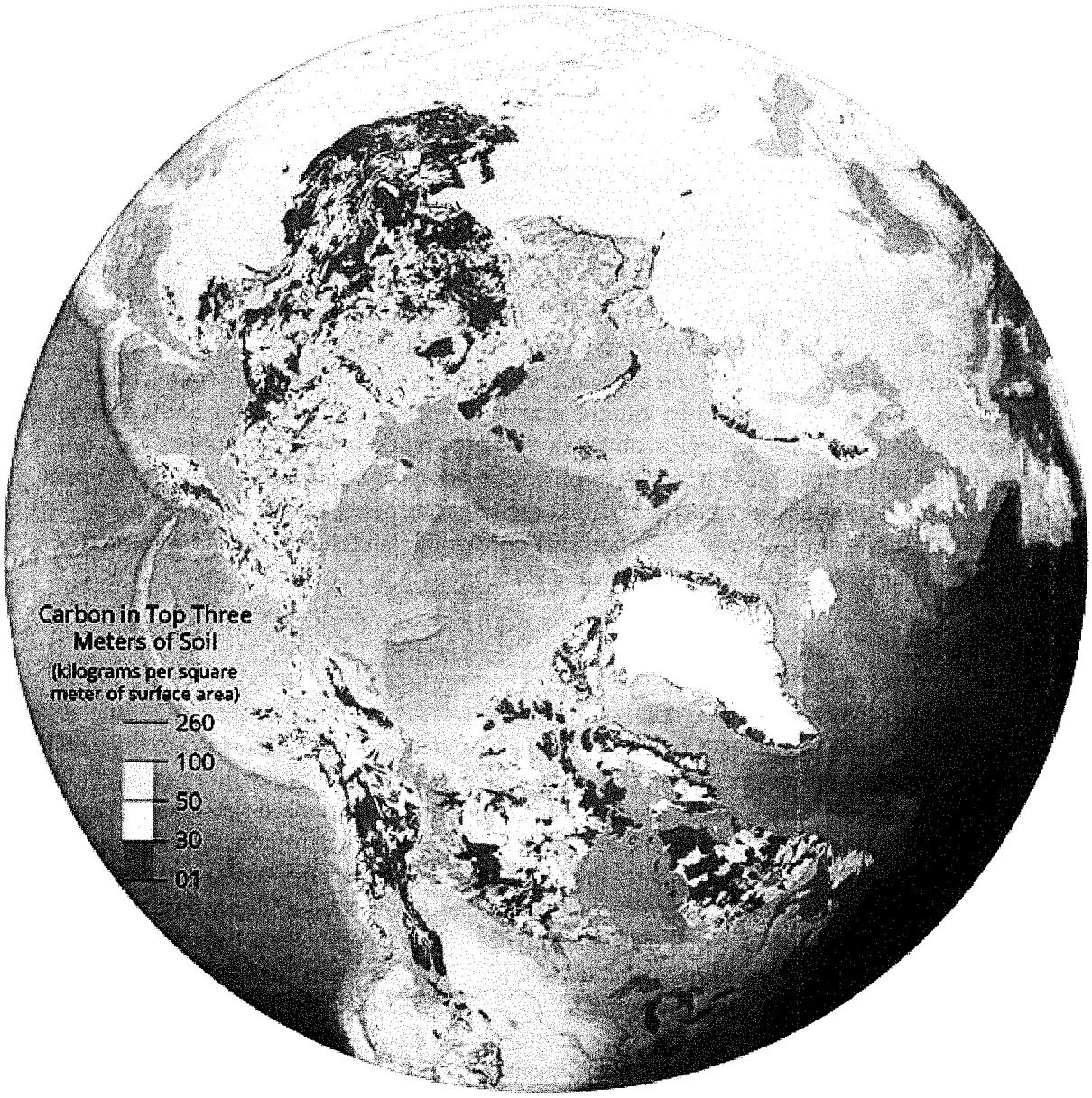

Fig. 1. Soil organic carbon pools (0-3 m depth) for the northern circumpolar permafrost region. (modified from Scientific American, November 2016) Produced by Mapping Specialists, Ltd.

A significant amount of carbon (25-30%) is also stored deeper (> 3 m depth) due to unique processes that bury carbon in permafrost region soils. In particular, the Yedoma region of Siberia and Alaska remained ice-free during the last Ice Age and accumulated silt (loess) soils, which buried large quantities of organic matter deep into the permafrost (Strauss et al. 2013). Recent work has reconciled several estimates for the Yedoma region, placing 327-466 Pg C in these deep loess deposits, which can be tens of meters thick (Schuur et al. 2018). This region contains intact Yedoma deposits that have remained primarily frozen since the last glacial period, and also deposits where abrupt permafrost thaw led to ground subsidence (**thermokarst**) and lake formation. These thermokarst lakes accumulated more carbon as lake ecosystems developed, and these deposits later re-froze into permafrost when the lakes drained (Anthony et al. 2014; Strauss et al. 2017). The remaining deep carbon accounted for in the total permafrost carbon inventory is contained in Arctic river deltas, which contain 96 ± 55 Pg C (< 10%).

Permafrost thaw occurs when a warming climate affects permafrost temperature gradually from the surface downward. At the same time, abrupt permafrost thaw, related to the destabilization of and melting of ground ice, can affect tens of meters of permafrost rapidly over a single season. As a result, the entire organic carbon inventory of surface and deep soil reported here may be vulnerable to thaw in a changing climate.

Ecosystem-atmosphere carbon exchange: Is the Arctic currently releasing additional net carbon dioxide emissions to the atmosphere?

Permafrost thaw and increased microbial decomposition releases stored organic carbon from the terrestrial biosphere into the atmosphere as greenhouse gases. At the same time, plant growth sequesters atmospheric CO_2, which becomes stored as new plant biomass or deposited as new soil organic matter. Direct and indirect effects linked to climate warming can stimulate both processes, and whether Arctic ecosystems are currently a net carbon source (losses > gains) or sink (gains > losses) is an area of intense research. Ecosystem carbon balance (net gain or loss of ecosystem carbon) is the relatively small difference between two large, opposing fluxes: plant carbon uptake via plant photosynthesis and growth versus respiratory loss via metabolism by all living organisms (Fig. 2). Across the landscape, this biological carbon cycle is then modified by relatively rapid physical disturbances, such as fire and abrupt permafrost thaw (thermokarst) that accelerate carbon losses while modifying rates of carbon gain. Carbon dioxide represents the main form, by weight, of carbon exchanged between ecosystems and the atmosphere. Methane exchange is a much smaller amount by weight than CO_2, and consequently does not greatly alter ecosystem carbon balance at the landscape scale. The larger warming potential of CH_4 means that changing emissions can affect climate, but these impacts are outside of the scope of this report.

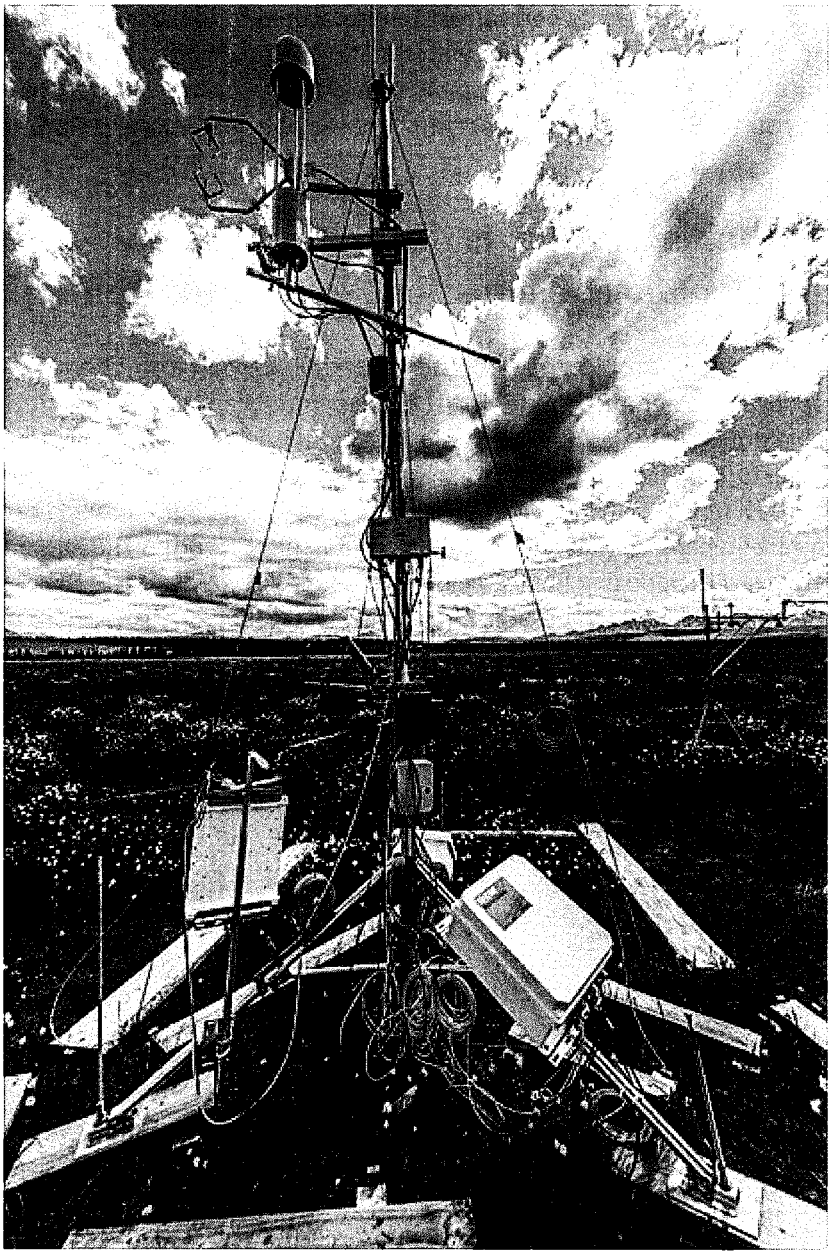

Fig. 2. Eddy covariance tower with micrometerological sensors and gas analyzers for measuring CO_2 and CH_4 concentrations used to determine the exchange of greenhouse gases between moist acidic tussock tundra and the atmosphere. This tower, located at the Eight Mile Lake research watershed near Denali National Park, Alaska, records aggregated greenhouse gas exchange over 30-minute intervals that can then be combined to determine daily, monthly, seasonal, and annual exchanges of carbon. The tower's sensing footprint is on the scale of tens to hundreds of meters from the tower, depending on windspeed and direction.

Northern tundra and boreal ecosystems typically gain carbon (**carbon sink**) stored in plant biomass and new soil organic matter during the short summer growing season when plant photosynthesis and growth is greater than carbon respired by plants and soil back to the atmosphere. In any given year, individual ecosystems can have gains or losses in net carbon due to changes in the physical and biological environment (Treat et al. 2018), and also depending on the successional stage of the

ecosystem, but what matters to future climate is the aggregate response across the regions over years to decades.

Previous efforts to synthesize ecosystem carbon balance focused on CO_2 flux measurements have produced results that have not agreed. For instance, a study that scaled plot CO_2 flux measurements to regional land area reported a net annual carbon exchange in the tundra region of 0.013 Pg C per year (i.e., a small **sink** but near neutral exchange) over the 1990s and 2000s (McGuire et al. 2012). A follow-up study focused on a subset of the same tundra sites and also included new sites with additional non-summer data to bolster the under-sampled cold season (Belshe et al. 2013). The second study supported the previous finding that the summer-season carbon sink increased in the 2000s compared with the 1990s. However, the second study also suggested that the mean tundra flux remained a carbon source annually across both decades when additional non-summer flux data were included. When scaled to a similar-sized region, the second study predicted that the tundra was acting as a current source of 0.462 Pg C per year. One potential explanation for the difference between these two comprehensive synthesis studies was the inclusion (in the former), and exclusion (in the latter) of fluxes measured in wetland ecosystems. Wetlands generally store more carbon in anaerobic soils, and typically act as annual net carbon sinks even while CH_4 is emitted (Lund et al. 2010). This differential response of individual ecosystem types and the relative scarcity of measurement sites across the Arctic region continue to make it difficult to upscale to the aggregate effect of ecosystems' greenhouse gas exchange on the atmosphere.

Another approach to this same question is to measure changes in atmospheric greenhouse gas concentrations and to separate out contributions from different sources. Given the extent of fossil fuel carbon emissions, it remains a challenge to quantify and separate the effect of ecosystem carbon exchange, but regional atmospheric measurement campaigns can help to focus in on local influences (Parazoo et al. 2016). Recent measurements of atmospheric greenhouse gas concentrations over Alaska by NASA aircraft have been used to the estimate the net regional impact on the atmosphere by those Arctic and boreal ecosystems for 2012 to 2014 (Commane et al. 2017). This recent NASA campaign was able to provide important insight into the aggregate influence of the carbon exchange for the Alaska permafrost region, across tundra, boreal forests, and wetland/lake/freshwater ecosystems as a whole. During this three-year time period, the tundra region of Alaska was found to be a consistent net CO_2 source to the atmosphere, whereas the boreal forest region was either neutral or a net CO_2 sink. The boreal forest region exhibited larger interannual variability due both to changes in the balance of photosynthesis and respiration and to the amount of combustion emissions by wildfire.

The Alaska study region as a whole was estimated to be a net carbon source of 0.025 ± 0.014 Pg C per year averaged over the land area of both tundra and boreal forest regions for the three-year study period. If this Alaskan region (1.6×10^6 km^2) was representative of the entire northern circumpolar permafrost region soil area (17.8×10^6 km^2), this amount would be equivalent to a circumpolar net **source** of 0.3 Pg C per year. Historically (over hundreds to thousands of years), the Arctic region was accumulating carbon in soils and vegetation and thus was acting as a net sink of atmospheric CO_2. Assuming this three-year snapshot provided by NASA aircraft monitoring is indicative of the Arctic's current physical and biological environment, a significant and major threshold has been crossed in the high latitude region whereas the aggregate effect of terrestrial ecosystems is now contributing to, rather than slowing, climate change.

Aircraft measurements of atmospheric greenhouse gas concentrations help to describe the combined regional impact of changing permafrost region ecosystems. However, the long cold Arctic winter (or

non-summer) season limits observations from the air, just as it has limited ground-based observations in the past due to the difficult operating conditions. For example, the NASA aircraft campaign made atmospheric measurements from April through November only. In one of the recent synthesis studies of ground-based measurements, the regional carbon balance estimate for the North American subregion, for example, had 80 study-years of summer measurements and only 9 study-years of non-summer measurements available for upscaling (McGuire et al. 2012). The summer growing season is typically a time when net carbon is stored within growing ecosystems acting as a seasonal carbon sink. However, summer carbon sequestration is partially offset by carbon losses in fall, winter, and spring when microbes remain metabolically active and release CO_2 during a period where plants are largely dormant. While absolute levels of CO_2 flux are low during the non-summer season, the long period of more than 250 days can be enough to offset the net carbon that accumulated during summer.

A new comprehensive synthesis study of non-summer ecosystem CO_2 fluxes across the circumpolar region showed that carbon release during the Arctic winter was 2 to 3 times higher than previously estimated from ground-based measurements (Fig. 3) (Natali et al. 2019). This circumpolar estimate suggests that carbon release in the cold season offsets net carbon uptake during the growing season (derived from models) such that the region as a whole could already be a source of 0.6 Pg C per year to the atmosphere. It was not possible to determine whether these higher flux estimates were a result of changing environmental conditions or the aggregation of more observations during this scarcely observed non-summer period. Regardless, similar to the regional extrapolation made by aircraft, this winter flux synthesis supports the idea that the accelerating feedback from changing permafrost ecosystems to climate change may already be underway.

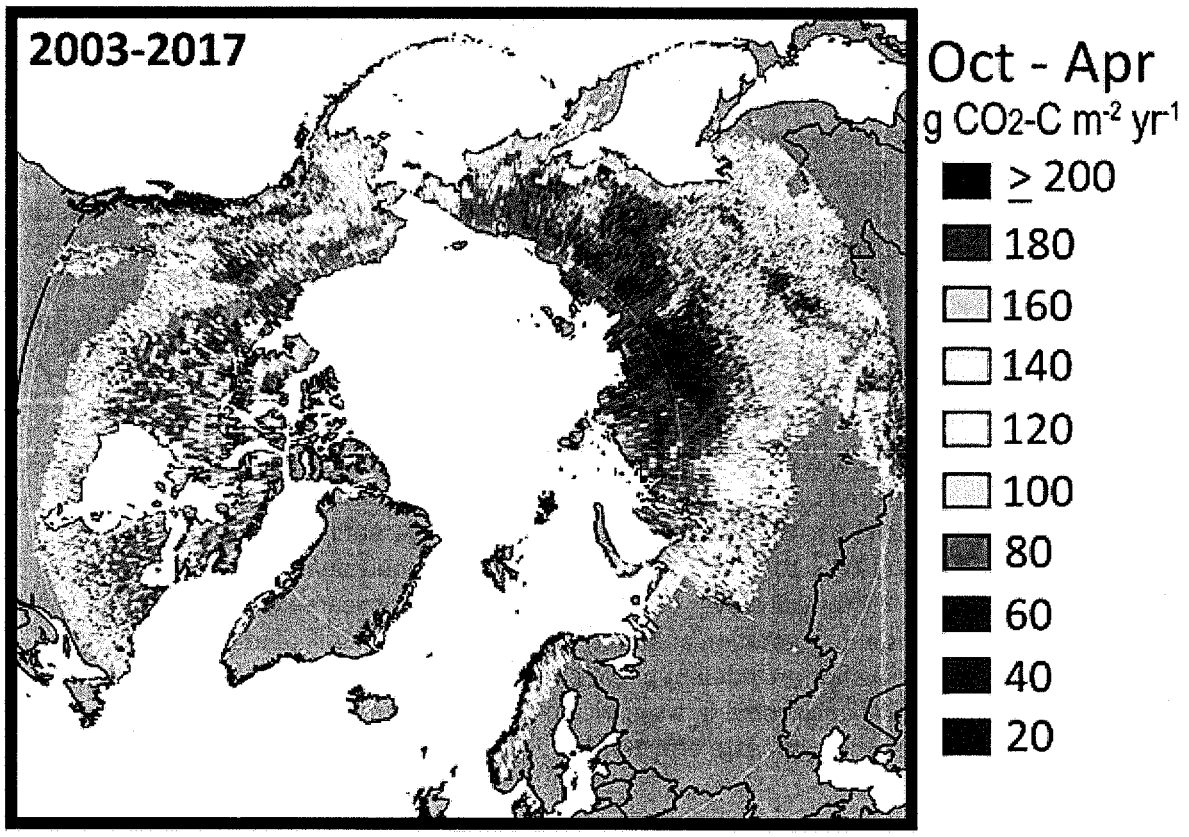

Fig. 3. Non-summer season CO_2 flux rates for the permafrost region, synthesized from individual study sites measured between 2003 and 2017 and extrapolated using environmental variables.

References

Anthony, K. M. W., and Coauthors, 2014: A shift of thermokarst lakes from carbon sources to sinks during the Holocene epoch. *Nature*, **511**, 452, https://doi.org/10.1038/Nature13560.

Belshe, F. E., A. G. Schuur, and B. M. Bolker, 2013: Tundra ecosystems observed to be carbon dioxide sources due to differential amplification of the carbon cycle. *Ecol. Lett.*, https://doi.org/10.1111/ele.12164.

Biskaborn, B. K., and Coauthors, 2019: Permafrost is warming at a global scale. *Nat. Commun.*, **10**(1), 264, https://doi.org/10.1038/s41467-018-08240-4.

Commane, R., and Coauthors, 2017: Carbon dioxide sources from Alaska driven by increasing early winter respiration from Arctic tundra. *P. Natl. Acad. Sci. USA*, **114**(21), 5361-5366, https://doi.org/10.1073/pnas.1618567114.

Hugelius, G., and Coauthors, 2014: Estimated stocks of circumpolar permafrost carbon with quantified uncertainty ranges and identified data gaps. *Biogeosciences*, **11**, 6573-6593, https://doi.org/10.5194/bg-11-6573-2014.

Jobbágy, E. G., and R. B. Jackson, 2000: The vertical distribution of soil organic carbon and its relation to climate and vegetation. *Ecol. Appl.*, **10**(2), 423-436, https://doi.org/10.1890/1051-0761(2000)010[0423:TVDOSO]2.0.CO;2.

Lund, M., and Coauthors, 2010: Variability in exchange of CO_2 across 12 northern peatland and tundra sites. *Glob. Change Biol.*, **16**(9), 2436-2448, https://doi.org/10.1111/j.1365-2486.2009.02104.x.

McGuire, A. D., T. R. Christensen, D. Hayes, A. Heroult, E. Euskirchen, J. S. Kimball, C. Koven, P. Lafleur, P. A. Miller, W. Oechel, P. Peylin, M. Williams, and Y. Yi, 2012: An assessment of the carbon balance of Arctic tundra: Comparisons among observations, process models, and atmospheric inversions. *Biogeosciences*, **9**(8), 3185-3204, https://doi.org/10.5194/bg-9-3185-2012.

Natali, S., and Coauthors, 2019: Large loss of CO_2 in winter observed across pan-Arctic permafrost region. *Nat. Climate Change*, **9**, 852-857, https://doi.org/10.1038/s41558-019-0592-8.

Parazoo, N. C., R. Commane, S. C. Wofsy, C. D. Koven, C. Sweeney, D. M. Lawrence, J. Lindaas, R. Y. -W. Chang, and C. E. Miller, 2016: Detecting regional patterns of changing CO_2 flux in Alaska. *P. Natl. Acad. Sci. USA*, **113**(28), 7733-7738, https://doi.org/10.1073/pnas.1601085113.

Schuur, E. A. G., and Coauthors, 2008: Vulnerability of permafrost carbon to climate change: Implications for the global carbon cycle. *Bioscience*, **58**, 701-714.

Schuur, E. A. G., and Coauthors, 2015: Climate change and the permafrost carbon feedback. *Nature*, **520**, 171-179, https://doi.org/10.1038/nature14338.

Schuur, E. A. G., and Coauthors, 2018: Chapter 11: Arctic and boreal carbon. In: Second State of the Carbon Cycle Report (SOCCR2): A Sustained Assessment Report, Cavallaro, N., G. Shrestha, R. Birdsey, M. A. Mayes, R. G. Najjar, S. C. Reed, P. Romero-Lankao, and Z. Zhu, Eds., U.S. Global Change Research Program, Washington, DC, USA, 428-468.

Schuur, T., and G. Hugelius, 2016: Terrestrial carbon cycle. *Arctic Report Card 2016,* J. Richter-Menge, J. E. Overland, and J. Mathis, Eds. http://www.arctic.noaa.gov/Report-Card.

Strauss, J., L. Schirrmeister, G. Grosse, S. Wetterich, M. Ulrich, U. Herzschuh, and H. -W. Hubberten, 2013: The deep permafrost carbon pool of the Yedoma region in Siberia and Alaska. *Geophys. Res.Lett.*, **40**, 6165-6170, https://doi.org/10.1002/2013gl058088.

Strauss, J., L. Schirrmeister, G. Grosse, D. Fortier, G. Hugelius, C. Knoblauch, V. Romanovsky, C. Schädel, T. Schneider von Deimling, E. A. G. Schuur, D. Shmelev, M. Ulrich, and A. Veremeeva, 2017: Deep Yedoma permafrost: A synthesis of depositional characteristics and carbon vulnerability. *Earth-Sci. Rev.*, **172**, 75-86, https://doi.org/10.1016/j.earscirev.2017.07.007.

Treat, C. C., M. E. Marushchak, C. Voigt, Y. Zhang, Z. Tan, Q. Zhuang, T. A. Virtanen, A. Räsänen, C. Biasi, G. Hugelius, D. Kaverin, P. A. Miller, M. Stendel, V. Romanovsky, F. Rivkin, P. J. Martikainen, and N. J. Shurpali, 2018: Tundra landscape heterogeneity, not interannual variability, controls the decadal regional carbon balance in the Western Russian Arctic. *Glob. Change Biol.*, **24**, 5188-5204, https://doi.org/10.1111/gcb.14421.

November 22, 2019

Ivory Gull: Status, Trends and New Knowledge

H. Strøm[1], D. Boertmann[2], M. V. Gavrilo[3], H. G. Gilchrist[4], O. Gilg[5], M. Mallory[6], A. Mosbech[2], and G. Yannic[5,7]

[1]Norwegian Polar Institute, Fram Centre, Tromsø, Norway
[2]Department of Bioscience, Arctic Research Centre, Roskilde, Denmark
[3]Association "Maritime Heritage: Explore & Sustain", St. Petersburg, Russia
[4]Environment Canada, Ottawa, ON, Canada
[5]Groupe de Recherche en Ecologie Arctique (GREA), Francheville, France
[6]Acadia University, Wolfville, NS, Canada
[7]Université Grenoble Alpes, CNRS, Université Savoie Mont Blanc, LECA, Laboratoire d'Écologie Alpine, Grenoble, France

Highlights

- The breeding population of ivory gull in the Arctic is **declining** in parts of its range. Especially dramatic is the situation in Canada, where 70% of the population has been lost since the 1980s.
- Satellite tracking of ivory gulls breeding in Canada, Greenland, Svalbard and Russia show that southern **Davis Strait and northern Labrador Sea** is an internationally significant wintering area for the species.
- Levels of **contaminants** in eggs, blood and feathers of the ivory gull are among the highest ever reported in arctic seabirds and may have **sub-lethal effects** in combination with other stressors.
- Studies on genetics in the ivory gull show **low population structure**, implying that conservation planning needs to consider ivory gulls as a **genetically homogeneous**, Arctic-wide metapopulation.

Introduction

The ivory gull (*Pagophila eburnea*) is a high-arctic seabird associated with sea ice throughout the year. It breeds at high latitudes, mostly in the Atlantic sector of the Arctic. Mainly small (i.e., 5 to 200 pairs), scattered colonies are found in Arctic Canada, Greenland, Svalbard and the northern islands of Russia in the Barents and Kara seas (Fig. 1). Ivory gulls breed on steep cliffs and inland nunataks (rocky outcrops emerging from icecaps), on flat, gravel-covered areas near coasts (Fig. 2) or on small islands and even gravel-covered ice floes. The species feeds on ice-associated fauna, primarily small fish and macro-zooplankton, and on remains of marine mammals killed by polar bear (Mallory et al. 2008). Migration between the high-arctic breeding grounds and the more southerly wintering areas takes place along the sea ice edge. Due to its reliance on sea ice for hunting, the ivory gull rarely moves far from sea ice. The species is listed as Near Threatened by the International Union for Conservation of Nature (IUCN), recognizing global warming and pollution as major threats (BirdLife International 2018). An international circumpolar "Conservation Strategy and Action Plan" has been presented by the Arctic Council to gain more insight into how this bird responds to increases in the disappearance of sea ice habitat, natural resource exploration and development and increases in contaminants (Gilchrist et al. 2008).

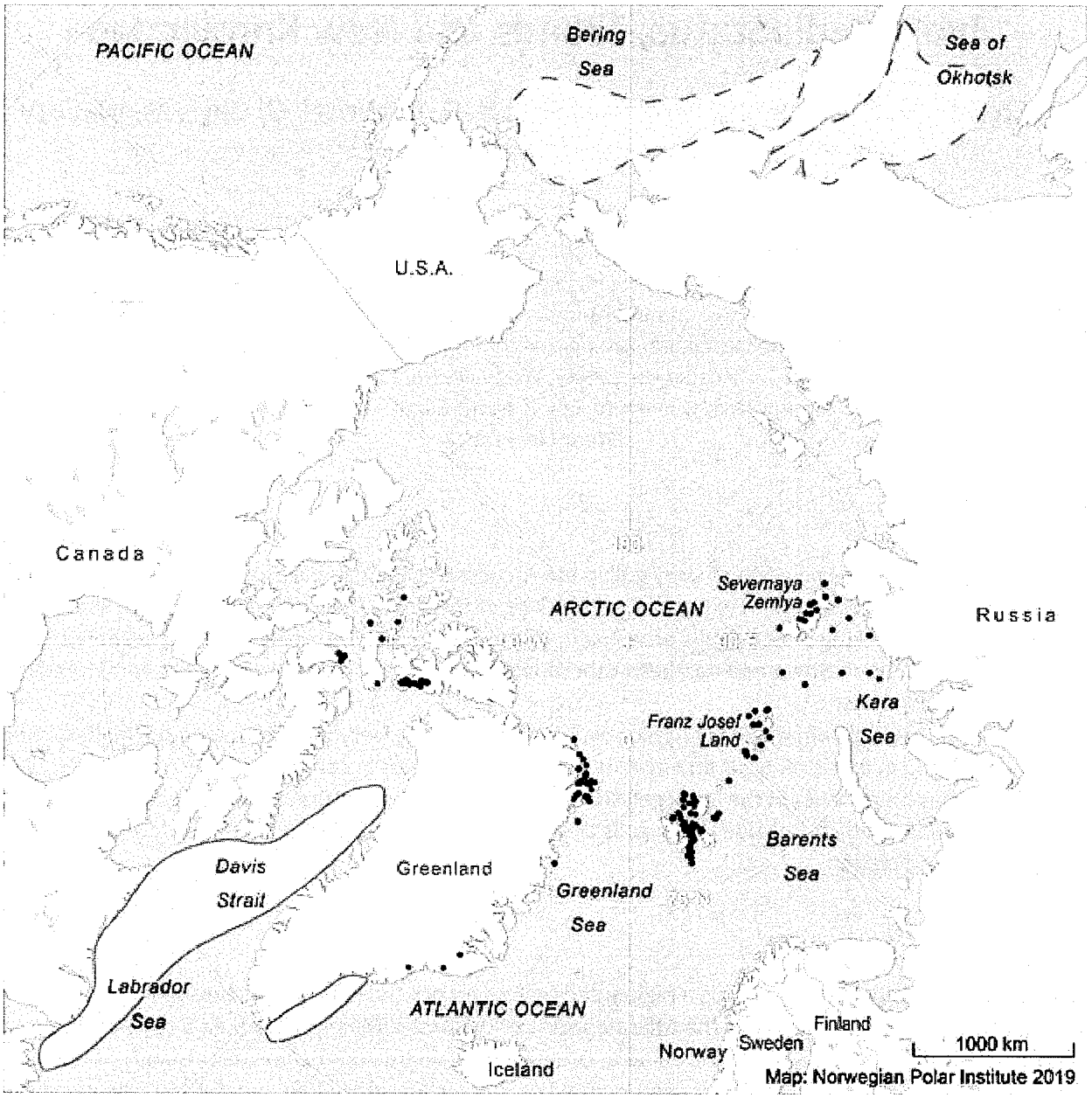

Fig. 1. The distribution of known ivory gull breeding colonies occupied for one or more years since year 2000 (shown here as black circles). Wintering areas are shown in light grey. Source: Circumpolar Seabird Group (CBird).

Fig. 2. Ivory gull breeding colony, Severnaya Zemlya, Russia. Photo: Alexey Lokhov.

Population Status

In 2008, the Circumpolar Seabird Group (CBird) of the Arctic Council's CAFF (Conservation of Arctic Flora and Fauna) Working Group estimated the total population of ivory gulls to be 6,325-11,500 breeding pairs (Gilchrist et al. 2008). Most occur at colonies in Arctic Russia (approx. 86% of the global population). The remaining populations are more or less equally distributed between Canada, Greenland and Svalbard. The population size is difficult to assess because breeding colonies are not consistently occupied each year and because some sites may still be unknown.

The breeding population of ivory gulls is declining in at least parts of its global range. The Canadian population has declined by 70% since the 1980s at colonies that were known before 2002 (Gilchrist and Mallory 2005; Gaston et al. 2012). The reason for this decline is an area of current active research but could be related to loss of sea ice due to climate change, contaminants and illegal harvesting in Greenland during migration. The Greenland population seems to be declining in the south of its breeding range, while in the north the trends are unclear (Gilg et al. 2009). In Greenland, unusual climate events, such as very wet (rain) storms, have been shown to cause breeding failure (Yannic et al. 2014). For Svalbard, the long-term population trend is difficult to assess as historical data are scarce, but annual surveys since 2009 show a decline (Strøm 2013). Surveys conducted in the Russian Arctic in 2006-08 and incidental observations from colonies in subsequent years infer stable populations in some key colonies and no signs of an overall decline (Gavrilo and Martynova 2017). However, more recent observations in the 2010s revealed multiple events of colony abandonment or breeding failure. One possible reason is increased colony depredation by polar bears. Both the IUCN and the OSPAR-commission urge for new population surveys in all countries to better assess the status of the species and the true magnitude of decline.

Migration routes and wintering areas

While the ivory gull has long been known to winter along the southern edge of the arctic pack ice in the waters of the North Atlantic Ocean, recent results from satellite tagging of breeding birds from Canada, Greenland, Svalbard and Russia have revealed that the Davis Strait and Labrador Sea is the key wintering area for the species, at least for the Atlantic breeding populations (Spencer et al. 2014; Gilg et al. 2016) (Fig. 1). Birds from Russia (Franz Josef Land), Svalbard and Greenland aggregate in a post-breeding area along the ice-edge north of Svalbard and Franz Josef Land, and as far east as Severnaya Zemlya, before migrating along the East Greenland ice-edge to winter in Labrador and the Davis Strait (Gilg et al. 2010). Here they mix with birds from Canadian colonies (Spencer et al. 2016), making the southern Davis Strait and northern Labrador Sea an internationally significant wintering area for the species. The Bering and Okhotsk Seas also seem to be important wintering areas for the easternmost breeding population in Russia and for some Greenland and Norwegian birds, but more tracking is necessary to confirm this (Gilg et al. 2010).

Contamination

As a top-predator and scavenger, the ivory gull is vulnerable to exposure to contaminants that concentrate through the food chain (biomagnifying contaminants). The levels of persistent organic pollutants (POPs) including organochlorine pesticides (OCPs) and polychlorinated biphenyls (PCBs), and a heavy metal (mercury (Hg)) in ivory gulls are among the highest ever reported in arctic seabirds (Braune et al. 2006; Miljeteig et al. 2009; Lucia et al. 2015). Concentrations are not thought to be at high enough levels to cause direct mortality, but there is a threat from combined effects that are likely to have a sub-lethal effect. This has been shown in other seabird species, with similar and higher contaminant levels, with effects on parental behaviour, endocrine distribution and neurological functions, as well as to potential reproductive disruptions (Miljeteig et al. 2012; Lucia et al. 2016). The concentration of methyl mercury in feathers of Canadian birds increased by a factor of 45 during 1877-2007 (Bond et al. 2015). Mercury can have wide-ranging deleterious effects on birds. Being bioavailable, Hg levels are expected to increase in the Arctic due to global warming (Krabbenhoft and Sunderland 2013). Hence, there is concern about population effects in high-latitude species such as the ivory gull, even though such species live far from the sources of such environmental contaminants (Bond et al. 2015).

Ivory gull genetics

The ability to cope with rapid habitat changes through distribution shifts or adaptation to new conditions depends on both evolutionary and demographic processes (i.e., plasticity, adaptation or migration). The level of genetic variance within a population can directly influence the outcome of a response to environmental change by providing the necessary genetic variation upon which selection can act (Bourne et al. 2014). Until recently, the population structure of the ivory gull and the degree of connectivity between the different breeding populations was virtually unknown. Based on mitochondrial DNA-samples from museum specimens, Royston and Carr (2014) found no strong population structure, except among the birds wintering in the Pacific that probably originated from the easternmost breeding population in the Kara Sea and Severnaya Zemlya. Using a population genetic model and based on samples from 343 individuals from 16 localities across the breeding range, Yannic et al. (2016) similarly found a high degree of genetic homogeneity of ivory gulls across their entire distribution range, but with sufficient genetic diversity to maintain a genetically healthy population. The lack of population genetic

structure suggests there is an effective dispersal across the Arctic region and implies that conservation planning needs to consider ivory gulls as a genetically homogeneous, Arctic-wide metapopulation (Yannic et al. 2016), with the potential to recover from other areas.

References

BirdLife International, 2018: *Pagophila eburnea*. The IUCN Red List of Threatened Species 2018: e.T22694473A132555020. https://doi.org/10.2305/IUCN.UK.2018-2.RLTS.T22694473A132555020.en. Downloaded on 10 September 2019.

Bond, A. L., K. A. Hobson, and B. A. Branfireun, 2015: Rapidly increasing methyl mercury in endangered ivory gull (*Pagophila eburnea*) feathers over a 130 year record. *Proc. R. Soc. B-Biol. Sci.*, **282**(1805), 20150032, https://doi.org/10.1098/rspb.2015.0032.

Bourne, E. C., G. Bocedi, J. M. J. Travis, R. J. Pakeman, R. W. Brooker, and K. Schiffers, 2014: Between migration load and evolutionary rescue: dispersal, adaptation and the response of spatially structured populations to environmental change. *Proc. R. Soc. B-Biol. Sci.*, **281**, 20132795.

Braune, B. M., M. L. Mallory, and H. G. Gilchrist, 2006: Elevated mercury levels in a declining population of ivory gulls in the Canadian Arctic. *Mar. Pollut. Bull.*, **52**(8), 978-982.

Gaston, A. J., M. L. Mallory, and G. H. Gilchrist, 2012: Populations and trends of Canadian Arctic seabirds. *Polar Biol.*, **35**(8), 1221-1232.

Gavrilo, M. V., and D. M. Martynova, 2017: Conservation of rare species of marine flora and fauna of the Russian Arctic National Park, included in the Red Data Book of the Russian Federation and in the IUCN Red List. *Nat. Conserv. Res.*, **2**(Suppl. 1), 10–42, https://doi.org/10.24189/ncr.2017.01 (in Russian with English summary).

Gilchrist, G., and M. L. Mallory, 2005: Declines in abundance and distribution of the ivory gull (*Pagophila eburnea*) in Arctic Canada. *Biol. Conserv.*, **121**, 303-309.

Gilchrist, G., H. Strøm, M. V. Gavrilo, and A. Mosbech, 2008: International Ivory Gull Conservation Strategy and Action Plan. Circumpolar Seabird Group (CBird). CAFF (Conservation of Arctic Flora and Fauna) Technical Report No. 18. 20 pp.

Gilg, O., D. Boertmann, F. Merkel, A. Aebischer, and B. Sabard, 2009: Status of the endangered ivory gull, *Pagophila eburnea*, in Greenland. *Polar Biol.*, **32**, 1275-1286.

Gilg, O., H. Strøm, A. Aebischer, M. Gavrilo, A. Volkov, C. Miljeteig, and B. Sabard, 2010: Post-breeding movements of northeast Atlantic ivory gull *Pagophila eburnea* populations. *J. Avian Biol.*, **41,** 532-542.

Gilg, O., L. Istomina, G. Heygster, H. Strøm, M. V. Gavrilo, M. L. Mallory, G. Gilchrist, A. Aebischer, B. Sabard, M. Huntemann, A. Mosbech, A., and G. Yannic, 2016: Living on the edge of a shrinking habitat: the ivory gull, *Pagophila eburnea*, an endangered sea-ice specialist. *Biol. Lett.*, **12**, 20160277, https://doi.org/10.1098/rsbl.2016.0277.

Krabbenhoft D. P., and E. M. Sunderland, 2013: Global change and mercury. *Science*, **341**, 1457-1458, https://doi.org/10.1126/science.1242838.

Lucia, M., N. Verboven, H. Strøm, C. Miljeteig, M. V. Gavrilo, B. M. Braune, D. Boertmann, and G. W. Gabrielsen, 2015: Circumpolar contamination in eggs of the high-arctic ivory gull *Pagophila eburnea*. *Environ. Toxicol. Chem.*, **34** (7), 1552-1561.

Lucia, M., H. Strøm, P. Bustamante, and G. W. Gabrielsen, 2016: Trace element accumulation in relation to the trophic behaviour of endangered ivory gulls (*Pagophila eburnea*) during their stay at a breeding site in Svalbard. *Arch. Environ. Contam. Toxicol.*, **71**(4), 518-529, https://doi.org/10.1007/s00244-016-0320-6.

Mallory M. L., I. J. Stenhouse, G. Gilchrist , G. Robertson, J. C. Haney, and S. D. Macdonald, 2008: Ivory gull (*Pagophila eburnea*). *The Birds of North America Online*, A. Poole, Ed., Cornell Lab of Ornithology, Ithaca, accessed 11 February 2014. http://bna.birds.cornell.edu/BNA/species/175/

Miljeteig, C., H. Strøm, M. G. Gavrilo, A. Volkov, B. M. Jenssen, and G. W. Gabrielsen, 2009: High levels of contaminants in ivory gull *Pagophila eburnea* eggs from the Russian and Norwegian Arctic. *Environ. Sci. Tech.*, **43**(14), 5521-5528.

Miljeteig, C., G. W. Gabrielsen, H. Strøm, M. V. Gavrilo, E. Lie, and B. M. Jensen, 2012: Eggshell thinning and decreased concentrations of vitamin E are associated with contaminants in eggs of ivory gulls. *Sci. Total Environ.*, **431**, 92-99.

Royston, S., and S. M. Carr, 2014: Conservation genetics of high-arctic Gull species at risk: I. Diversity in the mtDNA control region of circumpolar populations of the Endangered Ivory Gull (*Pagophila eburnea*). *Mitochondrial DNA*, **27**(6), 3995-3999, https://doi.org/10.3109/19401736.2014.989520.

Spencer, N. C., H. G. Gilchrist, and M. L. Mallory, 2014: Annual movement patterns of endangered ivory gulls: The importance of sea ice. *PLoS ONE*, **9**(12), e115231, https://doi.org/10.1371/journal.pone.0115231.

Spencer, N. C., G. H. Gilchrist, H. Strøm, K. A. Allard, and M. L. Mallory, 2016: Key winter habitat of the ivory gull *Pagophila eburnea* in the Canadian Arctic. *Endanger. Species Res.*, **31**, 33-45, https://doi.org/10.3354/esr00747.

Strøm, H., 2013: Birds of Svalbard. *Birds and Mammals of Svalbard*, K. M. Kovacs and C. Lydersen, Eds., Polarhåndbok No. 13, Norwegian Polar Institute, 86-191. https://www.npolar.no/en/species/ivory-gull/.

Yannic, G., A. Aebischer, B. Sabard, and O. Gilg, 2014: Complete breeding failures in ivory gull following unusual rainy storms in North Greenland. *Polar Res.*, **33**, 22749.

Yannic, G., J. M. Yearsley, R. Sermier, C. Dufresnes, O. Gilg, A. Aebischer, M. Gavrilo, H. Strøm, M. Mallory, R. I. G. Morrison, H. G. Gilchrist, and T. Broquet, 2016: High connectivity in a long-lived high-Arctic seabird, the ivory gull *Pagophila eburnea*. *Polar Biol.*, **39**(2), 221-236, https://doi.org/10.1007/s00300-015-1775-z.

December 3, 2019

Comparison of Near-bottom Fish Densities Show Rapid Community and Population Shifts in Bering and Barents Seas

J. T. Thorson[1], M. Fossheim[2], F. J. Mueter[3], E. Olsen[4], R. R. Lauth[1], R. Primicerio[5], B. Husson[2], J. Marsh[3], A. Dolgov[6,7,8], and S. G. Zador[1]

[1]Alaska Fisheries Science Center, NOAA, Seattle, WA, USA
[2]Institute of Marine Research, Tromsø, Norway
[3]College of Fisheries and Ocean Sciences, University of Alaska Fairbanks, Juneau, AK, USA
[4]Institute of Marine Research, Bergen, Norway
[5]University of Tromsø, Tromsø, Norway
[6]Polar Branch of the Federal State Budget Scientific Institution "Russian Federal Research Institute of Fisheries and Oceanography" (PINRO), Murmansk, Russia
[7]Federal State Educational Institution of Higher Education "Murmansk State Technical University" (FSEI HE MSTU), Murmansk, Russia
[8]Tomsk State University, Tomsk, Russia

Highlights

- The northern edge of distribution for fishes associated with the Bering Sea shelf (e.g., walleye pollock and Pacific cod) shifted northward from 2010 to 2017/18.
- The spatial distribution of boreal fishes in the Barents Sea in 2017 resembles their distribution in 2012, showing a northward shift relative to their previous distribution in 2004.
- In both Bering and Barents Seas, recent shifts are associated with changes in bottom water temperature and loss of sea ice.
- Density estimates for individual species show that responses vary among species, and boreal species can maintain high densities in southern habitats even during shifts in the northward edge of distribution.

Introduction

Marine populations are expected to remain within their preferred thermal conditions, and therefore to shift their spatial distributions to track changes in ocean temperatures (Pinsky et al. 2013). Many different indicators show changes in Arctic physical conditions, with an increased rate of change from 2005 to present day (Overland et al. 2019). Given these rapid physical changes and expected responses of marine populations to changing thermal conditions, the spatial distribution of Arctic and subarctic fish communities will likely be a sensitive indicator for contemporary and ongoing Arctic climate change.

Here we present changes in the fish communities of the Bering and Barents Seas during 2017/18 relative to baseline conditions 10-15 years earlier. This involves mapping shifts in the spatial distribution of boreal (southern) and Arctic (northern) fish communities in each ecosystem, as well as identifying indicator species associated with each community. The Bering Sea has shown substantial and rapidly warming ocean temperatures and associated decreases in the thickness and extent of sea ice from 1982

to 2019, with pronounced changes occurring since 2014, while the sea surface temperature trends in the Barents Sea are varied both spatially and seasonally (see essay *Sea Surface Temperature*). Fish populations in both the Bering and Barents Seas are expected to expand into new areas in a warming climate if certain pre-conditions are met, including suitable bottom topography, water temperatures, salinities and distance to spawning grounds (Hollowed et al. 2013). The patterns and rates of documented shifts are species-specific and tend to follow temperature gradients (Pinsky et al. 2013), although observed shifts have trailed behind and are sometimes poorly correlated with the actual rates of climate shifts (Alabia et al. 2018).

Bering Sea community shifts

On the shallow Bering Sea shelf, the summer distribution of fishes and invertebrates living near the sea floor (i.e., demersal fishes) is tied to the extent of the cold pool (bottom temperatures < 2°C) as determined by the southern extent of sea ice during the preceding winter (Mueter and Litzow 2008). Until recently, there was a general expectation that sea ice would continue to persist throughout the winter over the shallow northern Bering Sea and Chukchi Sea shelf, limiting the northward expansion of boreal species (Stabeno et al. 2012). However, latent heat from the warm conditions of summer 2016, combined with less sea-ice formation in the 2017 winter, resulted in an extensive but narrow cold pool on the eastern Bering Sea shelf during summer 2017 (see essay *Recent Warming in the Bering Sea*). This created a wide corridor within the shallow continental shelf for species to move northward, as observed with dramatic increases of Pacific cod, *Gadus macrocephalus*, walleye pollock, *G. chalcogrammus* and several flatfish species into the northern Bering Sea (Stevenson and Lauth 2019). A delayed freeze-up in the Chukchi Sea and unusual southerly winds resulted in near-complete lack of sea ice in the northern Bering Sea the following winter, in 2018. Maximum sea-ice extent subsequently reached the lowest levels on record in 2019 (see essay *Recent Warming in the Bering Sea*).

We identify shifts in distribution for four assemblages in the eastern and northern Bering Sea (Fig. 1), and also identify indicator species that are associated with each assemblage (Table 1). Boreal groundfish were observed again in the northern Bering Sea during the 2018 summer (Duffy-Anderson et al. 2019; Stabeno et al. 2019). Although shifts in these large, abundant species are more apparent, Arctic taxa tend to be more sensitive to habitat changes. Arctic cod (*Boregadus saida*) in particular can serve as a sentinel species that responds quickly to changes in temperature and ice extent (Alabia et al. 2018; Marsh and Mueter 2019). Changes in individual species result in community-level changes (Fig. 1) that reflect a transition from a 'Northern Shelf' (Arctic) community dominated by relatively few, smaller and less abundant species with Arctic affinities to a community dominated by larger boreal species. In particular, the Arctic and northern shelf community is represented by butterfly sculpin, *Hemilepidotus papilio*, and Bering flounder, *Hippoglossoides robustus* (see Table 1 for full list), and this community retreated northward from 2010 to 2018. This Arctic community was then replaced by the southern shelf community represented by northern rock sole, *Lepidopsetta polyxystra*, and sturgeon poacher, *Podothecus accipenserinus* (i.e., comparing the spatial distribution of light and dark blue in Fig. 1).

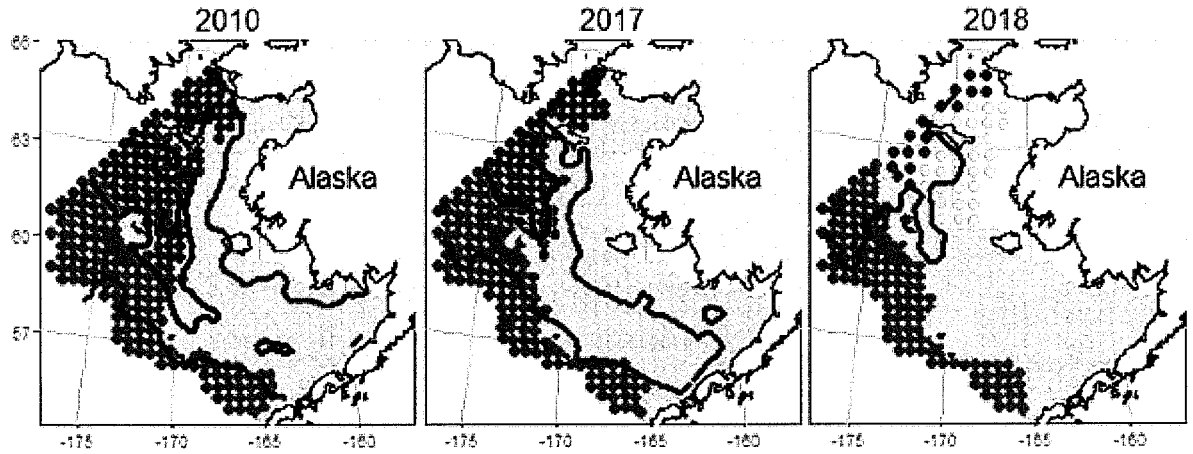

Fig. 1. Major fish assemblages identified in the eastern Bering Sea, including two boreal assemblages on the southern shelf (light blue) and in the outer shelf/slope region (green), as well as a mixed Norton Sound (light green) and an Arctic / northern shelf assemblage (dark blue). Contours denote -1°C (black) and 3°C (red) isotherms of bottom temperature. Assemblages are based on Ward's minimum variance clustering of pairwise Bray-Curtis distances among 1463 hauls sampled during summer trawl surveys. Bray-Curtis distances were computed from fourth-root transformed catch-per-unit-effort (kg/ha) of 44 common demersal fish and macroinvertebrate species.

Table 1. Indicator species associated with each of four fish communities in the Bering Sea; shifts in spatial distribution for these communities are mapped in Fig. 1. Species are shown that have a statistically significant association ($p < 0.001$) for each community, following methods in Dufrêne and Legendre (1997). Only species for which specificity exceeds 0.5 and group fidelity exceeds 0.2 are shown.

Community	**Species**	
	Scientific Name	Common Name
Boreal: outer shelf / slope	*Atheresthes evermanni*	Kamchatka flounder
	Atheresthes stomias	arrowtooth flounder
	Lycodes brevipes	shortfin eelpout
	Hippoglossoides elassodon	flathead sole
	Hemitripterus bolini	bigmouth sculpin
	Icelus spiniger	thorny sculpin
	Chionoecetes bairdi	tanner crab
	Bathyraja interrupta	sandpaper skate
	Glyptocephalus zachirus	rex sole
	Reinhardtius hippoglossoides	Greenland halibut/turbot
	Leptagonus frenatus	sawback poacher
Boreal: southern shelf	*Lepidopsetta polyxystra*	Northern rock sole
	Podothecus accipenserinus	sturgeon poacher

Community	Species	
	Paralithodes camtschaticus	red king crab
Norton Sound	*Eleginus gracilis*	saffron cod
	Myoxocephalus jaok	plain sculpin
	Platichthys stellatus	starry flounder
	Limanda proboscidea	longhead dab
	Gymnocanthus pistilliger	threaded sculpin
	Telmessus cheiragonus	helmet crab
	Lumpenus fabricii	slender eelblenny
Arctic: northern shelf	*Hemilepidotus papilio*	butterfly sculpin
	Liparis gibbus	variegated snailfish
	Limanda sakhalinensis	Sakhalin sole
	Hippoglossoides robustus	Bering flounder
	Boreogadus saida	Arctic cod
	Lycodes raridens	marbled eelpout
	Myoxocephalus verrucosus	warty eelpout

Barents Sea community shifts

In the Barents Sea, the warming ocean temperatures and retraction of the sea ice was concurrent with a northeastward displacement of Arctic fish (Fig. 2). This region includes three communities: Arctic (represented by Arctic cod, *Boreogadus saida* and bigeye sculpin, *Triglops nybelini*), boreal (represented by haddock, *Melanogrammus aeglefinus* and saithe, *Pollachius virens*) and a transition community (see Table 2 for full list of species associated with each community). The decreasing extent of Arctic water masses was associated with a northward shift in the transition zone separating Arctic and boreal fish communities from 2004 to 2012 (Fossheim et al. 2015a,b). During these years, the southern (boreal) fish community gradually expanded northward while the northern (Arctic) community retracted (Fossheim et al. 2015a,b). In 2017 the Arctic fish communities continued to have a displaced spatial distribution similar to 2012; there was neither a recovery to previous distributions (like 2004), nor a further displacement (beyond 2012). The boreal community includes large-bodied generalist feeders. These species took advantage of favorable conditions in the Barents Sea, both by increasing in abundance (demography) and by expanding their distribution (behavior). By contrast, many Arctic species are small-sized bottom-associated specialists and their spatial distribution has retracted to smaller areas in the northeast. We hypothesize that new areas for boreal species opened as Arctic waters warmed and primary and secondary production increased (see essay *Arctic Ocean Primary Productivity*). These changes likely favored the boreal generalists competitively over the arctic specialists. In some cases, the larger predatory species (i.e., boreal fish) might also exert feeding pressure on the smaller benthivore species (i.e., Arctic fish).

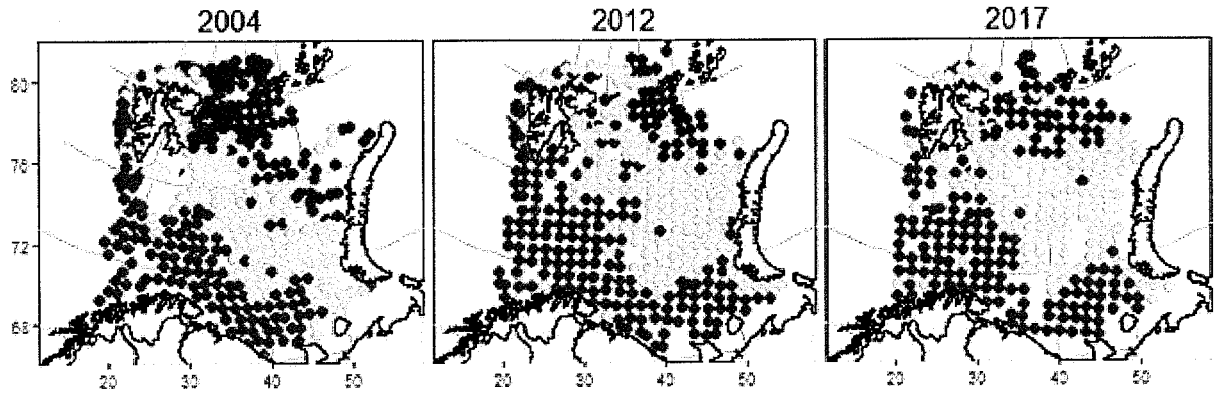

Fig. 2. Major fish assemblages identified in the Barents Sea, showing a boreal (dark green), mixed (light green) and Arctic (blue) assemblage. Fish assemblage classification of 1199 hauls, sampled during summer trawl surveys, was based on log transformed catch-per-unit-effort data for 66 demersal fish taxa. The classification was obtained using linear discriminant functions trained on 2004 fish assemblages identified via Ward's minimum variance clustering of Bray-Curtis dissimilarities.

Table 2. Indicator species associated with each of three estimated fish communities in the Barents Sea; shifts in spatial distribution for these communities are mapped in Fig. 2. See Table 1 caption for details.

Community	**Species**	
	Scientific Name	Common Name
Boreal	*Melanogrammus aeglefinus*	Haddock
	Micromesistius poutassou	blue whiting
	Sebastes mentella	deepwater redfish
	Amblyraja radiata	thorny skate
	Sebastes norvegicus	golden redfish
	Trisopterus esmarkii	Norway pout
	Anarhichas minor	spotted wolffish
	Pollachius virens	saithe
Mixed	*Leptoclinus maculatus*	daubed shanny
	Lumpenus lampretaeformis	snakeblenny
	Triglops murrayi	moustache sculpin
Arctic	*Triglops nybelini*	bigeye sculpin
	Boreogadus saida	Arctic cod
	Liparidae spp.	snailfish spp.
	Reinhardtius hippoglossoides	Greenland halibut/turbot
	Icelus spp.	sculpin spp.

Single-species analyses

We next illustrate these same patterns for individual, large-bodied species in each region. For walleye pollock and Pacific cod in the eastern Bering Sea, northward shifts in distribution are clearly apparent between bottom-trawl surveys occurring first in 2010 and repeated in 2017 and 2018 (Fig. 3a-f). Hotspots of increased density for Pacific cod are apparent south of St. Lawrence Island (63° N -170° W) and for walleye pollock along the limits of the Russian exclusive economic zone near the Bering Strait (64° N -172° W) in 2017/18. The locations of these hotspots along the northern portion of the Bering Sea have contributed to a rapid northward shift in the population centroid for these and other commercially important species (e.g., northern rock sole, *Lepidopsetta polyxystra*, see Stevenson and Lauth (2019)). Distribution shifts in the Barents Sea are also apparent by comparing densities of Atlantic cod and haddock in the summer bottom-trawl survey from 2003 with surveys in 2017/18 (Fig. 3g-l). For example, Atlantic cod show increased densities in the central Barents Sea (75° N 35° E) while haddock show increased densities near Bear Island (75° N 19° E). These species-specific results show that the areas with the greatest changes vary from species to species. These results also show that northward shifts can occur even while population densities for boreal species remain high within the southern portion of their range, e.g., elevated estimates of walleye pollock density near Unimak Island (65° N -165° W) in 2010 and 2018 (Fig. 3a,c).

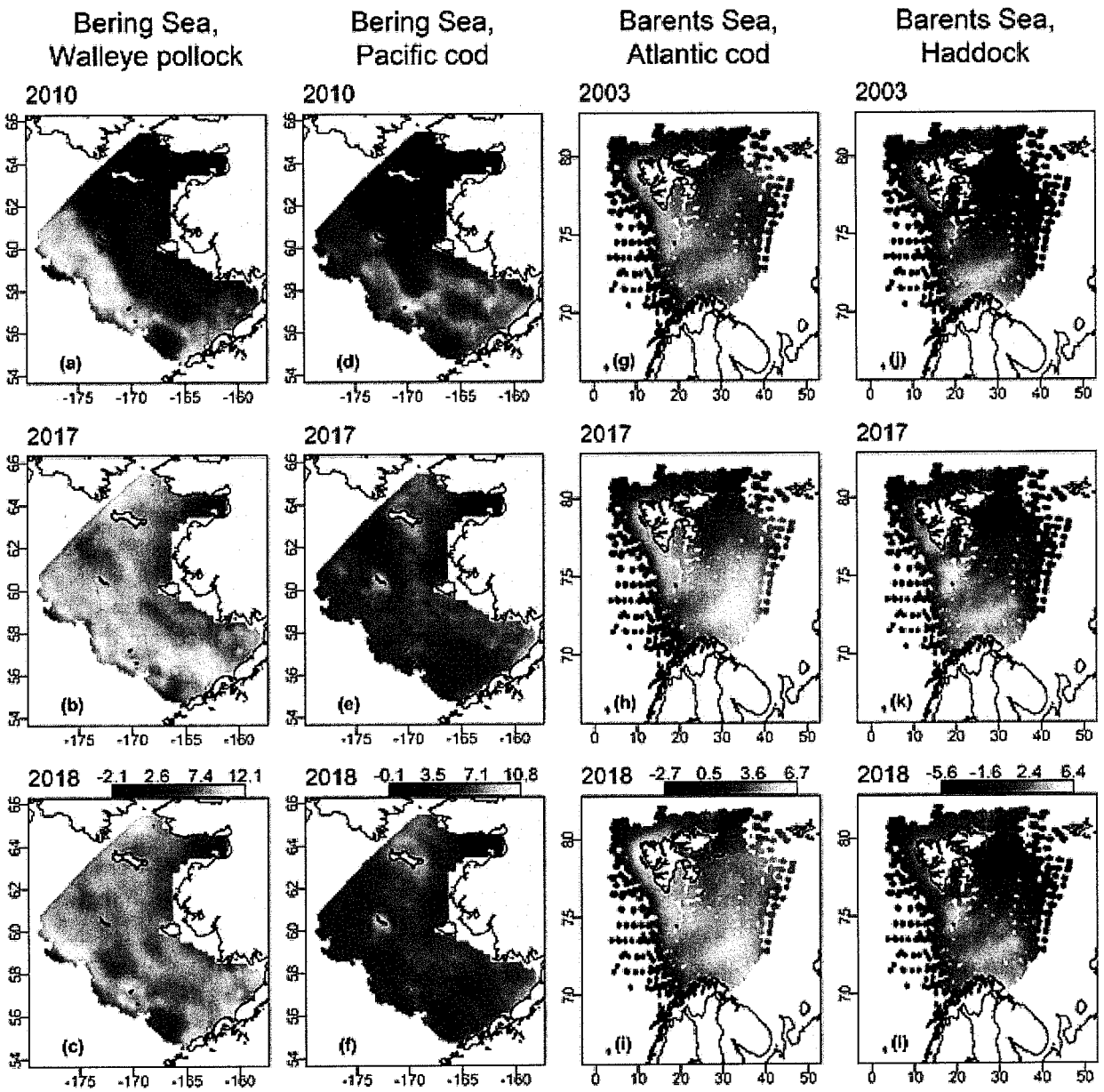

Fig. 3. Visualization of density estimates for Pacific cod and walleye pollock in the eastern and northern Bering Sea (EBS) shelf in 2010, 2017 and 2018 (a-f), and Atlantic cod and haddock in Barents Sea (BS) summer survey in 2003, 2017 and 2018 (g-l); see colorbar in bottom row for each species, with units of natural-logarithm of biomass per area. Years are chosen to show the first year with sampling data spanning the full spatial domain, as well as the two most recent years available at the time of analysis. Estimates are generated using a spatio-temporal delta-model (Thorson 2019) applied to all years of data for each species individually, and predicting density within the footprint of the survey (EBS) or for all locations within 20 km of any survey observation (BS). We estimate density at 500 modeled locations, which are distributed in proportion to the spatial area being estimated, and using bilinear interpolation to predict densities between modeled locations. The models for the EBS shelf estimate the magnitude of first-order autoregression among years in the spatio-temporal term.

Consequences for Arctic ecosystems

In the Bering Sea, the expansion of nearshore ('Norton Sound') and southern shelf species into the northern Bering Sea is likely to have profound effects on the benthic ecology of the northern Bering Sea, due to an increase in demersal fish biomass by several orders of magnitude (Stevenson and Lauth 2019). The observed high densities of fish in Bering Strait suggest that boreal species may shift their summer feeding migrations into the Chukchi Sea, which has also shown large decreases in summer sea-ice extent (see essay *Sea Ice*). Movement northward into the Chukchi Sea highlights the need for additional fisheries surveys north of Bering Strait, ongoing monitoring of benthic ecosystem components in the northern Bering and Chukchi seas, as well as synthesis of data from the western portion of the Bering Sea within Russian waters. In the Barents Sea, fish communities shifted rapidly from 2004 to 2012, and then remained relatively stable from 2012 to 2017. Increasing water temperatures opened new feeding habitats in the Barents Sea for Atlantic cod and haddock. So far, these species have been benefiting from the effects of climate change on the Barents Sea. These recent bottom-trawl surveys suggest that the spatial distributions of fish communities in the Barents Sea are stable for the moment at a new state, associated with warmer waters, less sea ice, and northward displacement of boreal species. However, different processes drive density changes in leading (northern) and trailing (southern) edges of species distribution (Pinsky et al. 2020), and contemporary warming could still result in future (lagged) changes. We encourage further comparison between climate-driven distribution shifts for these Atlantic and Pacific gateways to the Arctic. In particular, we note the importance of separating mechanisms occurring on the leading (northward) edges where populations are colonizing new habitats, relative to trailing (southward) edges where populations are likely to be extirpated from existing habitat given future warming.

Acknowledgments

We thank the many scientists who have contributed to these long-term surveys of the eastern and northern Bering Sea, and the Barents Sea. We also thank L. Britt, L. Barnett, E. Yasumiishi, and three anonymous reviewers for comments on an earlier draft.

References

Alabia, I. D., J. G. Molinos, S. -I. Saitoh, T. Hirawake, T. Hirata, and F. J. Mueter, 2018: Distribution shifts of marine taxa in the Pacific Arctic under contemporary climate changes. *Divers. Distrib.*, **24**, 1583-1597, https://doi.org/10.1111/ddi.12788.

Duffy-Anderson, J. T., and Coauthors, 2019: Responses of the northern Bering Sea and southeastern Bering Sea pelagic ecosystems following record-breaking low winter sea ice. *Geophys. Res. Lett.*, **46**(16), 9833-9842, https://doi.org/10.1029/2019GL083396.

Dufrêne, M., and P. Legendre, 1997: Species assemblages and indicator species: The need for a flexible asymmetrical approach. *Ecol. Monogr.*, **67**, 345-366, https://doi.org/10.1890/0012-9615(1997)067[0345:SAAIST]2.0.CO;2.

Fossheim, M., R. Primicerio, E. Johannesen, R. B. Ingvaldsen, M. M. Aschan, and A.V. Dolgov, 2015a: Climate change is pushing boreal fish northwards to the Arctic: The case of the Barents Sea. *Arctic*

Report Card 2015, M. O. Jeffries, J. Richter-Menge, and J. E. Overland, Eds., https://www.arctic.noaa.gov/Report-Card.

Fossheim, M., R. Primicerio, E. Johannesen, R. B. Ingvaldsen, M. M. Aschan, and A.V. Dolgov, 2015b: Recent warming leads to a rapid borealization of fish communities in the Arctic. *Nat. Climate Change*, **5**, 673-677, https://doi.org/10.1038/nclimate2647.

Hollowed, A. B., and Coauthors, 2013: Projected impacts of climate change on marine fish and fisheries. *ICES J. Mar. Sci.*, **70**, 1023-1037, https://doi.org/10.1093/icesjms/fst081.

Marsh, J. M., and F. J. Mueter, 2019: Influences of temperature, predators, and competitors on polar cod (*Boreogadus saida*) at the southern margin of their distribution. *Polar Biol.*, https://doi.org/10.1007/s00300-019-02575-4.

Mueter, F.J., and M. A. Litzow, 2008: Sea ice retreat alters the biogeography of the Bering Sea continental shelf. *Ecol. Appl.*, **18**, 309-320, https://doi.org/10.1890/07-0564.1.

Overland, J. E., M. Wang, and J. E. Box, 2019: An integrated index of recent pan-Arctic climate change. *Environ. Res. Lett.*, **14**, 035006, https://doi.org/10.1088/1748-9326/aaf665.

Pinsky, M. L., B. Worm, M. J. Fogarty, J. L Sarmiento, and S. A. Levin, 2013: Marine taxa track local climate velocities. *Science*, **341**, 1239-1242.

Pinsky, M. L., R. L. Selden, and Z. J Kitchel, 2020 (in press): Climate-driven shifts in marine species ranges: Scaling from organisms to communities. *Annu. Rev. Mar. Sci.*, **12**, https://doi.org/10.1146/annurev-marine-010419-010916.

Stabeno, P. J., E. V. Farley Jr., N. B. Kachel, S. Moore, C. W. Mordy, J. M. Napp, J. E. Overland, A. I. Pinchuk, and M. F. Sigler, 2012: A comparison of the physics of the northern and southern shelves of the eastern Bering Sea and some implications for the ecosystem. *Deep-Sea Res. Pt. II*, **65-70**, 14-30, https://doi.org/10.1016/j.dsr2.2012.02.019.

Stabeno, P. J., S. W. Bell, N. A. Bond, D. G. Kimmel, C. W. Mordy, and M. E. Sullivan, 2019: Distributed biological observatory region 1: Physics, chemistry and plankton in the northern Bering Sea. *Deep Sea Res. Pt. II*, **162**, 8-21, https://doi.org/10.1016/j.dsr2.2018.11.006.

Stevenson, D. E., and R. R. Lauth, 2019: Bottom trawl surveys in the northern Bering Sea indicate recent shifts in the distribution of marine species. *Polar Biol.*, **42**, 407-421, https://doi.org/10.1007/s00300-018-2431-1.

Thorson, J. T., 2019: Guidance for decisions using the Vector Autoregressive Spatio-Temporal (VAST) package in stock, ecosystem, habitat and climate assessments. *Fish. Res.*, **210**, 143-161, https://doi.org/10.1016/j.fishres.2018.10.013.

November 19, 2019

Recent Warming in the Bering Sea and Its Impact on the Ecosystem

P. J. Stabeno[1], R. L. Thoman[2], and K. Wood[1,3]

[1]Pacific Marine Environmental Laboratory, NOAA, Seattle, WA, USA
[2]International Arctic Research Center, University of Alaska Fairbanks, Fairbanks, AK, USA
[3]Joint Institute for the Study of the Atmosphere and Ocean, University of Washington, Seattle, WA, USA

Highlights

- There has been a marked decrease in sea-ice extent in the Bering Sea during the last two years.
- Record-breaking warm ocean temperatures occurred in 2019 on the southern Bering shelf, while bottom temperatures on the northern Bering shelf exceeded 4°C for the first time in November 2018.
- Loss of sea ice and increasing ocean temperatures have impacted the Bering Sea ecosystem, including northward migration of fish species.

The Bering Sea is the third largest semi-enclosed sea in the world and forms the transition between the subarctic North Pacific Ocean and the Arctic Ocean (Fig. 1). The western half of the sea consists of a basin (<3500 m depth) and a narrow (<100 km wide) shelf along the Russian coast south of Cape Navarin. The eastern half of the sea is a broad (~500 km) shelf stretching >1100 km northward from the Alaska Peninsula. This article focuses on the eastern shelf, which has an exceptionally productive ecosystem, supporting large numbers of seabirds and marine mammals, subsistence harvests for native communities across Alaska, and more than 40% of the annual U.S. catch of fish and shellfish (valued at > $1 billion annually). Sea ice is a critical factor in structuring this ecosystem. For the past two winters (2018 and 2019), maximum sea-ice extent in the Bering Sea has been at record lows, less than half of the long-term mean (1980-2010). These highly visible declines in sea ice occurred against a background of long-term warming and ice volume loss across the Arctic (see essay *Sea Ice*; Kwok 2018).

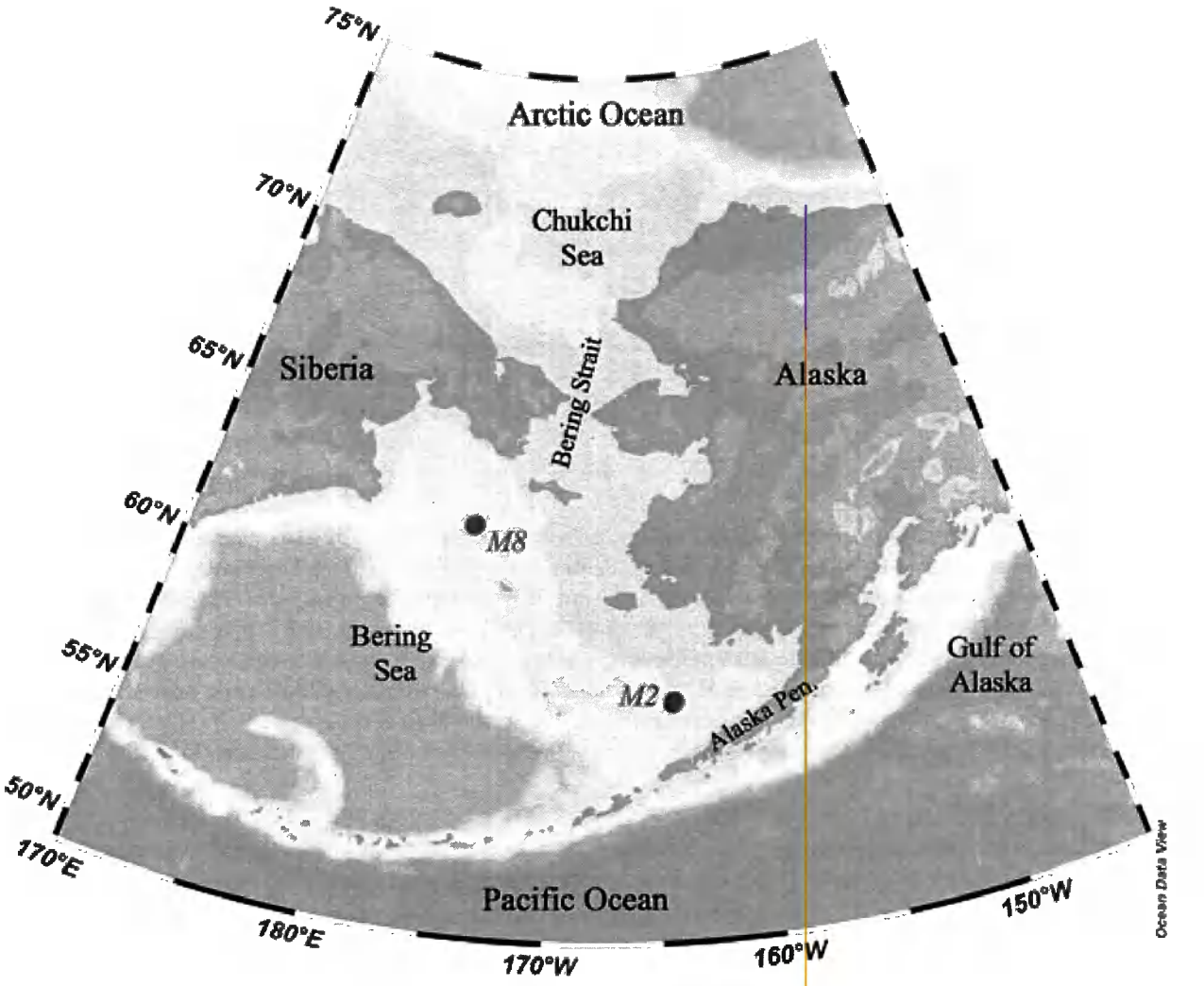

Fig. 1. Map of the Bering Sea, with location of the mooring sites indicated in red.

Historically, the eastern Bering Sea shelf (EBS; that region east of 178° E) has been seasonally ice-covered. The highest maximum sea-ice extent in the region, during the satellite era (1979-present), was 1.1×10^6 km^2 on 21 March 2012. The lowest maximum sea-ice extent (3.8×10^5 km^2) occurred just six years later on 17 March 2018 (Stabeno and Bell 2019). Maximum areal ice cover in winter 2019 was more extensive (4.9×10^5 km^2) than the 2018 record and occurred almost two months earlier on 25 January (Fig. 2a). The sea-ice extent in January 2019 was near average, but the ice was thin (Thompson 2018; Stabeno and Bell 2019). This thinness is attributable to: (1) late ice arrival (approximately a month later than usual) and its rapid advancement; and (2) warmer-than-average water temperatures (>0°C; Fig. 2b) in the northern Bering Sea (NBS) at mooring M8, which melted the bottom of ice floes and thus limited the thickness of the ice.

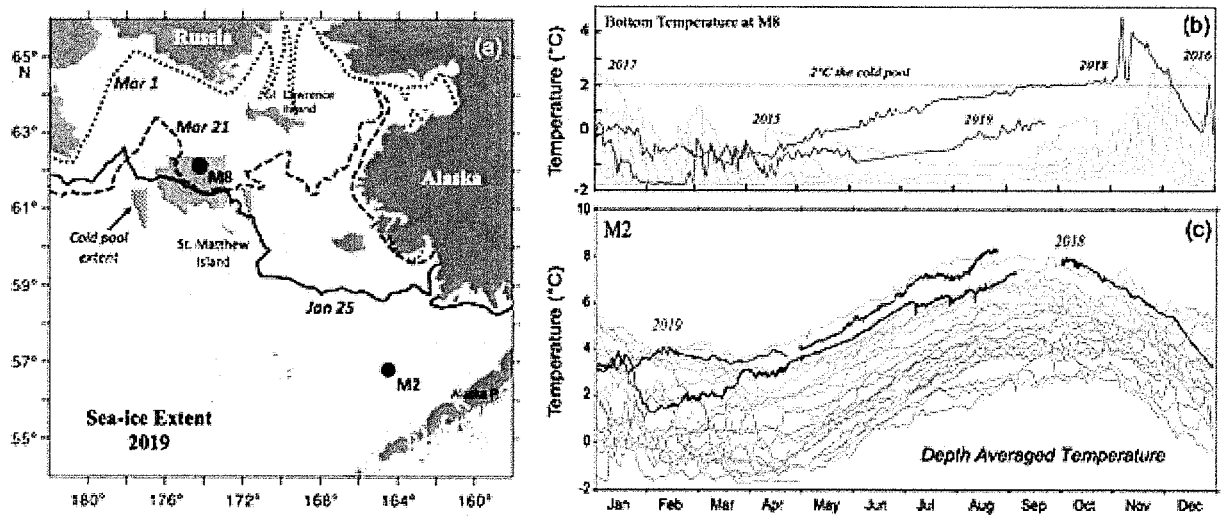

Fig. 2. (a) Sea-ice extent in the Bering Sea in 2019 for 25 January, 1 March, and 21 March derived from satellite passive microwave data (National Snow and Ice Data Center, http://nsidc.org/data). The shaded (dotted) area around M8 is the areal extent of the cold pool (<2°C bottom temperatures); data were collected by the National Marine Fisheries Service bottom trawl surveys (L. Britt, AFSC, personal communication). (b) Near-bottom temperatures measured from 2005 to 2019 at mooring site M8. (c) Depth-averaged temperature at M2 each year (1995 to 2019). The gray lines represent years when sea-ice cover was extensive in March and April at the mooring site and yellow indicates years when there was virtually no sea ice (<5% areal coverage on any given day) at the mooring site in March and April. Depth-averaged temperature in 2018 and 2019 are indicated in red.

In late January 2019 wind patterns changed and a series of five strong, warm cyclones entered the Bering Sea (Fig. 3), breaking up the thin ice and driving it northward. Minimum winter sea-ice extent in the EBS occurred in early March (Fig. 2a). From late January to early March, areal ice cover was reduced by 82% (a retreat of 4.0×10^5 km^2), the largest percent retreat ever observed in the satellite record during January or February. The absolute magnitude of ice retreat was second only to 1989 (4.2×10^5 km^2), a year that had one of the most extensive January ice covers on record (1979-2019). The large ice retreat in winter 2019 was primarily a result of a >30 day period of warm, southerly winds. In mid-March 2019 the winds reversed and once again came out of the north, driving the ice southward (Fig. 2a). Consequently, the sea-ice extent recovered somewhat, but remained relatively low through the rest of the season (e.g., Mar 21 in Fig. 2a).

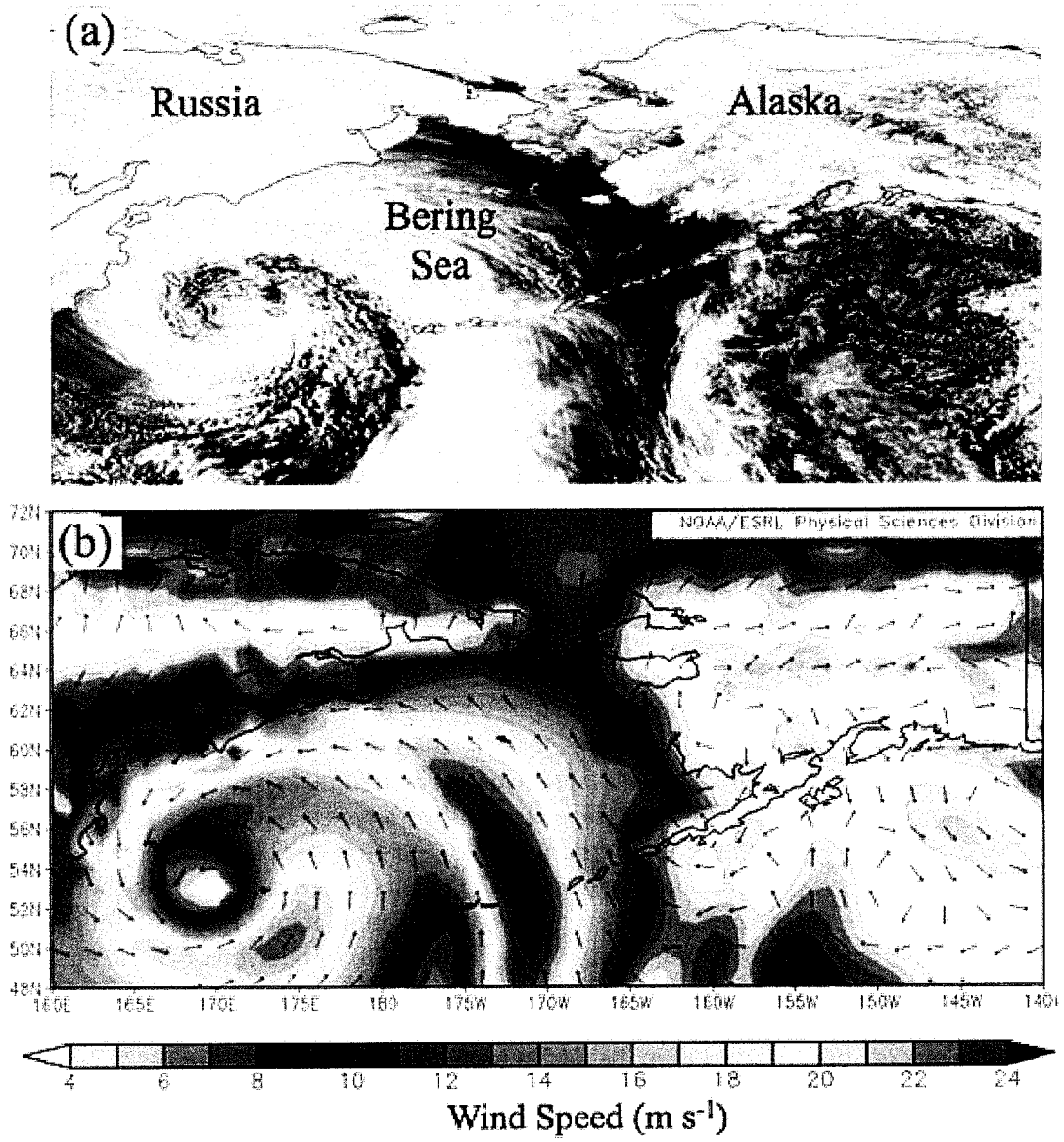

Fig. 3. (a) Satellite view of a strong cyclone in the Bering Sea on 2-3 March 2019 from NASA Worldview, and (b) its associated wind field from the North American Regional Reanalysis (NARR; Mesinger et al. 2006). This was one of a series of cyclones that affected the sea ice in the Bering Sea in late February and March 2019 by bringing strong, southerly winds and warmer temperatures to the region. During this period, air temperatures were 12-16°C above normal across the northern Bering Sea.

Sea-ice extent and timing of ice retreat have important impacts on the Bering Sea ecosystem. Depth-averaged water temperature was calculated at M2, a long-term (1995-2019) ecosystem mooring on the southern Bering Sea shelf (Fig. 2a). Ice extent at M2 in March-April is the primary determinant of ocean temperature for the following summer (Stabeno et al. 2012). Years with sea ice (>5% areal cover in the 50 km × 50 km box around M2) in March-April (gray lines; Fig. 2c) are characterized by cold ocean temperatures, while years with little-or-no sea ice (yellow lines) are characterized by warm water. The years with the warmest ocean temperatures (2016 and 2019) followed extremely warm years (2015 and

2018, respectively). That is, some heat from 2015 and 2018 persisted through the winter, providing warmer starting conditions for summer heating in 2016 and 2019, respectively.

Prior to 2016, the NBS (defined as north of 60° N) had extensive and persistent sea ice and bottom temperatures that remained <2°C throughout the year. In December 2016 and January 2017, bottom temperatures rose to above 2°C because of the late arrival of sea ice (Fig. 2b). Winds mixed the summer surface heat vertically, and the lack of cooling by subsequent ice growth resulted in >2°C near-bottom temperatures. Sea-ice extent the following year (February-March 2017) was low, but within the range of previous observations. Periods of warm, southerly winds in fall 2017 and winter 2018 resulted in extremely low ice extent and virtually no sea ice at mooring site M8 (Fig. 2a). This lack of ice resulted in very warm bottom waters at M8 in summer 2018 (Fig. 2b). Bottom temperatures in November 2018 were the warmest ever observed, ~2°C above the previous high. In 2019, there was more sea ice at M8; hence the bottom temperatures were not as warm as observed in 2018, but were warmer than observed in previous decades (Fig. 2b).

Unlike the pelagic-dominated southern Bering Sea ecosystem, the NBS is characterized by a productive benthic ecosystem (Grebmeier et al. 2006), aided by lipid-rich ice algae that fall to the sea floor as the sea ice melts (Duffy-Anderson et al. 2019). While there is often a subsurface summer phytoplankton bloom on the NBS shelf (Sigler et al. 2014), the largest increases in chlorophyll fluorescence at M8 usually occur with the retreat of sea ice. Chlorophyll fluorescence is related to phytoplankton and algal biomass. Fluorometers, which measure chlorophyll fluorescence, are positioned on moorings and the time series they collect provide an excellent indication of the timing of the primary production. The chlorophyll-fluorescence time series (depth of ~22 m) at M8 in 2018, and again in 2019, showed no evidence of elevated chlorophyll prior to the well-defined increases in June. In other words, there was no ice-associated increase in chlorophyll. Instead, these blooms were typical of open water, like the phytoplankton blooms characteristic of the southern shelf. In 2018, there was likely no export of lipid-rich ice algae to the benthos over much of the northern shelf. During spring/summer 2018, there was an abundance of small low-lipid-content zooplankton and low concentration of lipid-rich large zooplankton. This pattern is common in low ice years in the southern Bering Sea (Duffy-Anderson et al. 2019), but measurements in the NBS are more limited and patterns are less clear.

In 2018, there was a marked northward shift in the distribution of walleye pollock (*Gadus chalcogrammus*) and Pacific cod (*Gadus macrocephalus*) over the Bering Sea shelf. Typically, these species are found on the southern shelf and/or along the outer shelf where bottom temperatures are usually >2°C. In 2019, both pollock and Pacific cod were, once again, found in large numbers on the northern shelf. This change in distribution was likely related to the cold pool (the region on the shelf where summer bottom temperatures are <2°C). In 2018, the cold pool was almost non-existent (Stabeno et al. 2019). In 2019, while larger than in 2018, the cold pool was still well below its typical extent (Fig. 2a).

As in 2018, there were seabird die-offs on the Bering Sea shelf in 2019 (US Fish & Wildlife Service 2019). The largest die-offs, primarily on the southern shelf, affected short-tailed shearwaters (*Ardenna tenuirostris*), which washed ashore in July and August in Bristol Bay. While the underlying cause of the die-off is likely linked to warmer ocean conditions, the exact mechanism is not known. Possibilities

include: northward expansion of pollock and Pacific cod competing with shearwaters for food in the northern Bering Sea; increased toxins from harmful algal blooms; or other as yet unknown mechanisms.

These past two years of low ice extent were likely a result of three factors. First and foremost, abnormally warm, southerly winds during winter limited sea-ice extent and/or forced substantial ice retreat in the winter. Second, the late freeze-up in winter of 2017 and 2018 of the southern Chukchi Sea delayed ice arrival in the NBS. Finally, warm ocean temperatures slowed the advance of ice. Given the very late freeze-up in Chukchi Sea in 2019 (see essay *Sea Ice*), it is likely that ocean temperatures in the NBS will be above normal, however the influence of winter wind patterns on sea-ice extent and, in turn, on ocean temperatures remains difficult to predict.

Acknowledgments

We acknowledge the use of imagery from the NASA Worldview application (https://worldview.earthdata.nasa.gov), part of the NASA Earth Observing System Data and Information System (EOSDIS). NCEP Reanalysis data were provided by the NOAA/OAR/ESRL PSD, Boulder, Colorado, USA, from the Web site at https://www.esrl.noaa.gov/psd/. This research is contribution EcoFOCI 5024 to NOAA's Ecosystems and Fisheries Oceanography Coordinated Investigations program, and PMEL contribution number 5024.

References

Duffy-Anderson, J. T., P. Stabeno, A. G. Andrews, K. Cieciel, A. Deary, E. Farley, C. Fugate, C. Harpold, R. Heintz, D. Kimmel, K. Kuletz, J. Lamb, M. Paquin, S. Porter, L. Rogers, A. Spear, and E. Yasumiishi, 2019: Responses of the northern Bering Sea and southeastern Bering Sea pelagic ecosystems following record-breaking low winter sea-ice. *Geophys. Res. Lett.*, **46**(16), 9833-9842, https://doi.org/10.1029/2019GL083396.

Grebmeier, J. M., J. E. Overland, S. E. Moore, E. V. Farley, E. C. Carmack, L. W. Cooper, K. E. Frey, J. H. Helle, F. A. McLaughlin, and S. L. McNutt, 2006: A major ecosystem shift in the northern Bering Sea. *Science*, **311**(5766), 1461-1464, https://doi.org/10. 1126/science.1121365.

Kwok, R., 2018: Arctic sea ice thickness, volume, and multiyear ice coverage: Losses and coupled variability (1958-2018). *Environ. Res. Lett.*, **13**, 105005, https://doi.org/10.1088/1748-9326/aae3ec.

Mesinger, F., G. DiMego, E. Kalnay, K. Mitchell, P. C. Shafran, W. Ebisuzaki, D. Jović, J. Woollen, E. Rogers, E. H. Berbery, M. B. Ek, Y. Fan, R. Grumbine, W. Higgins, H. Li, Y. Lin, G. Manikin, D. Parrish, and W. Shi, 2006: North American regional reanalysis. *Bull. Amer. Meteor. Soc.*, **87**, 343-360, https://doi.org/10.1175/BAMS-87-3-343.

Sigler, M. F., P. J. Stabeno, L. B. Eisner, J. M. Napp, and F. J. Mueter, 2014: Spring and fall phytoplankton blooms in a productive subarctic ecosystem, the eastern Bering Sea, during 1995-2011. *Deep-Sea Res. Pt. II*, **109**, 71-83, https://doi.org/10.1016/j.dsr2.2013.12.007.

Stabeno, P. J., and S. W. Bell, 2019: Extreme conditions in the Bering Sea (2017-2018): Record breaking low sea-ice extent. *Geophys. Res. Lett.*, **46**(15), 8952-8959, https://doi.org/10.1029/2019GL083816.

Stabeno, P. J., S. W. Bell, N. A. Bond, D. G. Kimmel, C. W. Mordy, and M. E. Sullivan, 2019: Distributed Biological Observatory Region 1: Physics, chemistry and plankton in the northern Bering Sea. *Deep-Sea Res. Pt. II*, **162**, 8-21, https://doi.org/10.1016/j.dsr2.2018.11.006.

Stabeno, P. J., N. B. Kachel, S. E. Moore, J. M. Napp, M. Sigler, A. Yamaguchi, and A. N. Zerbini, 2012: Comparison of warm and cold years on the southeastern Bering Sea shelf and some implications for the ecosystem. *Deep-Sea Res. Pt. II*, **65-70**, 31-45, https://doi.org/10.1016/j.dsr2.2012.02.020.

Thompson, A., 2018: Shock and thaw - Alaskan sea ice just took a steep, unprecedented dive. *Sci. Am.*, May 2, 2018, https://www.scientificamerican.com/article/shock-and-thaw-alaskan-sea-ice-just-took-a-steep-unprecedented-dive/.

US Fish & Wildlife Service, 2019: 2019 Alaska Seabird Die-off Fact Sheet 508C (revised 9 September 2019), https://www.nps.gov/subjects/aknatureandscience/upload/9Sep2019-Die-Off-USFWS-Factsheet-508C-revised-29Aug.pdf.

December 6, 2019

Voices from the Front Lines of a Changing Bering Sea

An Indigenous Perspective for the 2019 Arctic Report Card

Richard Slats (from the community of Chevak), Carol Oliver (Golovin), Robert Bahnke (Nome), Helen Bell (Nome), Andrew Miller (Nome), Delbert Pungowiyi (Savoonga), Jacob Merculief (St. Paul Island), Norman Menadelook Sr. (Teller), Jerry Ivanoff (Unalakleet), and Clyde Oxereok (Wales)

M. L. Druckenmiller[1], R. Daniel[2], and M. Johnson[3], Eds.

[1]National Snow and Ice Data Center, Boulder, CO, USA
[2]The Pew Charitable Trust, U.S. Arctic Program, Washington, D.C., USA
[3]Bering Sea Elders Group, Anchorage, AK, USA

Introduction

The Bering Sea is home to over 70 Indigenous communities of the Iñupiat, Central Yup'ik, Cup'ik, St. Lawrence Island Yupik, Unangan, and Chukchi Peoples. We are peoples of the world's richest sea. We study the ocean and weather as a way of life, as a means for survival. The Bering Sea is undergoing changes that have never been observed in our lifetimes, but were foreseen by our elders decades ago. Global climate change is one of many forces beyond our control that are threatening the entire Bering Sea food chain, of which we are a part. Record-breaking temperatures, reductions in sea ice, and lack of snow are impacting our marine mammals, fish, seabirds, and ecosystem as a whole. The evidence exists along our coastlines, in our waters, and is revealed through the hardships we face in bringing harvests home to our families and communities.

Our resilience as Indigenous Peoples comes from our close proximity to the food resources that we depend on. In a warming Arctic, access to our subsistence foods is shrinking and becoming more hazardous to hunt and fish. At the same time, thawing permafrost and more frequent and higher storm surges increasingly threaten our homes, schools, airports, and utilities. Our environment has changed, but we remain vigilant. By adapting as we always have, we continue to hunt, fish, and harvest from the ocean and land. But, we fear for our young people; we worry that they will grow without the same foods and places that we have known throughout our lives. Maintaining what we inherited from our elders and thinking about our future generations, we offer this report as a glimpse into what we are observing and experiencing at the locations of our eight communities in the Bering Sea region of Alaska (Fig. 1).

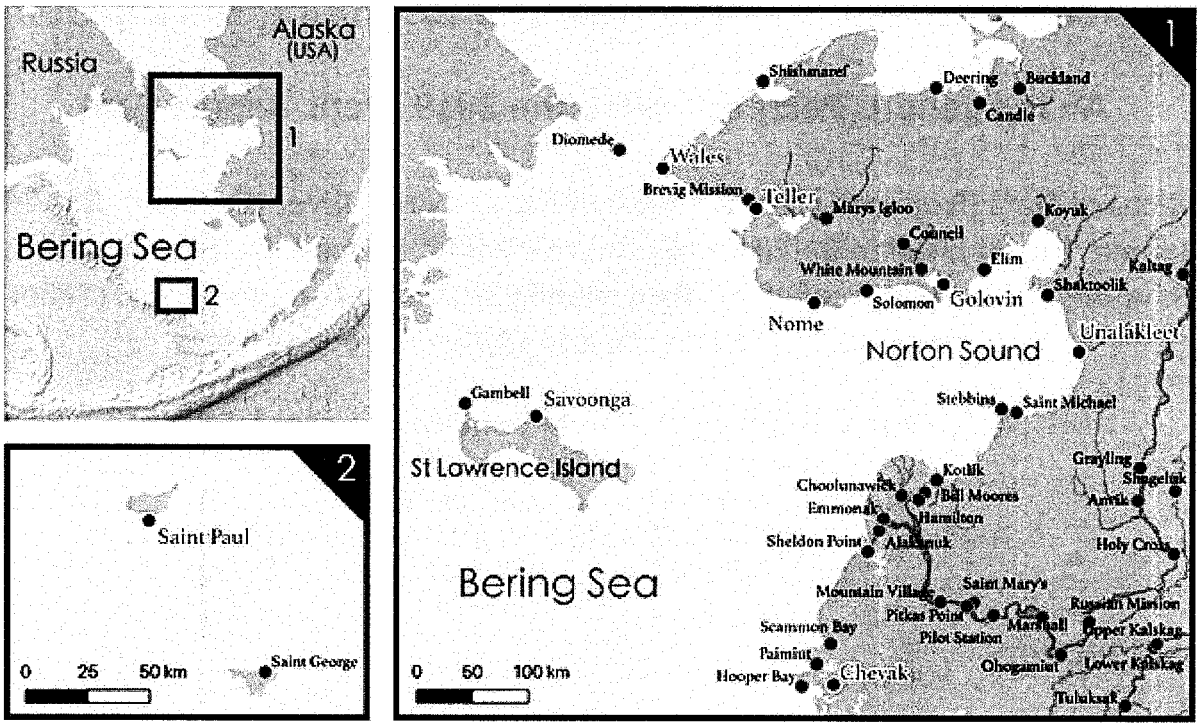

Fig. 1. Map of Alaska communities throughout the Bering Sea region. Authors are from communities denoted with the red markers.

An expanded version of this report with additional information and individual testimonials can be found at https://eloka-arctic.org/communities/bering-sea-voices.

Our changing world

Sea ice

We look for the return of the sea ice every fall season. Across our region, the ice provides access to seals, whales, walrus, fish, crabs, and other marine life for our subsistence harvests. Decades ago, we first saw the disappearance of the large floes of multiyear ice. This was the "mother ice" that would provide the big nails for securing our shorefast ice along the coast. Today, it is both the timing and overall thickness of the ice that has changed. Our sea ice arrives much later nowadays, with the largest shift occurring in the last five years (see essay *Recent Warming in the Bering Sea*). With a delayed and prolonged fall freeze-up, we are stranded for a growing part of the year when we can no longer use boats in the freezing waters, but also cannot yet safely travel across ice with snowmachines. Our traditional ice-based travel routes between communities (e.g., between Wales, Teller, and Brevig Mission) are no longer possible or are greatly limited in duration. At Diomede, a remote island community in the Bering Strait, the coastal sea ice has not been thick enough for an ice runway for the last 10 years or so, leaving the community to depend on less reliable helicopter access as their main means of resupply, mail delivery, and travel on and off the island throughout winter (e.g., to access health care and other social services). The warmer temperatures and delayed freeze-up also impact our river access. At Chevak, as in other coastal communities, the window of time for traveling our rivers and sloughs to set fish nets and traps is coming later, if it comes at all.

In the northern Bering Sea, sea ice used to be present with us for eight months a year. Today, we may only see three or four months with ice. We are used to generally assessing our ice thickness in feet, but now we are often looking at inches, even in the middle of winter. The anchored ridges of ice near our communities that we rely on to safely stabilize our shorefast ice are harder and harder to find, increasing the likelihood that storms or rising tides will break up and remove our ice throughout winter. This places at risk any stored fishing or hunting gear, including crab pots, that may be left on the ice for convenience and fuel-savings. At St. Lawrence Island, shorefast ice has been largely absent for the last five years. This lack of ice greatly hinders our ability to successfully hunt bowhead whales, which provide tons of meat and blubber for sharing throughout the island, as well as with other communities across the Bering Sea region and the whole state of Alaska. Walrus and seals are also no longer as reliably close to the island as they follow the drifting ice across greater distances. In particular, disruptions to our walrus hunting, which is a mainstay for the St. Lawrence Island Yupik, have a tremendous impact on our remote communities. The tomcod, which spawn under the island's shorefast ice, are also moving to new locations. Further south, at St. Paul Island, we have not experienced sea ice in winter since 2013. The loss of sea ice has been the biggest change across our region, and with its loss there is nothing to keep our waters cold.

Winds and weather

One of the biggest dangers we face is that we are no longer able to reliably predict the weather, which is less stable now than in the past. In today's world, we may see four weather patterns in a single day, typically with rapid shifts in wind direction. This limits our ability to spend time on the land or on the ocean (e.g., waiting for whales to come within chasing distance of our boats). It affects our planning and ability to collect and prepare our foods. For example, at Wales, due to more southerly winds in recent years (see essay *Recent Warming in the Bering Sea*), we see a change in when our clams show up; we used to harvest them in fall but now we do so in summer.

We are also experiencing changes in our precipitation—primarily less snow in winter, more frequent winter rain events, and wetter summers. The winter snow is needed to fill our creeks for safe crossings, to keep our ptarmigan nearby through providing shelter as they burrow and eat willows throughout the cold months, and to provide for bountiful salmon berry harvests in summer. Winter rains coat our runways in ice and prevent the planes from landing in our communities, the vast majority of which are not connected to road systems. At Nome, as we travel back and forth to our fish camps in summer, wetter weather with more unpredictable and heavy rains leaves us fewer days to dry our fish. As a result, we are increasingly using roofs (or hootches) over our fish drying racks. This past year's unusually warm air and water temperatures may also be linked to greater weeds seen in our lagoons. At Safety Lagoon near Nome, weeds rising through the water were clogging boat engines as we traveled to our cabins in summer.

Storms and erosion

Warning signs are found all around us of the challenges we face with our eroding shorelines and thawing permafrost. We are seeing coastal landslides, large sinkholes (Fig. 2), and methane bubbling up through our ponds in summer. Thawing permafrost combined with more frequent and higher storm surges, made possible by the diminishing sea ice, is threatening our roads, runways, schools, homes, fish camps, and utilities that carry our water and sewage. This strikes at the heart of our safety, health, and economic well-being. In Golovin, where many community members fish commercially, our only fish processing plant is falling into the ocean. We know that these types of losses are often only a matter of

time, but there is also a lot that we still have time to protect. We are encouraging our young people to build on higher ground.

Fig. 2. Sink hole in the permafrost along the Norton Sound coastline, south of Unalakleet, Alaska. Jerry Ivanoff from Unalakleet observed this as one of three large sinkholes that appeared along this stretch of coastline during summer 2019. Jerry Ivanoff's 22-foot boat can be seen offshore, at left, for scale. (Photo by Mwita Chacha on 24 September 2019)

Observing our animals

Multiple causes for concern

The ocean is our garden. As our well-being relies on the health of this garden, we observe the cumulative impacts on our food resources. The stresses of climate change are a major concern, yet we cannot necessarily separate those from the detrimental impacts that contamination and pollution also have had on our ocean, land, and air, and thereby on the animals and plants that sustain us. We acknowledge the risks that we continue to face as a legacy of the buried military materials around our communities (e.g., fuel drums that are rotting in the tundra), the past use of polychlorinated biphenyls (PCBs) and dichlorodiphenyltrichloroethane (DDT) on our lands, the bio-accumulation of mercury in our marine mammals, and the distant nuclear disasters of Chernobyl (1986) and Fukushima (2011). As we find black blisters on harvested tomcod, observe abnormal odors from the guts of harvested seals, unusual hair-loss on our ugruks (bearded seals, Fig. 3), or animals acting strangely with an extraordinary willingness to approach people, we are reminded that both local and global sources of contamination remain a very long-lived threat that has come to reside in Arctic ecosystems. Our ocean also brings garbage from all over the world. We find plastics as we dissect dead fish and birds found on our beaches. We increasingly must guard against plastic bags being sucked into boat engines. Styrofoam and lost fishing equipment are continually deposited up and down our coastlines.

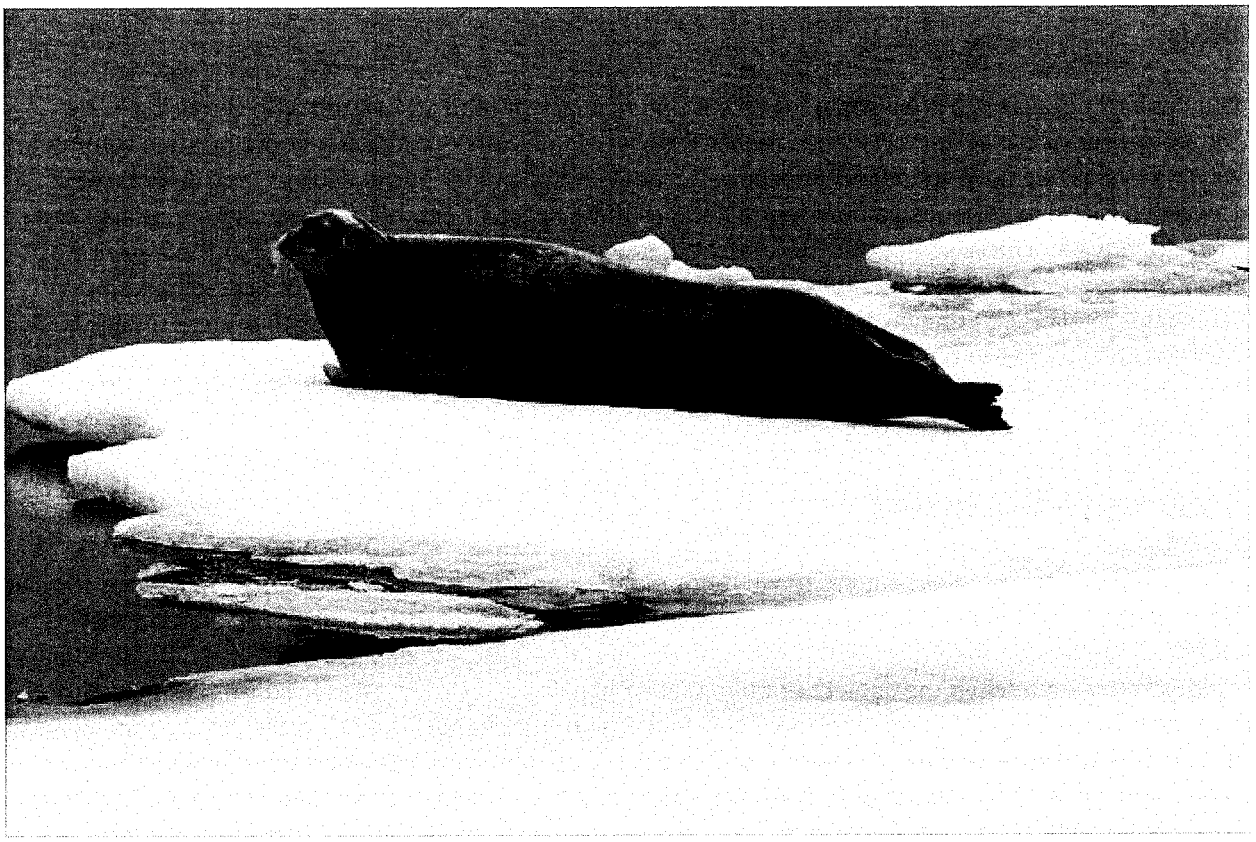

Fig. 3. An ugruk, also known as a bearded seal, resting on sea ice. Ugruks are a critical food source for many Bering Sea communities. (Photo by Gary Bembridge, 2015)

Fish

The fisheries of the Bering Sea are vital to our food security and economic well-being. We harvest fish from our rivers, from the sea ice, and in the open ocean. As the temperatures of ocean waters rise and winter sea ice diminishes, the health of our fisheries is of growing concern. At Teller and Nome, we have seen die-offs of our blue cod and tomcod, likely due to lack of food. During this past summer's record-breaking heat wave, large numbers of salmon were washing up dead along the Ninglikfak River near Chevak, the Kuskokwim River, and other waters across our region. We also see changes in fish migration timing and patterns (see essays *Recent Warming in the Bering Sea* and *Bering Sea Fisheries*). With a later fall freeze-up and an earlier spring thaw, the salmon runs are changing, requiring us to adjust when we fish. Some salmon are traveling further north altogether to spawn in colder waters.

Marine mammals

The media and scientific coverage of massive seal die-offs in Alaskan waters is confirmed by what we too observe. At Wales, we counted 20 dead young ugruks from this past spring that had presumably not had enough food. Similarly, on St. Lawrence Island, we observed 50 dead spotted seals and young ugruks along a 15-20 mile stretch of beach. In recent years, near Chevak, various species of seals with bald patches have been found floating dead on our rivers. While the messages we receive from biologists point to starvation, as opposed to disease, these observations are nonetheless alarming and cause worry regarding the security and safety of our food sources. With sea ice diminishing, our walruses, ugruks, whales, and polar bears are in danger. Our whole marine ecosystem is in danger, threatening our traditional way of life.

Birds

Our seabird populations are also under threat due to a lack of food associated with the rising temperatures of our waters. We have regularly observed die-offs during at least the last five summers. Around Wales, we have found our beaches littered with dead eider ducks, murres, and auklets. St. Lawrence Island experienced a massive auklet die-off this past summer. The adults laid their eggs but abandoned their chicks soon after they hatched. It was the adults' survival strategy in the absence of food. Still, we found dead adult auklets across our beaches, which necropsies confirmed had empty stomachs. Similarly, at Chevak this past summer, we observed common murres that were unable to fly because they were too hungry. Our little birds are also indicators of change, and we see these less and less. The lack of songbirds around Nome and Wales has brought uncommon silence when we are out on the land.

Looking to the future

We are sharing today things similar to what our elders shared in the past. We have seen change coming. Now, we know it is here. When we were young, we learned to read the clouds to understand the weather. We laid on the ground for hours with our grandparents, looking upwards. It is difficult to pass on this knowledge when the subject of our study is changing so quickly. The world from our childhood is no longer here. Our young children today are seeing so much change, but it is difficult for them to understand the pace. We are losing so much of our culture and connections to the resources from our ocean and lands. Store-bought groceries and meat, which are flown in by airplane at great cost, are continually replacing our local, fresh and nutritious subsistence foods. Our food security is even more at risk as our young people increasingly face high rates of unemployment with few job opportunities, and are less likely to own a boat for hunting and fishing.

With the unprecedented retreat of sea ice, expected increases in marine traffic and expanding fisheries are only more likely to further stress our Bering Sea ecosystem. We already are experiencing an increase in the number of large cargo ships entering our waters, as well as the growing prospects of harmful mining along our rivers. What steps will we take to care for our environment, to conserve, and to spark real action to address climate change? Our children need to be prepared to respond to these questions. It is therefore vital that our young people participate in this process of documenting and sharing our observations of change and adaptation across our region.

Afterword and acknowledgments

This essay is a direct result of a workshop in Nome, Alaska, during 26-27 September 2019, when ten elders from eight communities met for two days of sharing and discussion (Fig. 4). Many of us have never had a chance to share our voices to such a report. We are grateful for this opportunity to contribute to the NOAA Arctic Report Card. We also acknowledge that our eight communities are few compared to the total number in our region. While the peoples of the Bering Sea are experiencing many of the same challenges related to climate and environmental change, each community exists within its unique location and has its own experiences.

Fig. 4. Participants of the Bering Sea Elders' Arctic Report Card Workshop in Nome, AK during 26-27 September 2019. Back (left to right): Richard Slats, Matthew Druckenmiller, Mellisa Johnson, Andrew Miller, Jacob Merculief, Robert (Bob) Bahnke, Clyde Oxereok, and Raychelle Daniel. Front (left to right): Mwita Chacha, Eli Kintisch, Delbert Pongowiyi, Jerry Ivanoff, Norman Menadelook Sr., and Carol Oliver. Absent: Helen Bell. (Photo by Mwita Chacha)

We thank the Study of Environmental Arctic Change (SEARCH) and the National Snow and Ice Data Center (NSIDC) that funded and supported the workshop. We are very grateful to the University of Alaska Fairbanks (UAF) Northwest Campus in Nome, Alaska, for hosting the workshop; we specifically thank Barb QasuGlana Amarok and Mariah Morgan for their assistance. Lastly, this report would not have been possible without the support of the tribal councils of Chevak, Golovin, Savoonga, St. Paul Island, Teller, Unalakleet, and Wales, and the coordination provided by the Bering Sea Elders Group and Pew Charitable Trusts.

November 22, 2019

Authors and Affiliations

J. K. Andersen, National Snow and Ice Data Center, Boulder, CO, USA; Institute for Marine and Atmospheric Research Utrecht, Utrecht University, Utrecht, The Netherlands

Robert Bahnke, Nome, AK, USA

T. J. Ballinger, Department of Geography, Texas State University, San Marcos, TX, USA

Helen Bell, Nome, AK, USA

L. T. Berner, School of Informatics, Computing, and Cyber Systems, Northern Arizona University, Flagstaff, AZ, USA

U. S. Bhatt, Geophysical Institute, University of Alaska Fairbanks, Fairbanks, AK, USA; International Arctic Research Center, University of Alaska Fairbanks, Fairbanks, AK, USA

J. W. Bjerke, Norwegian Institute for Nature Research, FRAM - High North Research Centre for Climate and the Environment, Tromsø, Norway

D. Boertmann, Department of Bioscience, Arctic Research Centre, Roskilde, Denmark

J. E. Box, Geological Survey of Denmark and Greenland, Copenhagen, Denmark

A. L. Breen, International Arctic Research Center, University of Alaska Fairbanks, Fairbanks, AK, USA

R. Brown, Climate Research Division, Environment and Climate Change Canada, Ottawa, ON, Canada

J. Cappelen, Danish Meteorological Institute, Copenhagen, Denmark

J. C. Comiso, Cryospheric Sciences Laboratory, Goddard Space Flight Center, NASA, Greenbelt, MD, USA

L. W. Cooper, Chesapeake Biological Laboratory, University of Maryland Center for Environmental Science, Solomons, MD, USA

R. Daniel, The Pew Charitable Trust, U.S. Arctic Program, Washington, D.C., USA

B. Decharme, Centre National de Recherches Météorologiques, Toulouse, France

C. Derksen, Climate Research Division, Environment and Climate Change Canada, Ottawa, ON, Canada

A. Dolgov, Polar Branch of the Federal State Budget Scientific Institution "Russian Federal Research Institute of Fisheries and Oceanography" (PINRO), Murmansk, Russia; Federal State Educational Institution of Higher Education "Murmansk State Technical University" (FSEI HE MSTU), Murmansk, Russia; Tomsk State University, Tomsk, Russia

M. L. Druckenmiller, National Snow and Ice Data Center, Boulder, CO, USA

H. E. Epstein, Department of Environmental Sciences, University of Virginia, Charlottesville, VA, USA

S. Farrell, NOAA Earth System Science Interdisciplinary Center, University of Maryland, College Park, MD, USA

R. S. Fausto, Geological Survey of Denmark and Greenland, Copenhagen, Denmark

X. Fettweis, University of Liege, Liege, Belgium

B. C. Forbes, Arctic Centre, University of Lapland, Rovaniemi, Finland

M. Fossheim, Institute of Marine Research, Tromsø, Norway

K. E. Frey, Graduate School of Geography, Clark University, Worcester, MA, USA

G. V. Frost, Alaska Biological Research, Inc., Fairbanks, AK, USA

M. V. Gavrilo, Association "Maritime Heritage: Explore & Sustain", St. Petersburg, Russia

S. Gerland, Norwegian Polar Institute, Fram Centre, Tromsø, Norway

H. G. Gilchrist, Environment Canada, Ottawa, ON, Canada

O. Gilg, Groupe de Recherche en Ecologie Arctique (GREA), Francheville, France

S. J. Goetz, School of Informatics, Computing, and Cyber Systems, Northern Arizona University, Flagstaff, AZ, USA

J. M. Grebmeier, Chesapeake Biological Laboratory, University of Maryland Center for Environmental Science, Solomons, MD, USA

E. Hanna, School of Geography and Lincoln Centre for Water and Planetary Health, University of Lincoln, Lincoln, UK

I. Hanssen-Bauer, Norwegian Meteorological Institute, Blindern, Oslo, Norway

S. Helfrich, Center for Satellite Applications and Research, NESDIS, NOAA, College Park, MD, USA

S. Hendricks, Alfred Wegener Institute, Helmholtz Centre for Polar and Marine Research, Bremerhaven, Germany

B. Husson, Institute of Marine Research, Tromsø, Norway

Jerry Ivanoff, Unalakleet, AK, USA

C. M. Iversen, Environmental Sciences Division and Climate Change Science Institute, Oak Ridge National Laboratory, Oak Ridge, TN, USA

M. Jeffries, Cold Regions Research and Engineering Laboratory of the Engineer Research and Development Center, U.S. Army Corps of Engineers, Hanover, NH, USA

M. Johnson, Bering Sea Elders Group, Anchorage, AK, USA

L. Kaleschke, Alfred Wegener Institute, Helmholtz Centre for Polar and Marine Research, Bremerhaven, Germany

S. -J. Kim, Korea Polar Research Institute, Incheon, Republic of Korea

C. Ladd, Pacific Marine Environmental Laboratory, NOAA, Seattle, WA, USA

M. J. Lara, Department of Plant Biology and Department of Geography, University of Illinois at Urbana-Champaign, IL, USA

R. R. Lauth, Alaska Fisheries Science Center, NOAA, Seattle, WA, USA

B. Loomis, Goddard Space Flight Center, NASA, Greenbelt, MD, USA

K. Luojus, Arctic Research Centre, Finnish Meteorological Institute, Helsinki, Finland

M. J. Macander, Alaska Biological Research, Inc., Fairbanks, AK, USA

M. Mallory, Acadia University, Wolfville, NS, Canada

K. D. Mankoff, Geological Survey of Denmark and Greenland, Copenhagen, Denmark

J. Marsh, College of Fisheries and Ocean Sciences, University of Alaska Fairbanks, Juneau, AK, USA

W. Meier, National Snow and Ice Data Center, Cooperative Institute for Research in Environment Sciences at the University of Colorado, Boulder, CO, USA

Norman Menadelook Sr., Teller, AK, USA

Jacob Merculief, St. Paul Island, AK, USA

Andrew Miller, Nome, AK, USA

T. Moon, National Snow and Ice Data Center, Boulder, CO, USA

A. Mosbech, Department of Bioscience, Arctic Research Centre, Roskilde, Denmark

T. Mote, Department of Geography, University of Georgia, Athens, GA, USA

L. Mudryk, Climate Research Division, Environment and Climate Change Canada, Ottawa, ON, Canada

F. J. Mueter, College of Fisheries and Ocean Sciences, University of Alaska Fairbanks, Juneau, AK, USA

Carol Oliver, Golovin, AK, USA

E. Olsen, Institute of Marine Research, Bergen, Norway

J. E. Overland, Pacific Marine Environmental Laboratory, NOAA, Seattle, WA, USA

Clyde Oxereok, Wales, AK, USA

D. Perovich, Thayer School of Engineering, Dartmouth College, Hanover, NH, USA

G. K. Phoenix, Department of Animal and Plant Sciences, University of Sheffield, Sheffield, UK

R. Primicerio, University of Tromsø, Tromsø, Norway

Delbert Pungowiyi, Savoonga, AK, USA

M. K. Raynolds, Institute of Arctic Biology, University of Alaska Fairbanks, Fairbanks, AK, USA

J. Richter-Menge, University of Alaska Fairbanks, Institute of Northern Engineering, Fairbanks, AK, USA

R. Ricker, Alfred Wegener Institute, Helmholtz Centre for Polar and Marine Research, Bremerhaven, Germany

A. V. Rocha, Department of Biological Sciences, University of Notre Dame, Notre Dame, IN, USA

V. G. Salmon, Environmental Sciences Division and Climate Change Science Institute, Oak Ridge National Laboratory, Oak Ridge, TN, USA

T. Schuur, Center for Ecosystem Science and Society, Northern Arizona University, Flagstaff, AZ, USA

Richard Slats, Chevak, AK, USA

C. J. P. P. Smeets, Department of Physical Geography, Utrecht University, Utrecht, The Netherlands

P. J. Stabeno, Pacific Marine Environmental Laboratory, NOAA, Seattle, WA, USA

L. V. Stock, Cryospheric Sciences Laboratory, Goddard Space Flight Center, NASA, Greenbelt, MD, USA

H. Strøm, Norwegian Polar Institute, Fram Centre, Tromsø, Norway

M. Tedesco, Lamont Doherty Earth Observatory of Columbia University, Palisades, NY, USA; Goddard Institute of Space Studies, NASA, New York, NY, USA

R. L. Thoman, International Arctic Research Center, University of Alaska Fairbanks, Fairbanks, AK, USA

P. E. Thornton, Environmental Sciences Division and Climate Change Science Institute, Oak Ridge National Laboratory, Oak Ridge, TN, USA

J. T. Thorson, Alaska Fisheries Science Center, NOAA, Seattle, WA, USA

X. Tian-Kunze, Alfred Wegener Institute, Helmholtz Centre for Polar and Marine Research, Bremerhaven, Germany

M. -L. Timmermans, Yale University, New Haven, CT, USA

H. Tømmervik, Norwegian Institute for Nature Research, FRAM - High North Research Centre for Climate and the Environment, Tromsø, Norway

M. Tschudi, Aerospace Engineering Sciences, University of Colorado, Boulder, CO, USA

D. van As, Geological Survey of Denmark and Greenland, Copenhagen, Denmark

R. S. W. van de Wal, Institute for Marine and Atmospheric Research Utrecht, Utrecht University, Utrecht, The Netherlands; Department of Physical Geography, Utrecht University, Utrecht, The Netherlands

D. A. Walker, Institute of Arctic Biology, University of Alaska Fairbanks, Fairbanks, AK, USA

J. E. Walsh, International Arctic Research Center, University of Alaska Fairbanks, Fairbanks, AK, USA

M. Wang, Joint Institute for the Study of the Atmosphere and Ocean, University of Washington, Seattle, WA, USA; Pacific Marine Environmental Laboratory, NOAA, Seattle, WA, USA

M. Webster, Geophysical Institute, University of Alaska Fairbanks, Fairbanks, AK, USA

K. Wood, Joint Institute for the Study of the Atmosphere and Ocean, University of Washington, Seattle, WA, USA; Pacific Marine Environmental Laboratory, NOAA, Seattle, WA, USA

S. D. Wullschleger, Environmental Sciences Division and Climate Change Science Institute, Oak Ridge National Laboratory, Oak Ridge, TN, USA

G. Yannic, Groupe de Recherche en Ecologie Arctique (GREA), Francheville, France; Université Grenoble Alpes, CNRS, Université Savoie Mont Blanc, LECA, Laboratoire d'Écologie Alpine, Grenoble, France

S. G. Zador, Alaska Fisheries Science Center, NOAA, Seattle, WA, USA